POLITECNICO DI MILANO

SCHOOL OF ENGINEERING

MASTER OF SCIENCE IN CIVIL ENGINEERING FOR RISK MITIGATION

THE INFLUENCE OF PORE PRESSURE ON THE FRACTURE BEHAVIOUR OF HIGH PERFORMANCE CONCRETE WITH AND WITHOUT POLYPROPYLENE FIBRES

MIAH MD JIHAD

AKTAR SHAMIMA

SUPERVISOR: PROF. ROBERTO FELICETTI

CO-ADVISOR: ENG. FRANCESCO LO MONTE

OCTOBER 2013

DECLARATION

We, the undersigned, hereby declare that the work contained in this thesis presented by **MIAH MD JIHAD** and **AKTAR SHAMIMA** entitled ***"The Influence of Pore Pressure on the Fracture Behaviour of High Performance Concrete with and without Polypropylene Fibres"*** is accepted as fulfilling the part of the requirements for the degree of Masters of Science in Civil Engineering for Risk Mitigation.

Signature: _____

Date: _____

ABSTRACT

The gradual or sudden separation of concrete layers or pieces from the surface of structural elements subjected to fire (spalling) is still a hot issue in structural design, since this phenomenon may lead (a) to a sizeable reduction of the cross-sectional area and (b) to the direct exposure of rebar's to flame. On this topic a great number of studies have been conducted, always looking into the role of both internal material factors (moisture content, porosity, tensile strength, fibre content) and external structural factors (heating rate, applied loads and constraints) in influencing the two main mechanisms responsible for this phenomenon. On the one hand heating generates temperature gradients that induce compressive stresses near the exposed surface (due to restrained thermal dilation) and tensile stresses in the cooler interior region (thermo-mechanical process). On the other hand, heating produces moisture transport and water vaporization (thermo-hygral process), causing the vapour pressure build-up in the pores, which, especially for HPC, substantially contributes to the explosive nature of spalling (explosive spalling). The latter evidence justifies the recent and increasing attention to the thermo-hygral behaviour of concrete exposed to fire, recognizing the vapour pressure build-up as the main provoking spalling phenomenon mechanism.

From the experimental point of view, several authors have directly measured the local pressure in concrete specimens subjected to thermal transients in different test conditions, obtaining values as high as 5 MPa in case of HPC and lower values for OPC. Another research trend is based on numerical models simulating heat and mass transport occurring in concrete exposed to high temperature. One of the critical problems of these models in assessing the risk of concrete spalling is the mutual interaction between pore pressure and the mechanical response of the material.

In order to clarify this point a special set-up has been designed aiming at performing simple indirect-tension tests (split-cube tests) under different level of sustained pore pressure. These levels are achieved by preliminary heating two opposite's faces of cubic specimens, whereas the lateral ones are sealed and thermal insulated, so as to create a mono-dimensional thermo-hygral transient field. The fracture is induced in the symmetry plane, where both temperature and pressure are monitored using a customized probe. The self-tensioning effects on the mechanical response of specimens are estimated by means of numerical simulations of heat transfer, based on back-analysis of some experimental results.

The numerical results emphasize a good correspondence with experimental evidence in assessing the thermal field and the self-tensioning effects on mechanical response. Moreover, the experimental results show that the pore pressure and the reduction of the apparent tensile strength have comparable values. This evidence, corroborated by simple considerations based on linear-elastic fracture mechanics, contrasts some other models, proposed in literature. In fact, these

models assume that gas pressure is exerted inside the pores and suggest to multiply it by the material porosity value, much smaller than the unitary value.

After all the experimental campaign show that pore pressure might be, in itself, a sufficient driving force to trigger explosive spalling in concrete members exposed to fire.

SOMMARIO

La graduale o improvvisa espulsione di strati o frammenti di calcestruzzo dalla superficie esposta all'incendio di un elemento strutturale (spalling) è tuttora un importante argomento di discussione nella progettazione strutturale, in quanto tale fenomeno può comportare una significativa riduzione della sezione resistente e l'esposizione diretta delle barre di armatura alle fiamme. A riguardo sono stati condotti numerosi studi, volti alla valutazione dell'influenza che sia fattori interni al materiale (contenuto di umidità, porosità, resistenza a trazione, contenuto di fibre) che esterni (velocità di riscaldamento, carichi applicati e condizioni di vincolo) esercitano sui due principali meccanismi responsabili del fenomeno (processi termo-meccanico e termo-igrometrico). Da un lato, infatti, il riscaldamento genera dei gradienti termici che inducono sforzi di compressione negli strati prossimi alla superficie esposta (a causa della dilatazione termica impedita) e sforzi di trazione nelle regioni interne, più fredde (processo termo-meccanico). Dall'altro induce il trasporto di acqua (sia allo stato liquido che gassoso) e la sua vaporizzazione, causando l'aumento della pressione di vapore all'interno dei pori (processo termo-igrometrico), contribuendo così, specialmente per i calcestruzzi ad alte prestazioni (HPC), alla natura esplosiva del fenomeno (explosive spalling). La violenza dello spalling sembra giustificare la grande attenzione rivolta, in tempi relativamente recenti, al comportamento termo-igrometrico del calcestruzzo, riconoscendo nello sviluppo della pressione di vapore il principale meccanismo scatenante.

Da un punto di vista sperimentale, alcuni autori hanno misurato direttamente la pressione dei pori localmente in provini di calcestruzzo soggetti a diversi cicli di riscaldamento, ottenendo valori elevati (fino a 5 MPa) per i calcestruzzi ad alte prestazioni (HPC) e valori più bassi per i calcestruzzi ordinari (OPC). Una seconda metodologia di ricerca, invece, è basata sulle modellazioni numeriche volte a simulare il trasporto di calore e di massa all'interno del calcestruzzo esposto ad alta temperatura. Un problema critico di questi modelli atti alla valutazione del rischio di spalling, consiste nella definizione dell'interazione tra pressione nei pori e risposta meccanica del materiale.

Al fine di chiarire tale aspetto, è stato messo a punto un set-up sperimentale, il cui scopo è quello di permettere l'esecuzione di prove di trazione indiretta (prove di splitting su provini cubici) per diversi livelli di pressione interna nei pori. Questi livelli vengono raggiunti attraverso il riscaldamento dei provini cubici su due facce opposte, mentre le rimanenti facce vengono preventivamente impermeabilizzate ed isolate termicamente, in modo da creare un processo termo-igrometrico pressoché monodimensionale. La frattura è indotta sul piano di simmetria del provino, dove vengono costantemente monitorate sia la pressione nei pori che la temperatura, per mezzo di un apposito sensore. L'effetto delle autotensioni termiche sulla risposta meccanica è stato studiato attraverso simulazioni numeriche incentrate unicamente sul trasferimento di calore e, quindi, su una stima

sufficientemente attendibile del campo termico che si viene ad instaurare nella tipologia di prova sopra descritta, sfruttando l'analisi inversa di risultati sperimentali precedentemente ottenuti.

I risultati delle modellazioni numeriche hanno evidenziato una buona corrispondenza con la realtà sperimentale per quanto riguarda la stima del campo termico e dell'effetto delle autotensioni. I risultati delle prove mostrano, invece, come la pressione nei pori misurata e la conseguente riduzione della resistenza a trazione apparente abbiano valori dello stesso ordine di grandezza. Tale evidenza, corroborata da semplici considerazioni basate sulla meccanica della frattura lineare elastica, si contrappone ad altri modelli proposti in letteratura, che, ipotizzando la pressione agente unicamente all'interno dei pori, suggeriscono di moltiplicarla per il valore della porosità (di molto inferiore all'unità).

In definitiva la pressione nei pori sembra essere, da sola, una forza sufficiente all'innesco dello spacco esplosivo di elementi strutturali di calcestruzzo esposto al fuoco.

ACKNOWLEDGEMENTS

We would like to express our sincere appreciation and deepest gratitude to our supervisor, Professor Roberto FELICETTI and Co-advisor, Eng. Francesco LO MONTE for their kind supervision, guidance, suggestions, encouragement and insight throughout this important study. We also would like to express thanks to the staff of the laboratory and workshop of the Structural Department, at Politecnico Di Milano.

We express sincere thanks to our Italian friends Marina Pistor, Sara Pistor and their family members for their helping attitude, appreciation and encouragement during this thesis period. We are grateful to our family especially our father, mother and brothers for their encouragement during our stay abroad.

Many technical papers are used in this research work for discussion of the results obtained by us. We would like to thank to all authors listed in the bibliography.

The authors would like to dedicate the whole work to their beloved parents.

THESIS LAYOUT

CHAPTER 1: INTRODUCTION

This chapter briefly introduces the reader to the topic of the issues of fire, fire design guidance, and problems related to fire accidents. This chapter also serves the choice of materials for fire design structures and the heat transmission system during fire.

CHAPTER 2: BEHAVIOUR OF CONCRETE AT HIGH TEMPERATURE

In this chapter general discussion about the temperature effects on chemical composition of concrete, problems of the deterioration of thermal properties (i.e. porosity, density, gas permeability, thermal expansion of cement, aggregate and concrete, thermal conductivity, diffusivity, specific heat and thermal inertia) and mechanical properties (i.e. compressive strength, tensile strength, poisson's ratio and modulus of elasticity) due to high temperature. Also this chapter covered the brief discussion about the behaviour of high strength concrete, spalling due to (a) pore pressure, (b) thermal stress, and (c) thermal cracking of concrete. It also covered the spalling in different types of concrete and the role of polypropylene fibre at high temperature.

CHAPTER 3: LITERATURE REVIEW

In this chapter an overview of the literature about the heating systems, measurements of temperature and pressure due to thermo-mechanical and thermo-hygrometric process are presented to the reader. Many factors can influence the pore pressure during heating, such as water cement ratio (w/c), heating rate, water content, aggregates type and the role of polypropylene fibres. Hence, the literature review was necessary to define the mix design, the experimental procedures and the content of polypropylene fibre used in the presented experimental work.

CHAPTER 4: EXPERIMENTAL CAMPAIGN

In this chapter a detailed overview of the proposed mix design, experimental set-up, procedure of the measurement of temperature, pore pressure and indirect tensile strength of the cubes in hot and virgin condition, is described. In order to understand the behaviour of concrete spalling, the experimental procedures of microstructure (scanning electron microscopy and mercury intrusion porosimetry) and thermal properties (porosity, vapour permeability, diffusivity and pore pressure measurement) were discussed. This chapter also serves the influence of tensile strength by pore pressure with different heating rate and different dosages of polypropylene fibres. Here also

discussed the preliminary experimental works (experimental and numerical analysis) which have already done in the year of 2011 and 2012 by two M.Sc. thesis to compare with our results.

CHAPTER 5: EXPERIMENTAL RESULTS

This chapter presents the details discussion of the experimental results in terms of: time-temperature, time-pore pressure, time-temperature-pore pressure, temperature-pore pressure, temperature at peak pressure and effect of pore pressure on the apparent tensile strength of concrete, with particular care on the role played by the pp-fibres, with different heating rates. This chapter also discussed the results of microstructure and thermal properties: pore-size distribution at different temperatures, porosity, vapor permeability, thermal diffusivity, pore pressure and microcracking inside the cementitious matrix.

CHAPTER 6: CONCLUSIONS AND RECOMMENDATIONS

This chapter contains a sum up of all results and an overall conclusion about the effect of pore pressure on the fracture behaviour of high performance concrete, with particular attention the role played by the polypropylene fibres.

NOTATIONS

T: Temperature

T_0: Initial temperature

q: Thermal flux

λ: Thermal conductivity coefficient

T_1, T_2: Temperature of wall faces

A: Area

L: Thickness of the wall

D: Thermal diffusivity coefficient

α_c: Thermal convection coefficient

$T_{surface}$: Surface temperature

T_{fluid}: Fluid temperature

φ: Configuration factor

ε: Emissivity

σ: Stefan-Boltzmann constant (5.67 X 10^{-8} W/m^2K^4)

T_r: Absolute temperature of receiving surface

T_e : Absolute temperature of emitting surface

ε_e: Emitting body emissivity

ε_r: Receiving body emissivity

C_p: Specific heat of concrete

ρ: Density of concrete

K: Thermal conductivity

H: Enthalpy

P: Pressure

ε_{th}: Thermal strain

ε_σ: Stress related strain

σ: Applied stress

ε_{cr}: Creep strain

t: Time

ε_{tr}: Transient strain

$f_{c,\theta}$: Peak stress

$\varepsilon_{1,\theta}$: Strain at the peak stress

$\varepsilon_{cu,\theta}$: Ultimate strain

$K_{c,t}$:Tensile strength reduction factor

$f_{ck,t}$: Characteristic tensile strength

f_c: Compressive strength

f_t: Tensile strength

t^{tot}: Total stress

t^{eff}: Effective stress

p^s: Solid phase pressure

I: Unit tensor

χ: Curvature of the water free surface

p^{gw}: Vapor water pressure

p^{ga}: Dry air pressure

p^w: Liquid water pressure

f_{ct}: Tensile strength

L: Length of the specimen

d: Designated dimension of specimen

F: Maximum load

P_{sv}: Saturation vapour pressure

f_{ct}^{ex}: Experimental tensile strength

f_{ct}^{th}: Theoretical tensile strength

E: Young's modulus of elasticity

G_f: Fracture energy

f_{ct}^{num}: Numerical tensile strength

f_{ct}^{app}: Apparent tensile strength

p_{gas}: Gas pressure

Δf_{ct}: Chemo-physical detrimental effect induced by temperature

K_I: Stress intensity factor

K_{Ic}: Critical stress intensity factor

T_{ext}: External temperature

T_{int}: Internal temperature

R: Heating rate

CONTENTS

CHAPTER 3: LITERATURE REVIEW

CHAPTER 4: EXPERIMENTAL CAMPAIGN

CHAPTER 5: EXPERIMENTAL RESULTS

LIST OF FIGURES

LIST OF TABLES

CHAPTER - 1

INTRODUCTION

1.1 FIRE DESIGN

Fire is a destructive force that causes many thousands of deaths and billions of euros of property loss each year. People around the world expect that their homes and workplaces will be safe from the ravages of an unwanted fire. Unfortunately, fires can occur in almost any kind of building, often when least expected. The safety of the occupants depends on many factors in the design and construction of buildings, including the expectation that certain building and parts of building will not collapse in a fire or allow the fire to spread. Designing a building or an infrastructure, engineers should take into account that there are several environmental hazards, among which one of the most severe can be fire. Fire safety refers to two strategies, depending on the evolution of fire: (a) in the early stages of a fire the aim is to prevent fire spreading outside the compartment to other parts of the building and (b) in the latter structural collapse. The first one can be achieved by sprinklers, fans or other devices against smoke or suitable materials and interior linings that retard flame spread. If fire keeps growing despite the previous presented measures, the structure needs to have sufficient fire resistance to remain structurally stable for a period of time. Therefore, an important and critical parameter involved in these strategies is time.

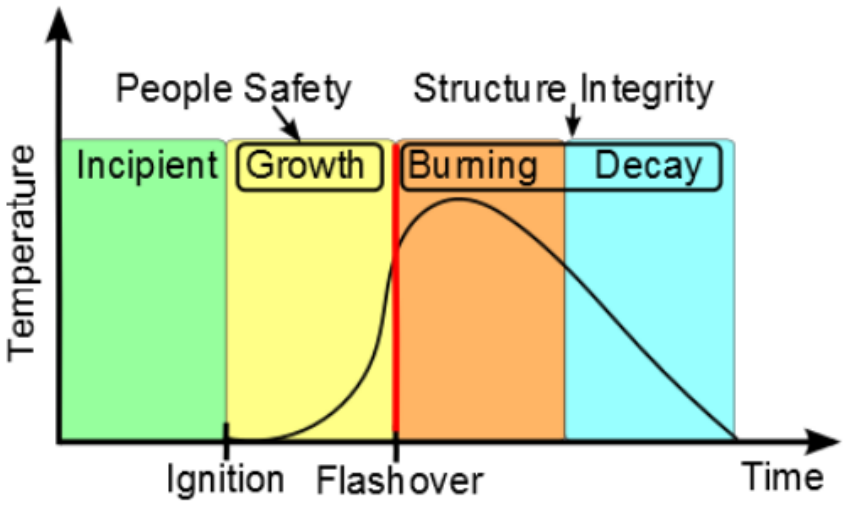

Figure 1.1: Time-temperature curve for full process of fire development (Andrew H.Buchanan, 2001).

Figure 1.1 presents the abovementioned strategies in a typical fire evolution inside a room assuming there are no suppression devices or fire fighters to stop the fire spread. The flashover represents the transition phase between the growth (pre-flashover) and the burning period, known also as a fully developed stage or post-flashover. In this thesis, only the burning phase is taken into account. Structural engineers should take enough measures when designing the structures so that there is sufficient time for people to escape towards safe places. Time is closely related to the type of material used for design: steel, timber or concrete. Steel should be more ductile and concrete should not suddenly spall due to the internal pressure created by the high temperature.

So far a lot of research works were focused on spalling caused by internal pore pressure due to high temperature. In this research work, we focused on the influence of pore pressure on the apparent tensile strength of high performance concrete (HPC) to clarify whether the tensile strength of hot concrete may be exceeded by pore pressure, without any significant contribution of thermal stress. Also for prevention of the spalling phenomenon, we introduced the polypropylene fibres with different dosages to reduce the internal pressure of the concrete.

1.2 CONCRETE DESIGN GUIDANCE

The increasing use of high-performance concrete in structures exposed to extreme environmental conditions (tunnels, marine platforms, Liquefied Natural Gas - LNG terminals, containment shells for industrial facilities), and the need to repair / strengthen existing structures in order to adhere to the more recent codes, bring in new problems, which go beyond the excellent knowledge about the behavior of ordinary concrete in extreme conditions. Designs of new concretes introduced many unknowns; for example high-performance concrete (HPC) are more sensitive to spalling under certain thermal and mechanical conditions. Progressive spalling involving gradual fall out of small pieces of concrete from the surface of the element or sudden failure with large release of energy and slough off of large pieces, in the case of explosive spalling, are phenomena that threaten the load- bearing capacity of the structure, and, in the worst scenario can lead to complete failure of the element (an example of spalling can be seen in Figure 1.2).

For this reason spalling should be taken into account when designing for fire resistance of the structures. Being a function of several different factors such as temperature, moisture content, vapor pressure, concrete type, cements paste, etc., it is difficult to fully understand the mechanism behind spalling and to quantify the risk of it to occur.

Figure 1.2: Seriously damaged due to spalling of columns (Explosive spalling).

The best economical method to prevent spalling is the addition of polypropylene fibres to the concrete mix within a range of 0.15% to 0.3% (Buchanan, 2001). During fire exposure, the polypropylene fibres melt and therefore increase the porosity of the element by creating cavities through which water vapour can escape. In this way the likelihood of spalling is decreased.

Hence, with these new materials, also a new approach of building design is required. Technical solutions should focus on improving the structural design within parameters such as type of reinforcement, external protection, element dimensions but also factors as the microstructure of the material, aggregate mix, cement paste, etc. Concerning people safety, until further development, usage of these concretes should be limited to lower areas of fire risk, for example foundations (Kalifa et al., 2000).

1.3 FIRE SCENARIO

Fire is one of the most severe conditions in which a structural system may be subjected during its useful life. From the significance of this phenomenon we can understand the need to design the structures that can withstand the destructive fire and can save the human life. The main categories of structures subjected to fires are:

- residential buildings or office buildings and warehouses;
- offshore structures and petrochemical plants;
- tunnels;
- bridges and viaducts;
- nuclear power plants.

1.3.1 BUILDINGS (ISO-834)

The standard furnace curve represents a typical building temperature development based upon a cellulosic fire in which the fuel source is wood, paper, fabric, etc. In BS 476, the temperature increases from 20 to 842°C after the first 30 min (i.e. equivalent to an average heating rate of 27.43°Cmin^{-1}). This fire profile has a slow temperature rise up to 1000°C over a period of 120 min; it is representing only a single exposure condition to a fully developed fire and does not include a final cooling branch present in real conditions (the temperature decreases once the most of the combustible material has been consumed).

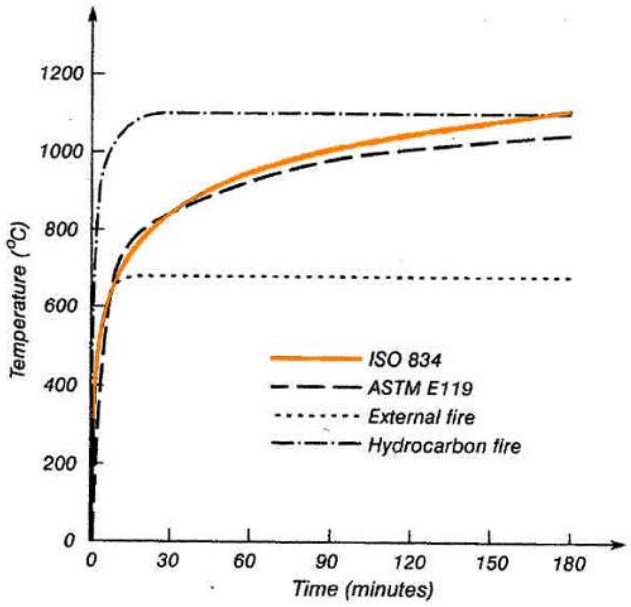

Figure 1.3: Standard Fire Curves.

By comparison, real fires can have a slower or longer growth phase, and once they are established, temperatures can be higher than the furnace temperatures, though they are rarely sustained because they are subject to pronounced fluctuations. The standard temperature–time curve, therefore, corresponds to a severe fire, but not the severest possible fire. Furthermore, as regards breaking phenomena mainly influenced by the speed of heating, as the gap in the concrete surface, the more severe condition is represented by a rapid development of the fire, which achieves high pressures of water vapor in the pore sand high thermal gradients.

In reality, it frequently happens that the heating rate in the first phase is higher than specified by the standard curve. In substance, in case of a fire that develops in a building, it is possible to perform the analysis of the individual structural elements (beams, columns, slabs etc.) by reference to different standard curves, depending on the regulations taken into consideration. In Italy, NTC2008 to the

point 3:6:1:5:1 implementing the ISO-834, of which are set the mathematical expression (1.1) and graphics, Figure 1.4, assumed initial temperature T_0 is 20°C.

$$T = 345 \log(8t + 1) + T_0 \quad (1.1)$$

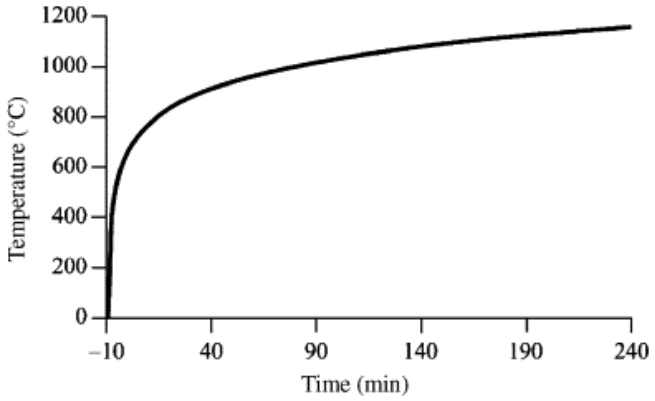

Figure 1.4: Standard Fire ISO-834.

1.3.2 OFFSHORE STRUCTRURES AND PETROCHEMICAL PLANTS

In the 1970s, the oil company Mobil investigated hydrocarbon fuel fires and developed a temperature–time profile with a rapid temperature rise in the first 5 min of the fire up to 900°C (i.e.176°C min^{-1}) and a peak of 1100°C. This research laid the foundation for test procedures to assess fire-protecting materials for the offshore and petrochemical plants.

1.3.3 TUNNELS

Since the second half of the 19th century, tunnels became of primary importance for connecting people and towns. Italy (that represents 12% of the population and 6% of the surface of all Europe) has the 30% of the railway tunnels and the 37% of the roadway tunnels of all Europe. Italy has, in fact, more than 1200 km of railway tunnels and more than 600 km of roadway tunnels, of which more than 75% have been built before 1940, i.e. when the problems related to fire were disregarded in the structural design. These few data show as the problem of assessing spalling sensitivity of existing tunnels is a big issue for Italy.

More recently, a spate of major tunnel fires have indicated that an even more severe fire scenario (RWS and RABT German fire curves) needs to be considered. In the Netherlands, the Ministry of Public Works, the Rijswaterstaat (RWS), and the TNO Centre for Fire Research have established a fire

curve for the evaluation of passive protecting materials in tunnels. This RWS Dutch fire curve models a most severe hydrocarbon fire, rapidly exceeding 1200°C and peaking at 1350°C (melting temperature of concrete) after 60 min and then falling gradually to 1200°C at 120 min, end of the curve. RWS is intended to simulate tankers carrying petrol in tunnels with a fire load of 300 MW causing a fire for 2 h, and was established on the basis of Dutch experience in tunnel fires. However, the maximum temperatures attained in recent major fires did not reach RWS levels, e.g. railway tunnel under the England Channel (Great Britain/France, November 1996, $T_{max} = 1100$°C), in road tunnels of Mont Blanc (Italy /France, April 1999, $T_{max} = 1000$°C), the Tauern (Austria, June 1999, $T_{max} = 1000$°C). The RWS fire curve, therefore, represents the severest form of tunnel fire in terms of initial heating rates and maximum temperatures. The RABT German fire curve, with a descending branch, represents a less severe fire scenario in tunnels than the RWS curve, reaching a maximum temperature of 1200°C (melting point of some aggregates) sustained up to 1 h before decaying to ambient.

Many standard (building) insulation materials decompose and lose their function above 1200°C. It may be that insulation materials behave well in BS 476, ISO 834, Eurocode hydrocarbon fires and even the RABT fire, but may not withstand a fire under RWS conditions. For this reason, the manufacturer of thermal insulation coatings for tunnel concrete linings, Lightcem, have recently developed two different thermal types of insulation materials: one for temperatures up to 1200°C based on Portland cements, and another for temperatures up to 1350°C based on aluminous cements. It should, however, be noted that structural aluminous cement concretes have been banned because of the risk of conversion and weakening that can take place under certain temperature/humidity conditions.

Fire in Channel Tunnel

A large fire involving ten HGVs occurred in the 50 km Channel tunnel between France and England on November 18th, 1996. A shuttle train travelling from France to the UK caught fire and stopped approximately 19 km from the French portal. The tunnel was made using a high-performance concrete (R_{ck}= 55 MPa). The flames were developed in an area coated with high-performance concrete; the fire lasted 9 h and reached locally temperatures exceeding 1000°C.

The concrete spalled over a length of about 500 meters, with the spalling depth being up to approximately 30 cm. Permanent operational equipment had to be renewed over a length of about 3 km.

Figure 1.5: Damage to the lining of the Channel Tunnel caused by the fire.

Soiling from the smoke was found over a length of about 3-5 km. This incident has clearly demonstrated that the high-performance concrete tract was not considered capable of withstanding the high temperatures reached at the center of the fire; however, given the intensity of the phenomenon, no other building material would have been able to resist to thermal gradients that accompanied the development of the flames.

Fire in Mont Blanc tunnel

The Mount Blanc tunnel is 11.6 km long, with a cross-section of approximately 46 m^2. The tunnel section is formed like a vault with the highest point 6 m above the road surface. The width is 8.5 m.

The total fire duration was about 53 h, the temperatures reached and locally exceeded 800 to 1000^{o}C and a stretch of over 900 m of the tunnel ceiling were considerably damaged. Most of the low-grade and highly permeable concrete remained in place, despite the lack of reinforcement and the sizeable damage undergone by 20–40% of the 0.5 m wall thickness.

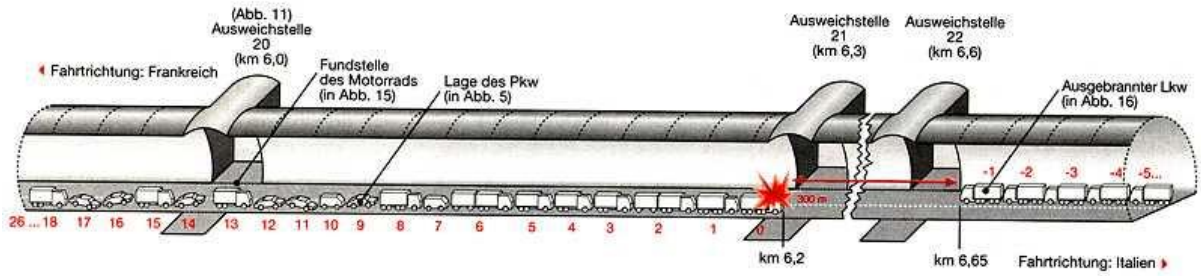

Figure 1.6: The Mont Blanc Tunnel, left to France, right to Italy.

Nonetheless, explosive spalling was observed in about 40% of the underground traffic systems experiencing fires in the last 40 years and specific measures for passive protection are currently adopted in the design of new tunnels (application of boards, cladding panels or sprayed-on materials, admixture of polypropylene fibres).

1.3.4 BRIDGES

The MacArthur Maze is a multilevel freeway inter-change bridge near Oakland, CA, serving several major cities in California. On 29 April 2007 it represented one of the most renewed and studied cases fire-induced collapses of bridges. The fire was triggered by a truck accident that occurred during the early morning hours. The truck was transporting 32600 l of gasoline, when it over-turned on the I-80 / I-880 interchange and burst into flames and the fire reached the very high temperatures of 1650°C.

Figure 1.7: McArthur Maze Collapse by Fire (L. Giuliani et al.).

The time resistance of the bridge was quite low, considering that a whole section of the overpass collapsed on the interchange beneath just 20 min after the beginning of the fire. The cause of the collapse has been imputed to the failure of the connections, overstressed by significant deflection of the road section, whose steel structure had been strongly weakened by the fire.

1.3.5 NUCLEAR POWER PLANTS

The containment structures of nuclear reactors generally have a double-shell: the internal made of prestressed concrete, the outer made of simply reinforced concrete. The inner shell, also called the primary shell, ensures the seal to gases and liquids; the outer (secondary shell) ensures instead the

Impact resistance off lying objects and, thanks to its high ductility, collaborates to the resistance to internal explosions. The eventual fusion of the reactor is subjecting both shells at elevated temperatures, thereby requiring a careful study of the behavior of concrete at high temperature; different material characteristics are required: good workability and compactness, low heat of hydration, low shrinkage, high resistance to traction, reduces rheology.

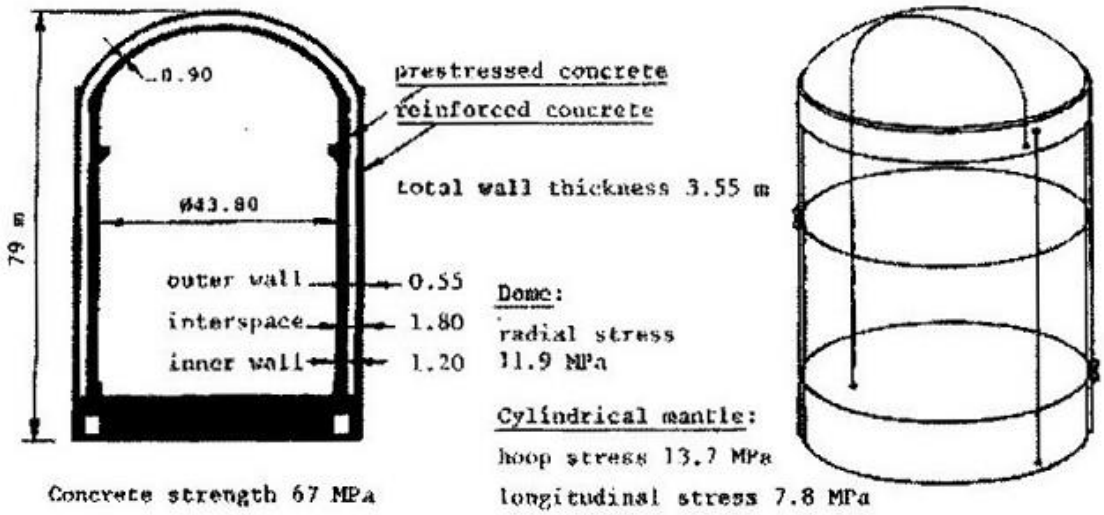

Figure 1.8: Secondary containment structure of the reactor of the nuclear power plant Civaux in Poitiers, France.

1.4 INCIDENTS OF FIRE

1.4.1 SOURCES AND MECHANISMS

Ignition occurs when a combustible mixture of gases is heated to temperatures that will trigger the exothermic oxidation reaction of combustion. Ignition almost always requires the input of heat from an external source. The few cases where self-heating within solid materials can cause spontaneous combustion is a special subject. There are numerous possible heat sources that cause building fires to ignite.

- sources with flame (matches, candles, gas heaters, open fires);
- smouldering sources (cigarettes);
- electrical sources (arcing, overheating);
- radiant sources (sunlight, hot items, heaters, fires).

There are other less common sources as related to mechanical factors (friction), hot surfaces, natural (lightning), transportation (car, bus and train accident), crime (arson) and socio-political (terrorism, war). With this sources fire can happen in the building and fire can spread from the first burning object to a second objet by flame contact if it is very close or by radiant heat transfer if it is further away. The time to ignition of a second object depends on the intensity of radiation from the flame and the distance between the objects.

The amount of heat and the temperature required to cause ignition depend on the material properties of the fuel, the size and shape of the ignited object, and in the time of exposure to heat.

A competent ignition source is one which has sufficient heat and temperature to cause ignition in the expected time of exposure. The time to ignition of materials depend on the thermo-physical properties, such as thermal conductivity, specific heat and density, whose product is defined thermal inertia. When exposed to the same heat source, the surface of material with low thermal inertia (e.g. polystyrene foam) will heat more rapidly than materials with higher material inertia (e.g. wood) leading to much more rapid ignition.

1.4.2 OUTLINE OF HEAT TRANSMISSION

The understanding of the evolution of the fire needs the knowledge of the phenomena and the laws that govern the transmission of heat, which occurs by the processes of conduction, convection and radiation. The following paragraphs recall the bases of these mechanisms.

•conduction, molecular phenomena;

•convection, conduction in a moving fluid;

•radiation, electromagnetic phenomena.

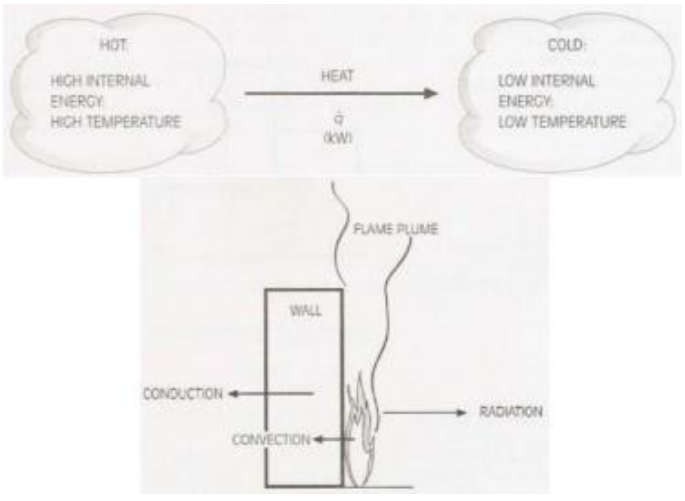

Figure 1.9: Example of Heat Transfer.

Conduction

Conduction is the transmission mechanism in solid materials. In materials which are good conductors of heat, the heat is transferred by the interaction of free electrons. In other materials which are poor conductors, the heat is transferred by mechanical vibrations of the molecular lattice. Conduction is an important factor in the ignition of solid surfaces, and in the fire resistance of barriers and structural members. For steady state situation the transfer of heat by conduction is directly proportional to the temperature gradient between 2 points. In porous materials some movement of fluids may occur. The simplest representation for conduction is the steady flow through wall.

Formula for conduction is as follows:

$$q = \lambda * A * (T_1 - T_2)/L \tag{1.2}$$

where, q is the thermal flux passing through solid body (W), λ is the thermal conductivity coefficient (W/m ^{o}C) and T_1, T_2 temperature of the two wall faces

Also same formula in another shape:

$$q = -\lambda * A * \frac{\partial t}{\partial x} \tag{1.3}$$

typical values of λ for concrete 0.8-1.4 W/m ^{o}C; for steel 10-70 W/m ^{o}C.

For transient heat flow when temperatures are changing with time, the amount of heat required to change the temperature of the material must be included.

For one dimensional (1-D) heat transfer by conduction in a material with no internal heat being released:

$$\frac{\partial^2 t}{\partial x^2} = \frac{1}{D} * \frac{\partial t}{\partial x} \tag{1.4}$$

where, D is the thermal diffusivity coefficient.

These equations state that the rate of heat flow between two temperatures (T_1, T_2) in a solid is proportional to a property of the solid known as thermal conductivity (K). [*reference, principles of fire behaviour, James G. Quintiere*].

It can be seen that materials with low thermal diffusivity will conduct less heat than materials with high thermal diffusivity, when exposed to increasing surface temperatures in unsteady-state conductive heat transfer.

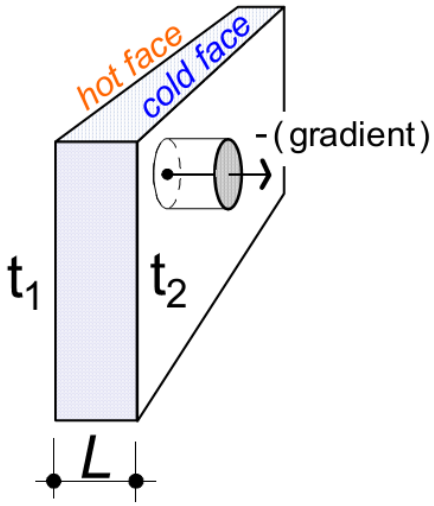

Figure 1.10: Heat transfer by conduction.

Convection

Convection is the heat transfer occurred by the movement of fluids, either gases or liquids. Convective heat transfer is an important factor in flame spread and in the upward transport of smoke and hot gases to the ceiling or out the window from a room fire. Convective heat transfer calculations usually involve heat transfer between the surface of a solid and a surrounding fluid which heats or cools the solid material. The rate of heating or cooling depends on several factors especially velocity of the fluid at the surface.

$$q = \alpha_c * A * (T_{surface} - T_{fluid}) \quad (1.5)$$

where, q is the thermal flux passing through fluid (W) and $\alpha_c$is the thermal convection coefficient (W/m^2 ^{o}C).

α_c depends on the surface geometry, the nature of flow, thickness of boundary layer. A typical value for structural elements exposed to fire (ISO-834 and external nominal) is 25 W/m^2 ^{o}C.

Radiation

Radiation is the transfer of energy by electromagnetic waves which can travel through vacuum, transparent solid or liquid. It is extremely important in fires because it is the main mechanism for heat transfer from flames to fuel surfaces, from hot smoke to building objects and from a burning building to adjacent once.

The radiation is mainly governed by the emissivity factor of the materials between the one which receives and the other which emits the heat.

$$q = \varphi * \varepsilon * \sigma * ({T_e}^4 - {T_r}^4) \quad (1.6)$$

where, T_r is the absolute temperature of receiving surface, T_e is the absolute temperature of emitting surface, φ is the configuration factor (measure of how much of the emitter is seen by the receiving surface), ε resulting emissivity of two surface:

$$\varepsilon = \frac{1}{\frac{1}{\varepsilon_e} + \frac{1}{\varepsilon_r} - 1} \quad (1.7)$$

σ is Stefan-Boltzmann constant ($5.67*10^{-8}$ W/m^{2}K^4).

Emissivity indicates the efficiency of the emitting surface as a radiator ($0< \varepsilon <1$). Convection and radiation provide similar contributions on the unexposed sides. Radiation prevails above 200^{o}C on the exposed side.

CHAPTER - 2

BEHAVIOUR OF CONCRETE AT HIGH TEMPERATURE

Fire resistance is a concept applicable to elements of the building structure and not to a material, but the properties of the material affect the performance of the element of which it forms a part. Concrete structures are known for their good behaviour in the case of fire and, in this regard, this depends on some positive aspects of the material:

• concrete is incombustible (e.g. compared to wood) and has a good insulating property thanks to its low thermal diffusivity (e.g. when compared with steel);

• during heating, the cement paste under goes endothermic chemical and physical processes that delay the transmission of heat to the structures exposed to fire;

• during fire, concrete maintains its geometry, protecting, thanks to the concrete cover, steel reinforcements and allowing the inner cooler core to continue to perform its structural function.

However, there are two main problems of concrete in fire. These are: deterioration in mechanical properties as temperature rises, caused by physico-chemical changes in the material during heating, and explosive spalling, which results in loss of material, reduction in section size and exposure of the reinforcing steel to excessive temperatures.

The low thermal diffusivity of concrete, compared to steel, usually leads to high thermal gradients within the R/C members subjected to fire, i.e. it needs long time to heat up the core due to the high thermal inertia of the material. Therefore, while there is a rapid decrease in the compressive strength of concrete in the layers exposed to high temperature, the structural member might bear until the whole body exceeds a critical temperature (at which the external forces are greater than the bearing capacity). So it is required to analyze the thermal response of the entire R/C member. The thermal behaviour is driven by the physico-thermal properties that are conductivity, specific heat, and density while the mechanical behaviour is driven by the mechanical properties that are stiffness, compressive and tensile strength; all the properties of concrete are dependent on the temperature.

Concrete properties degradation under fire condition is caused by the chemo-physical mechanisms generated in the porous concrete media, resulting in thermal softening (due to the induced damage) as well as thermal expansion, drying shrinkage and internal pore pressure increase, (Figure 2.2).

2.1 TEMPERATURE EFFECTS ON CHEMICAL COMPOSITION

Concrete is a composite construction material consisting generally of mineral aggregate, cement and water. Cement and water together create the cement paste that glues the aggregates and fills the voids within. The microstructure of the concrete depending on different ratios of water/cement can be seen in Figure 2.1.

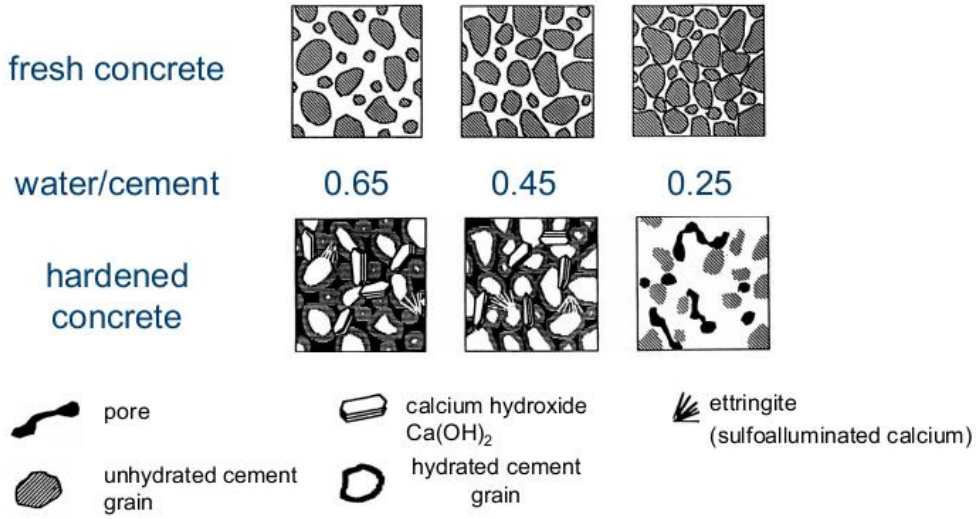

Figure 2.1: Microstructure of concrete(Aïtcin and Neville, 1993).

Concrete exposed to fire experiences chemical decomposition, depending on the temperature. A simple explanation will be given regarding of what happens with growing temperature following Figure 2.2.

• Above 100°C: There is an insignificant weight loss due to the expulsion of evaporable water from hardened cement paste and aggregate.

• 100°C to 200°C: Occurrence of vapor pressure in the micro pores and continuance of weight loss due to evaporation of water. Dehydration of cement gel begins at around 180°C.

• 200°C to 500°C: Weight loss increase mainly due to the loss of water from gel pores as well as the first stage of dehydration and breakdown of tobermorite gel occurs. Above 450°C the portlandite $Ca(OH)_2$ dissociates into calcium oxide (CaO) and water (H_2O).

• 500°C to 700°C: The rate of weight loss keeps increasing because of decomposition of calcium hydroxide in cement paste and decomposition of CSH (calcium silicate hydrate) phases. This is

followed by the formation of $\beta - C_2S$ (quartz silica). Above700°C concrete desegregations start.

• 700°C to 900°C: Decarbonation of calcium carbonate in the limestone aggregate, which occurs at about 800°C.

• Above 900°C: Melting of cement paste and aggregate at 1150°C and 1200°C. No further measurable weight loss. At 1270°C limestone aggregate concrete consists mostly of white porous calcium oxide. Glassy phase of basalt, quartzite and limestone concrete.

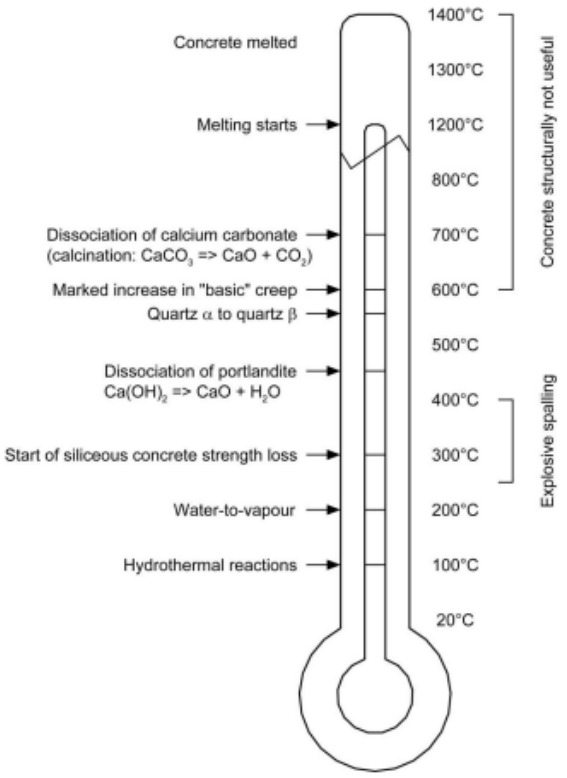

Figure 2.2: Concrete thermometer (Khoury, 2000).

2.2 THERMAL PHYSICAL PROPERTIES OF CONCRETE

To provide knowledge about thermal properties of concrete is essential to determine the distribution of temperature inside the concrete members in order to evaluate their mechanical response during fire and after fire (residual condition) in terms of cracks, loss of serviceability and durability. The type of aggregate, the original moisture content and the age of the concrete are important factors on which the thermal parameters depend. The type of coarse aggregate used in

concrete mix is one of the main factors affecting the change in concrete properties due to high temperature; it can be sorted out into 3 types: carbonate, siliceous and lightweight. Carbonate aggregates involve limestone and dolomite, siliceous aggregate involves silica, granite and sandstone, while lightweight aggregates are usually produced by heating shale, slate or clay.

2.2.1 POROSITY AND DENSITY

The loss of evaporable water does not affect porosity; however, dehydration creates additional pore space to effectively increase the porosity as the temperature increases. The average pore size increases with temperature as the ultrafine gel structure of the calcium silicate hydrate is progressively destroyed by dehydration. At 850˚C porosity is about 40% greater than it was at 105˚C, as noted in Figure 2.3. As a result of the pore size increase the bulk mass density of the cement paste decreases with temperature (i.e., from 1.45 g/cm^3 at 105˚C to 1.3 g/cm^3 at 850˚C), [20].

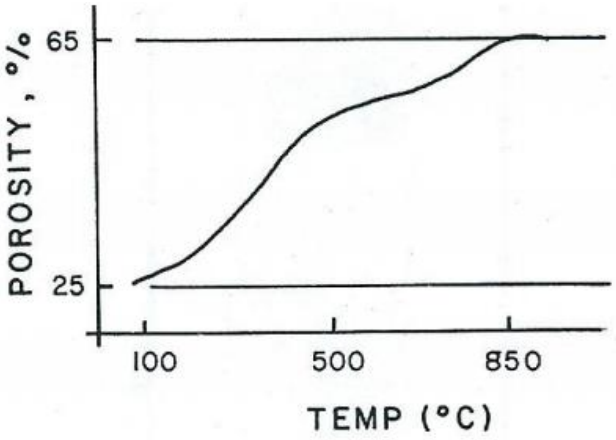

Figure 2.3: Variation of Portland cement paste porosity with temperature (T.Z. Harmathy, 1970).

As the volume of a given mass of concrete changes on exposure to elevated temperature, the mass density will also change. Changes in mass density result from thermal expansion and drying shrinkage, diffusion of water or released gases, and dehydration, melting, or sintering. The density of concrete depends on the density of its aggregate materials and its moisture content in the temperature range from 20°C to 150°C. Figure 2.4 presents variations of true density, bulk density, and porosity for a cement paste.

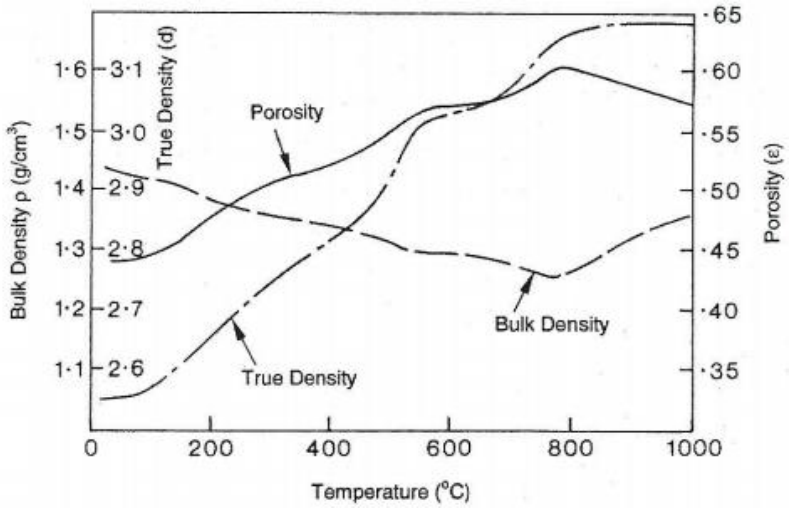

Figure 2.4: True density, bulk density, and porosity of cement paste versus temperature (T.Z. Harmathy, 1970).

In the unsealed condition results reflect the influences of chemical transformations that include water dilation up to about 80˚C, the loss of free and physically bound water at 100˚ to 200˚C depending on section size and heating rate, followed by loss of chemically-combined water at temperatures above 100˚C, the dissociation of calcium hydroxide at 400˚ to 500˚C, and decarbonation above 600˚C. In concrete the aggregate plays an important role in terms of thermal dilation and the dissociation of some aggregates such as carbonate aggregates that display a significant reduction in density above 600˚C and a marked increase in porosity, [20].

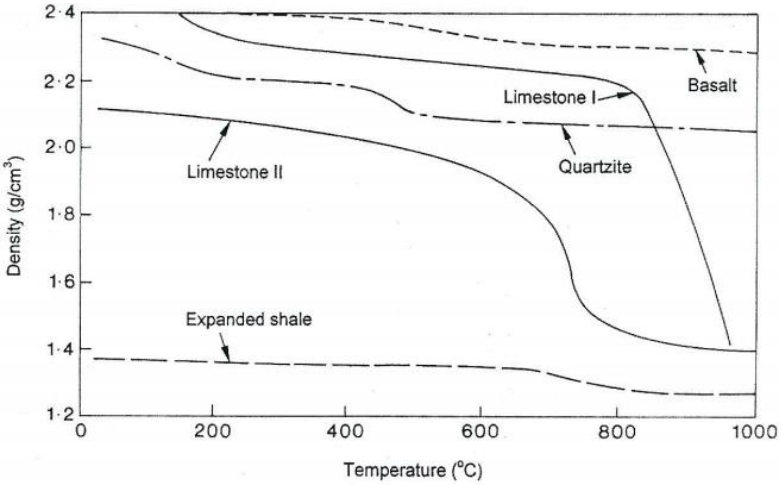

Figure 2.5: Density of concretes having different coarse aggregate types.

Figure 2.5 presents the effect of aggregate type on the density of concretes in the temperature range from room temperature to 1000°C. Storage (curing or preconditioning) conditions at lower temperature are also important because moist specimens will lose water and thus experience a greater decrease in density upon heating than specimens that have experienced drying. At temperatures from 150°C to 600°C the density of limestone concrete is relatively constant. At temperatures from 600˚ to 900˚C decarbonation of limestone commences and weight loss occurs as the concrete porosity increases until at higher temperatures sintering takes place and the density may increase slightly. Siliceous aggregates exhibit a somewhat steeper decrease in density with heating in the range from room temperature to 700°C due to the large thermal expansion of the quartz. Basalt exhibits the smallest decline in density because of its lower thermal expansion, [21].

2.2.2 GAS PERMEABILITY

Mindeguia et al. (2013) measured gas permeability of concrete based on the recommendations of the AFREM (Afrem, 1997) and consists in the gas (di-nitrogen) flow rate measurement, percolating through a 150 mm diameter and 50 mm thick concrete disc. For each measurement, two values of gas pressure are applied in order to assess the intrinsic permeability of the material according to the Klinkenberg approach (Klinkenberg, 1941). The evolution of the gas permeability of concrete with temperature is estimated after applying thermal cycles to samples. Samples were therefore heated up to 120, 250, 400 and 600°C. First, temperature evolves under a heat flow rate of 1°C/min, and the temperature is stabilized around the fixed value during 6 h. Tested samples at room temperature were in fact previously dried at 80°C.

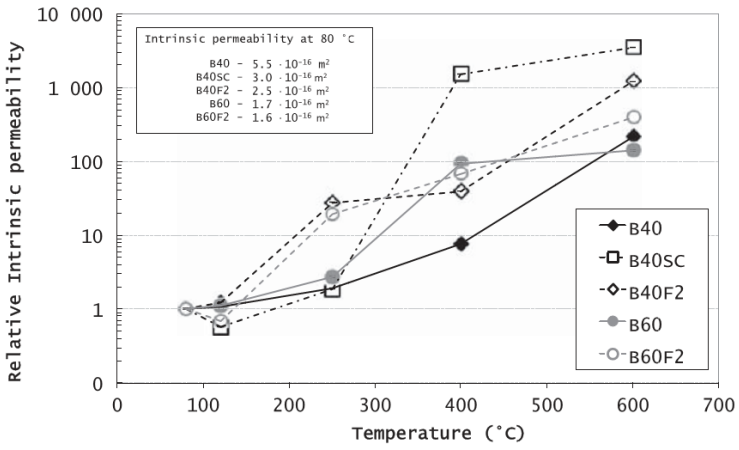

Figure 2.6: Change of the relative intrinsic permeability of the studied concretes vs. temperature (Mindeguia et al., 2013).

In the Figure 2.6, the change of the relative intrinsic concrete gas permeability, defined as the ratio between the permeability measured at high temperature and the one measured at room temperature (after drying at 80°C) is presented. For all tested concretes a more or less significant increase in intrinsic permeability with the temperature can be observed. On the one hand, note that for concretes without pp fibres, the permeability is little affected by heating up to 250°C; gas permeability essentially increases in the range 250–400°C. On the other hand, for concrete containing pp fibres, concrete gas permeability essentially increases in the range 120–250°C, that is, for temperatures around the melting point of pp fibres.

In particular, observe that the effect of the temperature on the intrinsic permeability of the B40 and the B40SC (see section 3.1, paragraph Mindeguia et al., 2013 for details of specimen) is almost the same up to a temperature of 250°C. Beyond that, the effect of temperature is clearly different for the two concretes: at 400°C, the intrinsic permeability of the B40SC is about 1.5 times higher than the one measured at room temperature (only 8 times higher than at room temperature for the B40). Indeed, in the case of B40SC, observed the creation of significant cracks due to heating, particularly around the siliceous aggregates (flint).

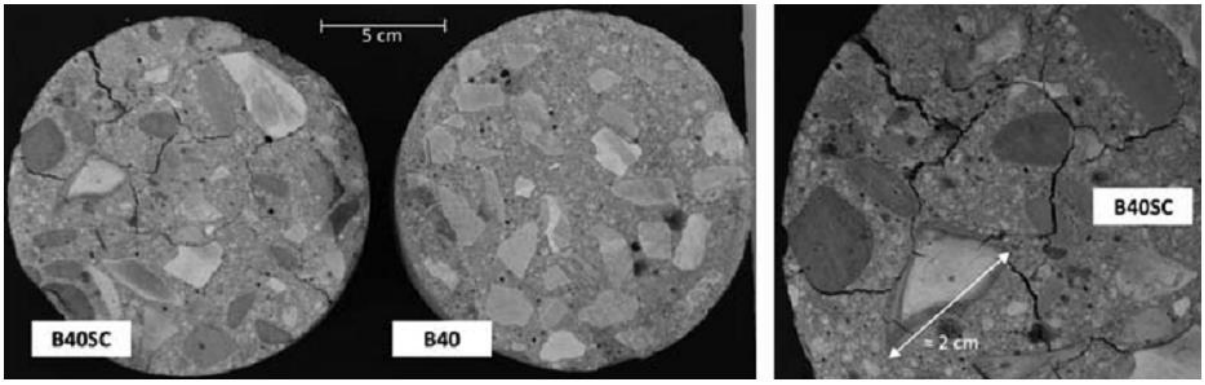

Figure 2.7: Pictures of the B40 and B40SC samples after heating at 400°C (Mindeguia et al., 2013).

This damage can be easily explained by the significant thermal expansion and instability of flint aggregates (compared with purely calcareous aggregates), leading to a thermal mismatch between cement paste and aggregates. Cracks in the B40SC (Figure 2.7) can be seen as percolation paths for the gas, which explains the high measured values of intrinsic permeability.

The intrinsic permeability of both concretes containing pp fibres (B40F2 and B60F2) similarly evolves. The effect of polypropylene fibres is particularly obvious from 250°C, that is, after their melting point (estimated around 160-170°C). The addition of pp fibres (in this case 2 kg per cubic meters of concrete) increases the intrinsic permeability of concrete once the fibre melting occurred.

For both concretes, the effect of the addition of fibres is identical: at 250°C, concrete intrinsic permeability is around 7 times higher than the one measured at room temperature. This phenomenon can be attributed to the melting of pp fibres and to the cracks that it involves. According to several authors (Kalifa et al., 2001; Khoury, 2008; Pistol et al., 2011), pp fibres first expand while melting (at 170°C) and then shrink. As soon as the fibre is shrinking, a void is created in the concrete (Khoury, 2008). This void can be seen as a weak mechanical point and stresses can be concentrated at the ends of the voids then these cracks can connect and a network of cracks appears (Pistol et al., 2011). This mechanism results in an increase of concrete porosity and permeability. So it can induce an easier transfer of fluid (liquid and steam water) and a reduction of the generated gas pore pressure (Figure 2.8), (Mindeguia et al., 2013).

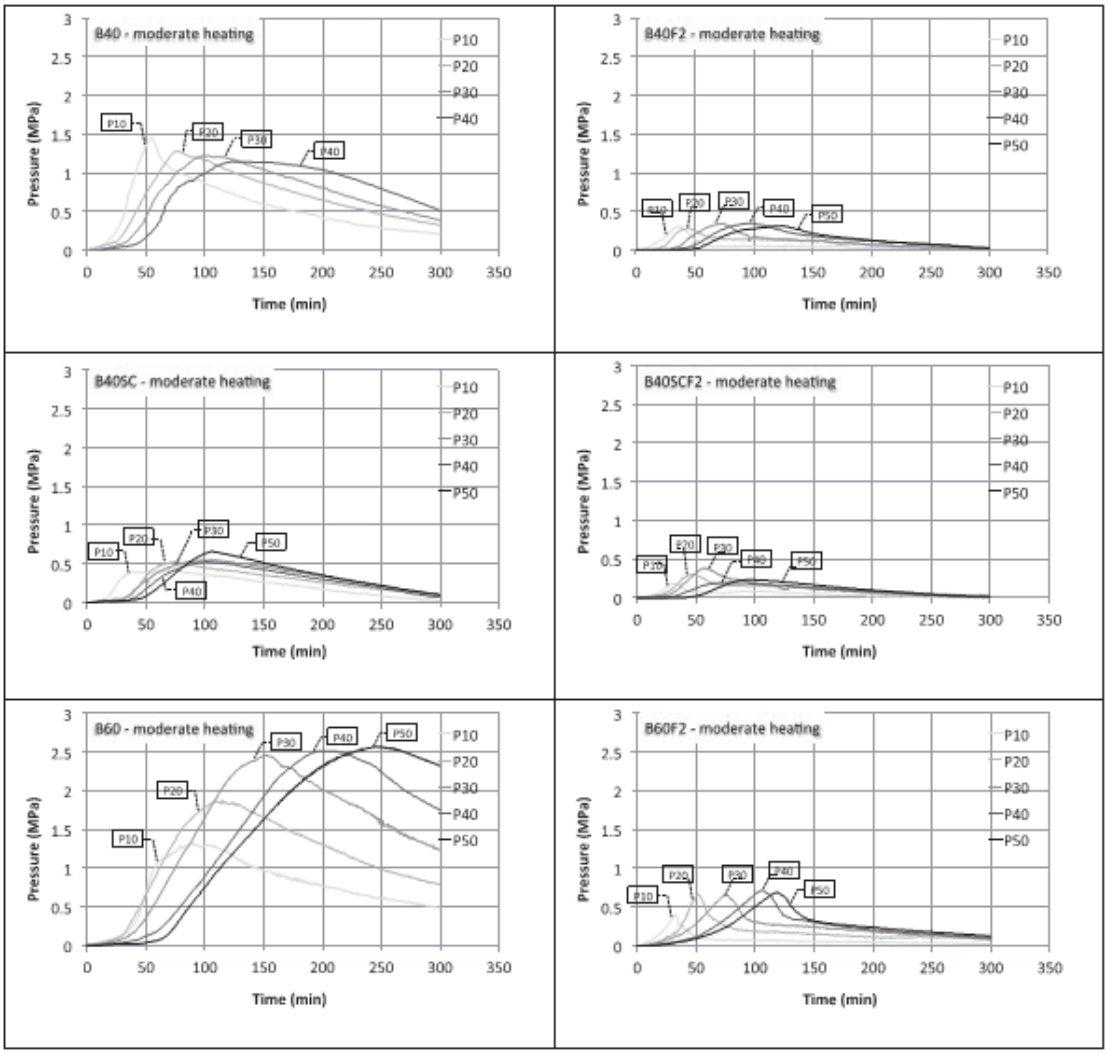

Figure 2.8: Temporal evolution of pore gas pressure of concrete without pp fibres (left) and with pp fibre (right).

2.2.3 COEFFICIENT OF THERMAL EXPANSION

The coefficient of thermal expansion represents the volume change of a material due to temperature change and is expressed as a change in length per degree of temperature change. The coefficient is important as a measure of the structural movement and thermal stresses resulting from a temperature change.

Concrete thermal expansion is a complicated phenomenon because of the interaction of its two main components (cement paste and aggregate) which each have their own coefficients of thermal expansion. When differences in the thermal expansion between the hardened cement paste and aggregate are large, heating causes microstresses and microcracking that can disrupt the concrete microstructure. Observations of thermal expansion are complicated by various extraneous effects that accompany the temperature change (e.g., additional volume changes caused by changes in moisture content, chemical reactions leading to dehydration and conversion, and creep and microcracking resulting from non-uniform thermal stresses).

2.2.3.1 THERMAL EXPANSION OF HARDEND CEMENT PASTE

Figure 2.9 presents data on the change of length of hardened Portland cement paste at elevated temperature. Initially the hardened cement paste expands on heating up to approximately 150˚C, the maximum expansion being on the order of 0.2%. Expansion ceases between 150 and 300˚C and then between 300 and 800˚C the hardened cement paste shrinks with the shrinkage being 1.6 to 2.2% at 800˚C, [22].

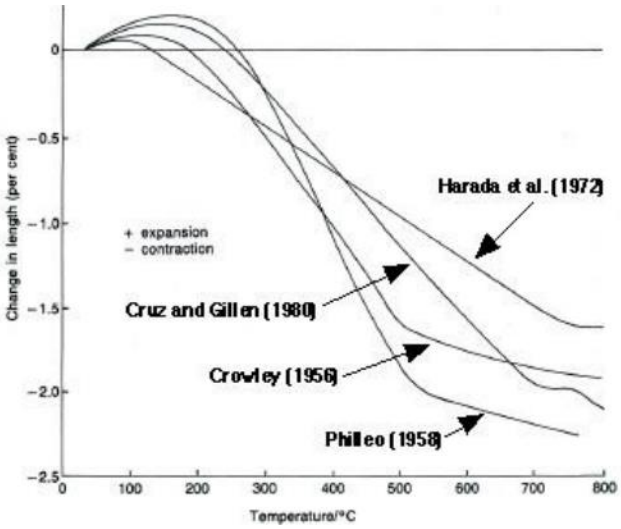

Figure 2.9: Length change of Portland cement paste specimens at elevated temperature (Z.P. Bazant and M.F. Kaplan, 1996).

The initial expansion has been attributed to kinetic molecular movements in the cement paste plus swelling pressures caused by a decrease in capillary tension of water as the temperature rises. Up to about 300˚C thermal shrinkage and thermal expansion both occur to produce a net expansion of the cement paste and at higher temperatures thermal shrinkage exceeds thermal expansion. Shrinkage of the cement paste results from loss of evaporable and chemically-combined water, [22].

2.2.3.2 THERMAL EXPANSION OF AGGREGATES

Aggregates generally constitutes a major proportion of the mix, it primarily influences the resultant coefficient of thermal expansion. Selection of an aggregate with a low coefficient of thermal expansion may help in crack prevention in mass concrete.

The main factor affecting the coefficient of thermal expansion of aggregate materials is the percentage by weight of silica present in the aggregate. Aggregates with little or no silica (e.g., limestone) have the lowest coefficients of thermal expansion. Processed lightweight aggregates (e.g., expanded slag, shale, or clay) have lower coefficients of thermal expansion than naturally-occurring rocks.

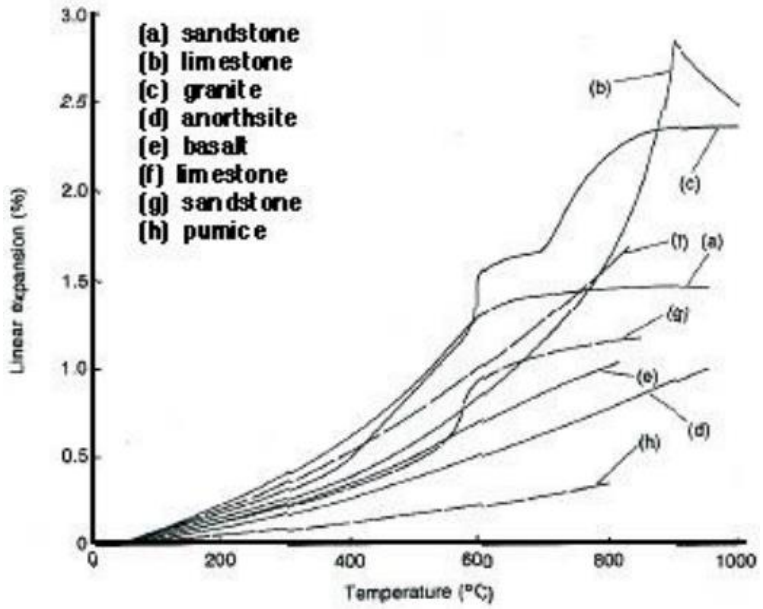

Figure 2.10: Linear thermal expansion of various rocks with temperature (Z.P. Bazant and M.F. Kaplan, 1996).

2.2.3.3 THERMAL EXPANSION OF CONCRETE

The resultant coefficient of thermal expansion for concrete is dominated by the aggregate material; however, the resulting coefficient tends to be somewhat higher due to the larger thermal expansion coefficient of the hardened cement paste, and will increase in proportion to the cement content. It has been indicated that up to 700˚C the concrete expansion is very similar to that for the aggregate used in the concrete. The values of the coefficient for concretes range from $\sim 2.2\ x\ 10^{-6}$ to $3.9\ x\ 10^{-6}$per °C with $3.1\ x\ 10^{-6}$per °C being a typical value. The coefficient of thermal expansion of hardened cement paste and concrete tend to initially increase slightly with age due to a decrease in internal relative humidity and then decrease slowly. The coefficient is influenced by the moisture condition (applies to paste component) and has minimum values for the two extremes: dry and saturated.

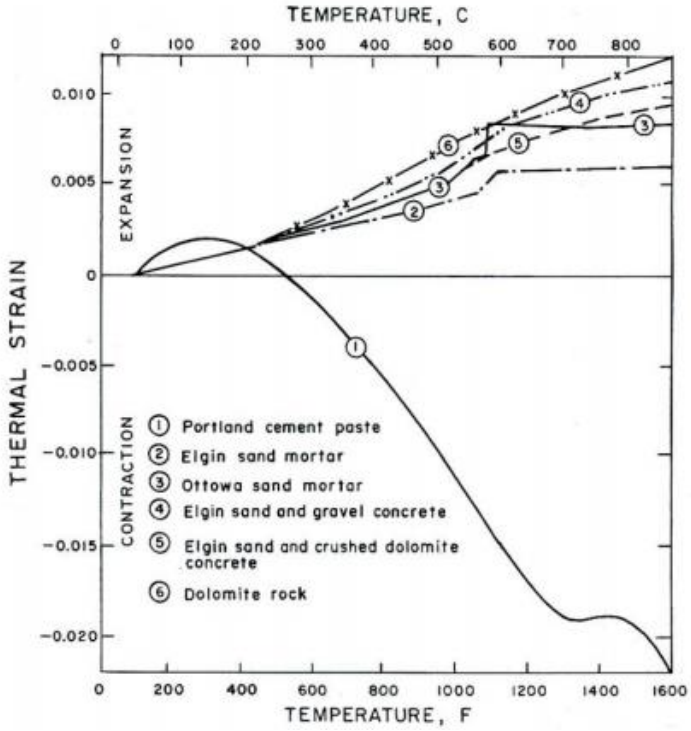

Figure 2.11: Thermal strain of Portland cement, mortar, and concrete during heating (C.R. Cruz and M. Gillen, 1980).

Figure 2.11 presents a comparison of thermal strain results for Portland cement paste, mortars, and concretes for temperatures up to 871˚C. The coefficient of linear expansion increases with increasing temperature due to the aggregate expansion dominating over contraction of the cement paste,

however, the effects of specimen moisture condition at test initiation (i.e., the number of thermal cycles that have been applied to the specimen) also has to be taken into consideration in determining the net specimen length change with temperature, [23].

Lightweight aggregate concretes (e.g., pumice and expanded shale aggregates) may shrink at temperatures greater than 300˚C. Tests of sealed concrete indicate that under thermal cycling (20 to 149 to 20˚C) permanent expansive set occurs after one cycle and the permanent expansion increases with increasing number of cycles, but at a decreasing rate. Also the coefficient decreased as the number of cycles increased and specimens permitted to dry after initial heating showed less expansion during subsequent thermal cycles.

Results indicate an almost monotonic increase in thermal expansion coefficient for the limestone concrete until decarbonation ($CaCO_3 \rightarrow CaO + CO_2$) leads to a decrease in the coefficient. The thermal expansion of the siliceous concrete is greater than that for the limestone concrete. Basalt, due to its fine crystalline structure, exhibits a lower expansion than the siliceous concrete. The presence of load reduces the thermal expansion as noted in Figure 2.12.

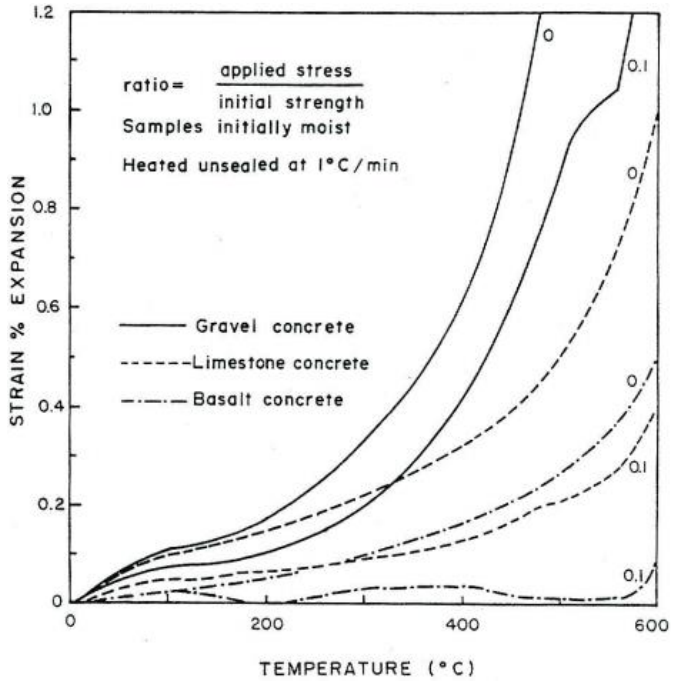

Figure 2.12: Variation of thermal strain with temperature and load for Portland cement concretes: 0 = no load, 0.1 = load corresponding to 10% f_c' (Sullivan et al., 1981).

According to Mindeguia et al. (2013), Figure 2.13 shows the thermal expansion of concretes curves of almost all the studied in the longitudinal direction of the sample. Except for the B40SC, all concretes present a nearly linear thermal expansion up to 570°C (coefficient of thermal expansion between 1 X 10^{-5} and 1.5 X 10^{-5} K^{-1}). Above this temperature, the thermal expansion of concrete suddenly increases. This may correspond to the transformation of quartz (which is accompanied by a strong swelling of the mineral), which is potentially present in the sand. The B40SC has the same behaviour as other concretes up to around 370°C.

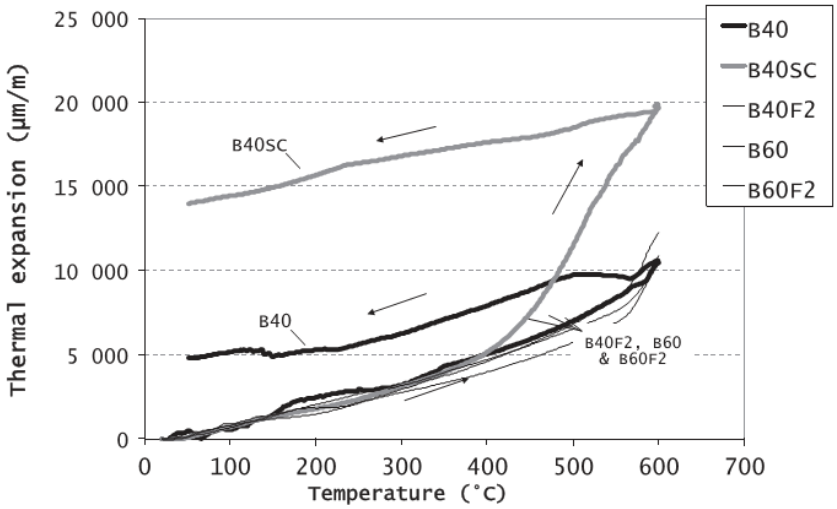

Figure 2.13: Thermal expansion curves of the studied concretes. Strain during cooling period has been measured for the B40 and the B40SC (Mindeguia et al., 2013).

Above this temperature, its thermal expansion heavily increases. At 600°C, the thermal expansion of the B40SC is twice higher than for other concretes. This behaviour is probably due to the presence of siliceous aggregates in the B40SC formula (flint rocks in particular). Indeed, this mineral is characterized by a high thermal expansion coefficient (Bazant & Kaplan, 1996) and by a possible breakdown of the aggregate by cleavage when subjected to temperatures higher than 110°C. High thermal expansion and the instability of flint aggregates also induced, after cooling, residual thermal strain about three times higher than for other concretes (Figure 2.13). Visually, this behaviour leads to a very significant cracking of the B40SC samples after the heating cycle. These observations are almost similar to the results presented in paragraph 2.2.2, which show a strong increase in the permeability of the B40SC between 300 and 400°C, due to the generation of many cracks, (Figure 2.7), (Mindeguia et al., 2013).

2.2.4 THERMAL CONDUCTIVITY

Thermal conductivity gives the heat flux transmitted through a unit area of a material under a unit temperature gradient (i.e., ability to conduct heat). For prestressed concrete pressure vessels, concrete with high thermal conductivity is generally desirable so thermal gradient through the thickness will be minimal. At normal temperatures the thermal conductivity of concrete depends primarily on the thermal conductivity of the aggregate and the moisture content at the time of heating (e.g., increase in aggregate-to-cement ratio and decrease in water-cement ratio tends to increase concrete conductivity).

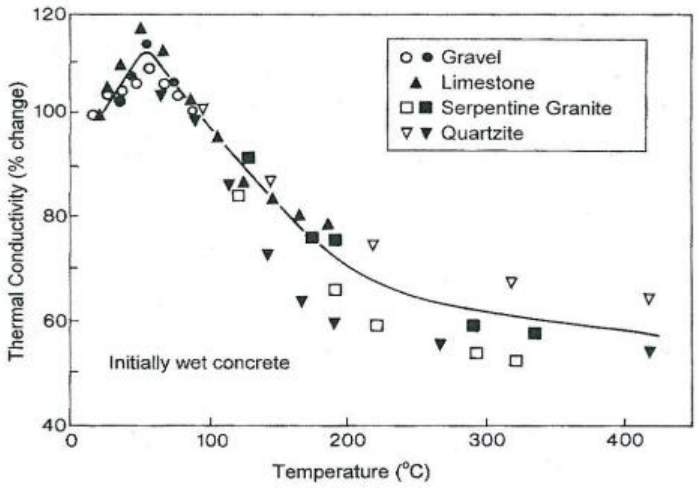

Figure 2.14: Effect of temperature on thermal conductivity of initially saturated concrete (Blundell et al., 1976).

Important factors influencing concrete thermal conductivity are the hardened cement paste, the pore volume and distribution, and the water content while age does not appear to have effects at high temperatures the thermal conductivity increases slightly, but decreases as it approaches 100°C. Up to 300°C to 400°C, the thermal conductivity decreases further, and as the temperature increases beyond 300°C increasing cracking develops. Figure 2.14 presents the effect of temperature on thermal conductivity of an initially saturated concrete, [25].

Although thermal conductivity of concrete depends on all its constituents, it is largely determined by the aggregate type since it makes up 60 to 80% the concrete volume. Lightweight aggregates have lower thermal conductivities due to their porosity. Because the conductivity of water is approximately half that of cement paste, the lower the mix-water content, the higher the conductivity of the hardened concrete.

As shown in Figure 2.15, thermal conductivity of concrete made with highly crystalline aggregate decrease with temperature up to 1000°C, while those of concrete made with amorphous aggregate are essentially constant.

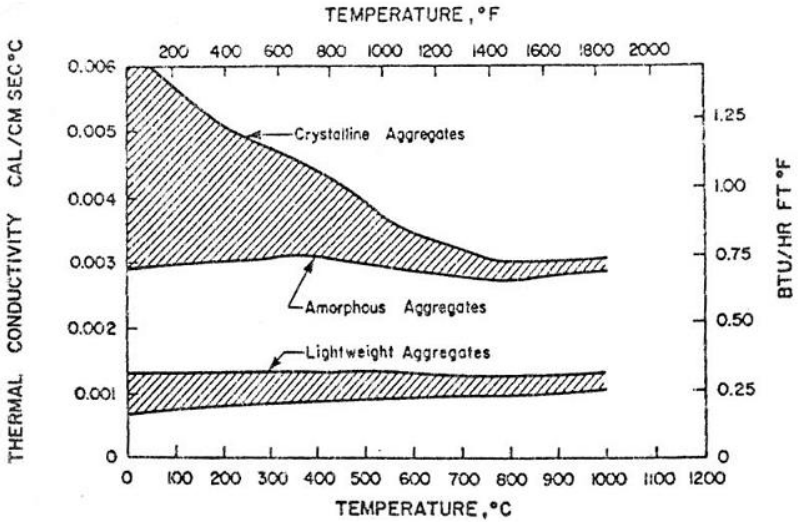

Figure 2.15: Thermal conductivity of different type of concretes (Harmathy and Allen, 1973).

Figure 2.16a and b presents thermal conductivity of concrete as a function of density and moisture content and the variation of thermal conductivity as a function of temperature for several mortars and concretes, respectively. The thermal conductivity on cooling depends on the maximum reached temperature, and after cooling to ambient conductivity falls to a level still below the original unheated level.

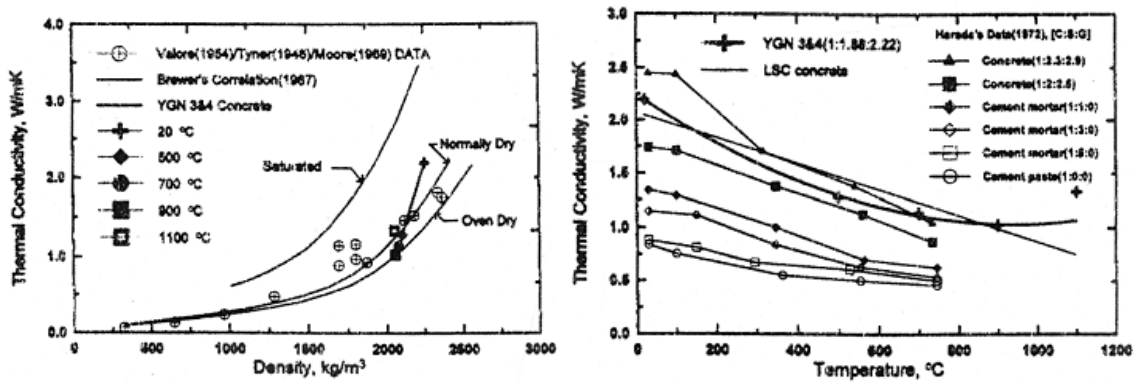

(a) (b)

Figure 2.16: Thermal conductivity as a function of density and moisture content (a), Thermal conductivity as a function of temperature (b), (K.-Y. Shin et al., 2002).

Results presented in the literature indicate that the major factors influencing concrete thermal conductivity are moisture content, aggregate type, hardened cement paste, and pore volume and distribution. The conductivity varies linearly with moisture content. As the conductivity of the aggregate material increases, the concrete thermal conductivity increases. Concretes with lower cement paste content can be expected to have a lower conductivity than lean concrete mixtures.

2.2.5 THERMAL DIFFUSIVITY

Thermal diffusivity is a measure of the rate at which heat will diffuse through a material in all directions due to a temperature change and is thus an index of the facility with which the material will transfer heat due to a temperature change. The diffusivity of concrete varies from 0.3 to 0.8 mm^2/s. It is described as follows:

$$D = \lambda/\rho C_p \tag{2.1}$$

where, D is the diffusivity (m^2/s), λ = thermal conductivity (W/mK), C_p = specific heat of concrete material (J/KgK) and ρ = density of concrete (Kg/m^3).

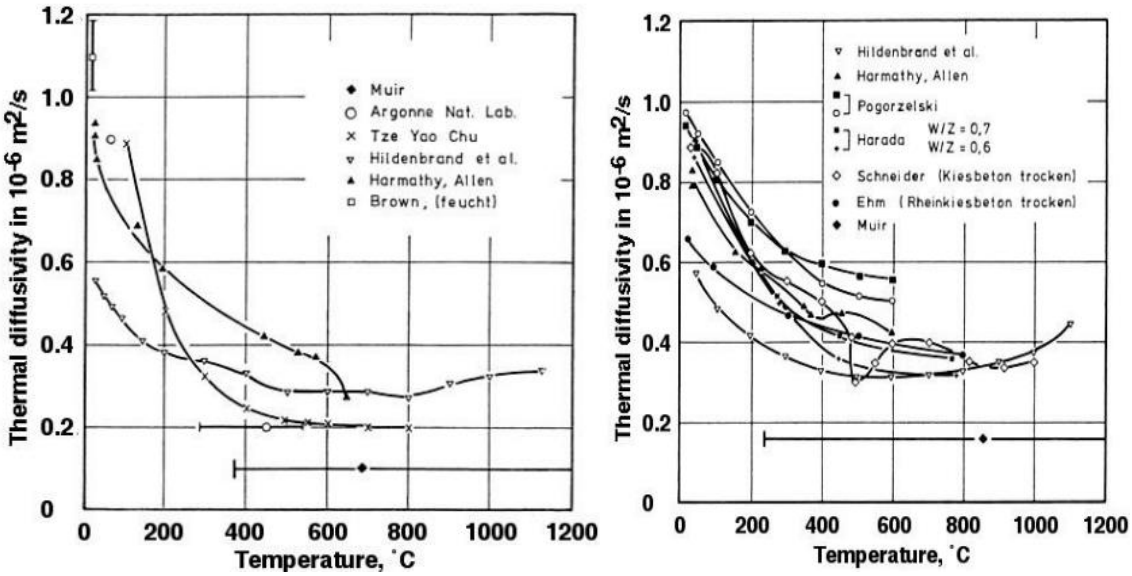

Figure 2.17: Thermal diffusivity of limestone aggregate and siliceous aggregate concrete respectively (Schneider, 1982).

Thermal diffusivity is important in nuclear power plant structures such as prestressed concrete pressure vessels for the same reasons cited for thermal conductivity. Concrete thermal diffusivity is

determined by the thermal properties of its constituents. At normal temperatures the diffusivity of concrete is mainly governed by the diffusivity of the aggregate. Aggregates with increasing values of thermal diffusivity include basalt, rhyolite, granite, limestone, dolerite, and quartzite. Factors that affect thermal conductivity generally have the same influence on thermal diffusivity.

Figure 2.18, presents thermal diffusivity results for three normal weight concretes and thirteen lightweight concretes. As noted in the Figure 2.18, at about 600˚C the thermal diffusivity of all concretes investigated becomes approximately 0.0033 cm^2/sec, [26].

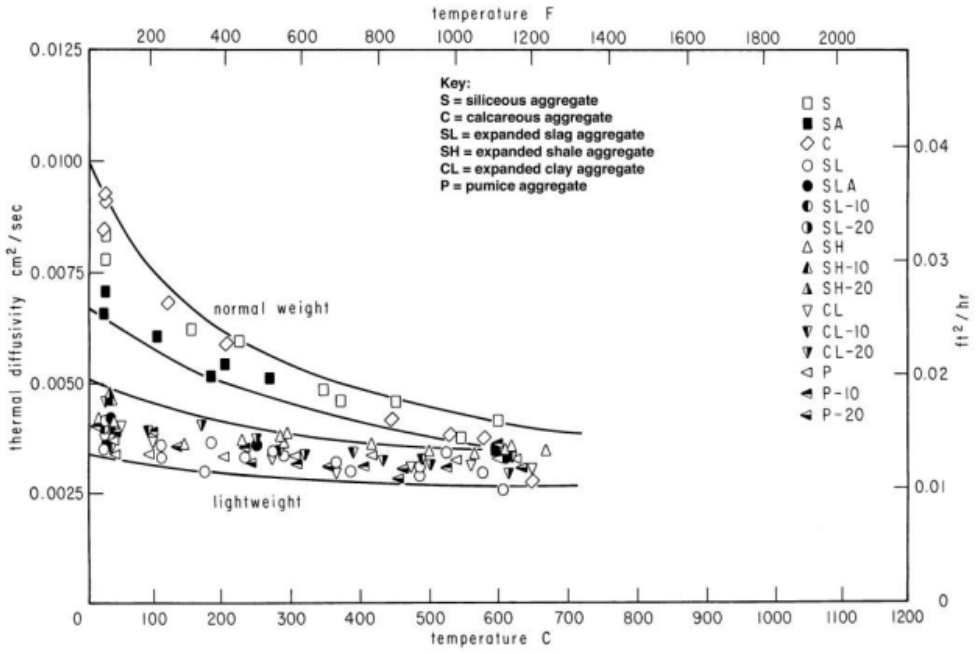

Figure 2.18: Thermal diffusivity of normal and lightweight concretes (Harmathy and Allen, 1973).

2.2.6 SPECIFIC HEAT

The thermal or heat capacity of a material, or specific heat, is the amount of heat per unit mass required to change the temperature of the material by one degree.

$$c_p = \left(\frac{\partial H}{\partial T_p}\right) \tag{2.2}$$

where, H is enthalpy, T is temperature, and p is pressure. The specific heat of ordinary concrete at room temperature ranges from 0.5 to 1.13 kJ $kg^{-1}K^{-1}$ while specific heat of hardened cement paste ranges from 0.63 to 1.72 kJ $kg^{-1}K^{-1}$. At room temperature aggregate type, mix proportions, and age

do not have a great effect on specific heat of concrete. However, as the moisture content in the concrete increases, the specific heat capacity increases at lower temperatures. The specific heat of aggregate can be calculated from its mineralogical content and the specific heat of concrete determined based on its relative proportions.

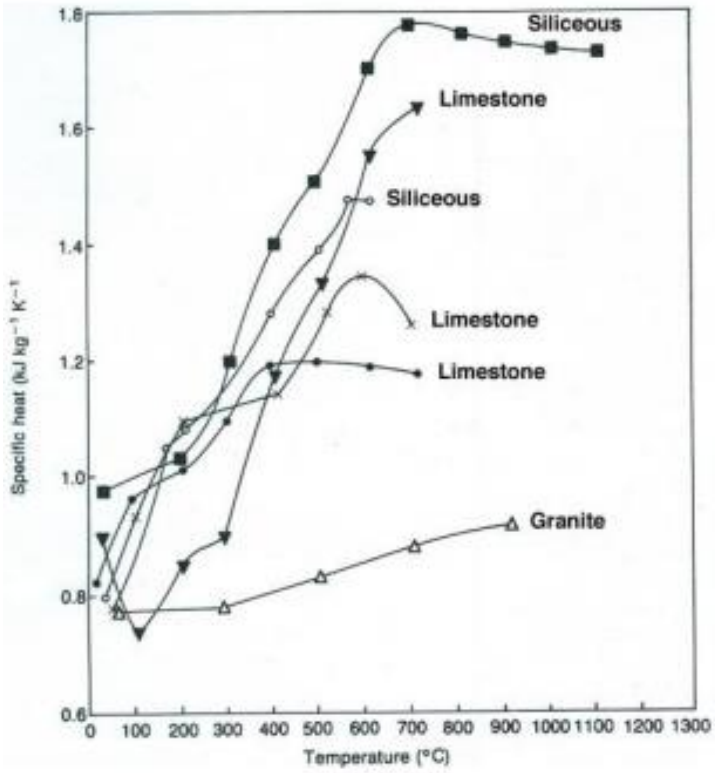

Figure 2.19: Specific heats of various concretes (Bazant and Kaplan, 1996).

Concrete specific heat increases with an increase in temperature. At elevated temperature the specific heat value is sensitive to the various transformations that take place in concrete. This includes the vaporization of free water at about 100˚C, the dissociation of $Ca(OH)_2$ at about 400˚C to 500˚C and the $\alpha - \beta$ quartz transformation in some aggregates. Heating of initially saturated concrete causes a rapid but temporary rise in the specific heat at about 90˚C due to the rapid release of latent heat of vaporization, [22].

Figure 2.20 presents specific heat as a function of temperature for a basaltic aggregate concrete (37.9 MPa, Type V cement) used in construction of Yonggwang Nuclear power plant units 3 and 4 in Korea. Results show that the specific heat increased to 500˚C, decreased from 700˚ to 900˚C, and then increased at temperatures above 900˚C, [28].

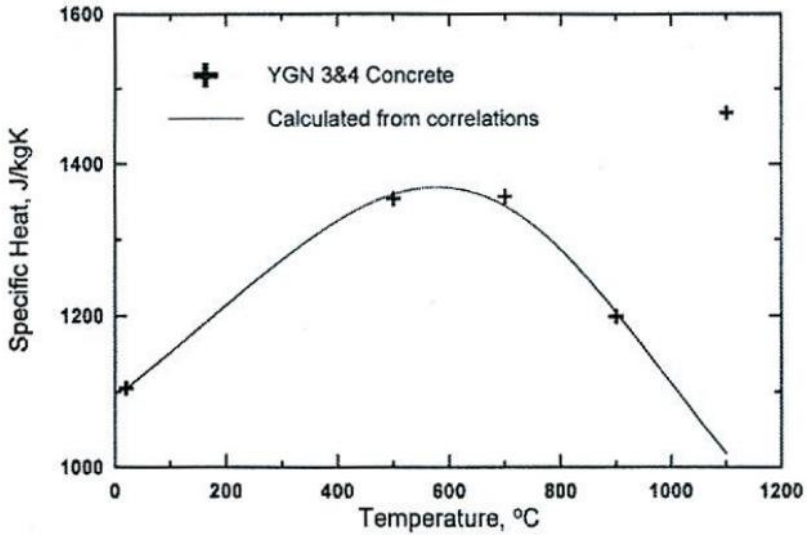

Figure 2.20: Specific heat of a Korean nuclear power plant concrete (Shin et al., 2002).

2.2.7 THERMAL INERTIA

Materials with low thermal inertia rapidly increase the surface temperatures.

$$a = K * \rho * C_p \tag{2.3}$$

where, K is the thermal conductivity, ρ is density of concrete, C_p specific heat of concrete material and $\rho * C_p$ governs the energy absorbed by walls of a room during a fire.

2.3 MECHANICAL PROPERTIES OF CONCRETE

Temperature rise has a great influence on the mechanical properties of concrete, causing a remarkable deterioration of concrete structural behavior during heating. Moreover, durability and serviceability are remarkably affected by high temperature due to physical deterioration processes which may lead to severe cracking, structural weakening and also to collapse. Thus, in order to reduce the harmful effects of high temperature, some preventative measures such as choosing right materials should be introduced. Deterioration in mechanical properties of concrete upon heating may be attributed to three material factors:

•physico-chemical changes in the cement paste;

•physico-chemical changes in the aggregate;

•thermal incompatibility between aggregate and cement paste.

However, all Portland-cement-based concretes lose their load-bearing capacity at temperatures above 550–600°C. At lower temperatures (i.e. that of the bulk of the concrete member during fire) the deterioration in mechanical properties during heating can be reduced by judicious concrete mix design whereby thermally stable aggregates of low thermal expansion are employed, and cement blends are selected that produce a low CaO/SiO_2 ratio, but not too low a permeability (also important to reduce the risk of spalling). Mechanical properties of concrete deal with strain, compressive strength, tensile strength and modulus of elasticity during heating.

The deformation of concrete is usually described by assuming that the total strain (ε) consists of four components being, (Buchanan, 2001):

$$\varepsilon = \varepsilon_{th}(T) + \varepsilon_{\sigma}(\sigma, T) + \varepsilon_{cr}(\sigma, T, t) + \varepsilon_{tr}(\sigma, T) \quad (2.4)$$

where, $\varepsilon_{th}(T)$ is thermal strain being a function of only temperature, $\varepsilon_{\sigma}(\sigma, T)$ is the stress related strain, being a function of both the applied stress σ and the temperature, $\varepsilon_{tr}(\sigma, T, t)$ is the creep strain, being also a function of time, t, and $\varepsilon_{tr}(\sigma, T)$ is the transient strain, being a function of both the applied stress and the temperature. Before explaining the changes in strength of concrete as a function of increasing temperature, two positive aspects of heated concrete need pointing out.

Transient creep

Concrete does not break up when heated above 100°C, because the differential strain resulting from the expansion of the aggregate and shrinkage of the cement paste is far too large to be accommodated by elastic strains. Because, transient creep (strictly, it should be called load-induced thermal strain, LITS) develops during first heating (and not during cooling) under load. LITS is unique to concrete amongst structural materials. Above 100°C it is essentially a function of temperature and not of time.

The existence of a master LITS for Portland-cement-based concrete in general for temperatures up to 450°C, irrespective of the type of aggregate or cement blend used (Fig. 2.21). LITS is much larger than the elastic strain (compare Figures 2.21 and 2.22 for 20% stress level), and contributes to a significant relaxation and redistribution of thermal stresses in heated concrete structures. Any structural analysis of heated concrete that ignores LITS will, therefore, be wholly inappropriate and will yield erroneous results, particularly for columns exposed to fire (Khoury, 2000).

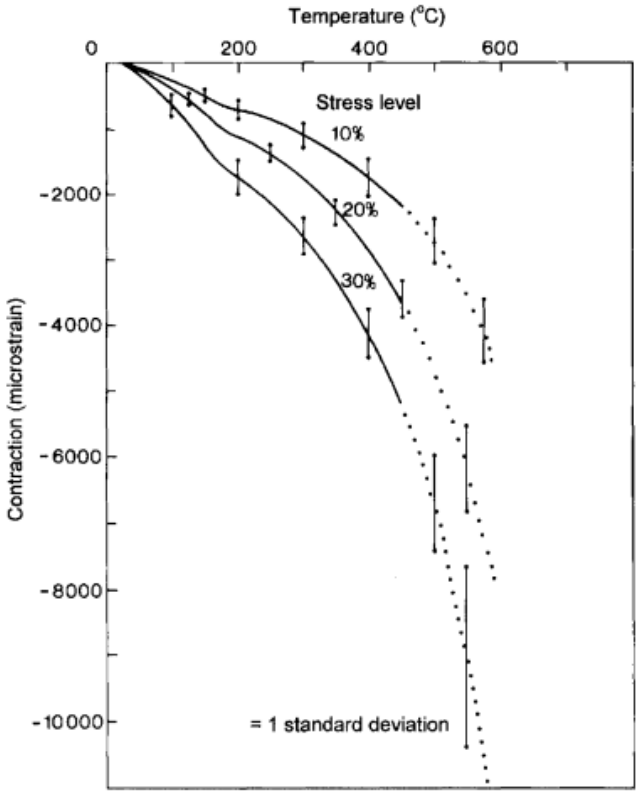

Figure 2.21: Load-induced thermal strains (or transient creep) of concrete during heating at 1°C min^{-1} to 600°C under compressive loads up to 30% of the unheated strength (Khoury, 2000).

Loading during heating

Another positive aspect of concrete at high temperature is the beneficial influence of loading which places the material into compression, compacts the concrete during heating and inhibits the development of cracks. An example of this phenomenon is given in Figure 2.22, comparing the stress–strain relation at levels of high temperature 20°C –700°C for concrete heated without load and under 20% compressive load. The influence of temperature can be markedly diminished. Both compressive strength and elastic modulus reduce far less with increase in temperature for the concrete heated under load. However, for concrete heated without load, tests consistently show the modulus of elasticity to reduce with increase in temperature by a larger proportion of the initial value than the compressive strength (Khoury, 2000).

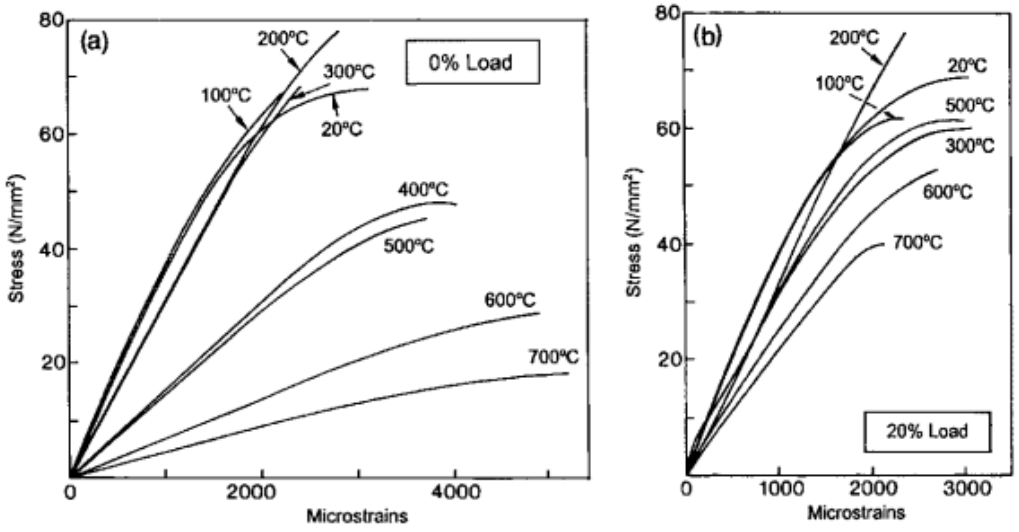

Figure 2.22: Effect of temperature and load level during heating-up upon the residual stress-strain relation in uniaxial compression tests conducted at constant stress rate (Khoury, 2000).

2.3.1 COMPRESSIVE STRENGTH

The behavior of concrete in compression is represented by means of a temperature-dependent stress-strain diagram, which depends on peak stress $f_{c,\theta}$ deformation at the peak stress $\varepsilon_{1,\theta}$ and ultimate strain $\varepsilon_{cu,\theta}$.

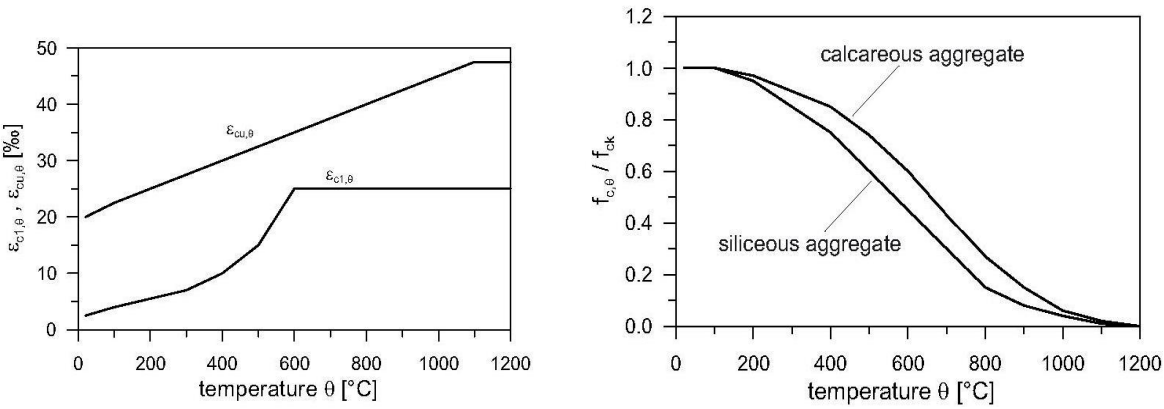

Figure 2.23: Relation between concrete strength and temperature.

The variation of these characteristics depends only upon the type of aggregate in the concrete (siliceous or calcareous). The residual strength for dense concrete after cooling varies depending on the maximum temperature attained mixes proportions and conditions of loading during heating.

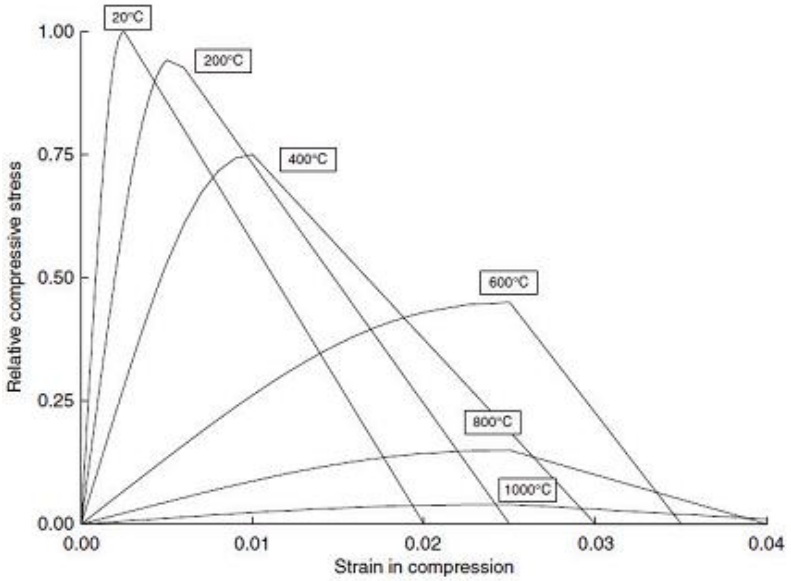

Figure 2.24: Typical temperature influence on the (normalized or relative) stress-strain relationship of concrete (normal weight, siliceous aggregates).

For temperatures up to 300°C, the residual strength of structural concrete is usually not severely reduced. The reduction is also determined by factors such as age which result in a high strength prior to the fire which may be in excess of design requirements. Temperatures greater than 500°C can reduce the compressive strength of structural concrete to only a small fraction of its original value, and such concrete is unlikely to possess any useful structural strength as it may contain a considerable amount of calcium oxide (CaO) which expands under moisture attack. Above 100°C the physically combined water is released from concrete. During the process the strength is not changed but above 100°C the elastic modulus decreases by about 10-20%. Above 300°C the silicate hydrates decompose and above 500°C the portlandite will be dehydrated, so the compressive strength is reduced slowly below 450-500°C and rapidly above 500°C. At temperatures above 600°C some aggregates begin to convert or to decompose. In general, the strength reduction of the structure is controlled by the fact that a strength reduction due to temperature effects will occur only in the outer 3-5 cm of the concrete, which are exposed to high temperatures. This layer itself, being demolished, forms an insulating layer which prevents a significant damage to the cross-section of the load bearing members. The effect of temperature on the compressive strength of concrete is shown in the following Figure 2.25:

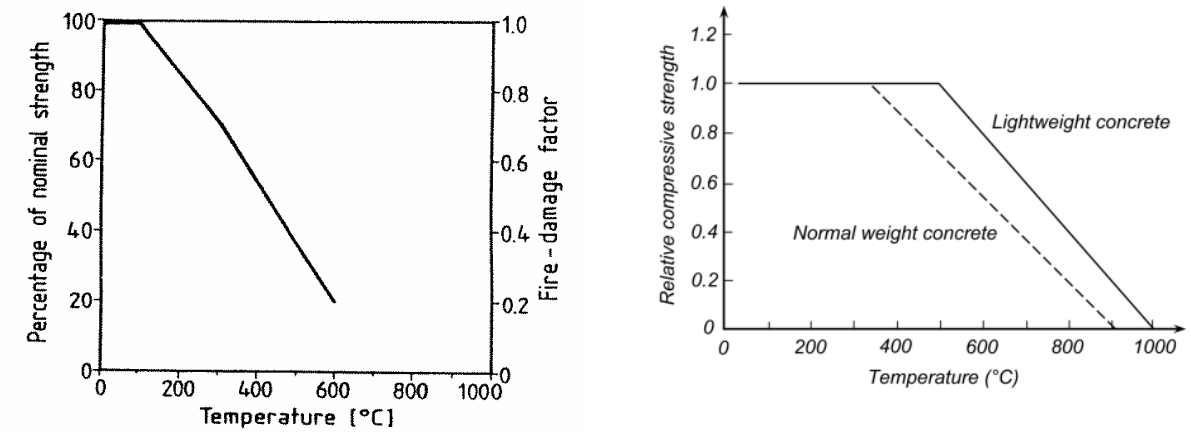

Figure 2.25: relations between percentage of nominal strength and temperature.

Recent research has extended the testing of compressive strength from normal-strength concrete to high-performance concrete (HPC; strengths 60–100 MPa) and even ultra-high performance concrete (UHPC containing steel fibres; strengths 100–300 MPa). The results shown in Figure 2.26 show that the hot strengths of the HPC concretes decline less with increase in temperature than those of the UHPC concrete, but that the reverse is true for the residual strength measured after cooling (possibly because of the steel fibres). The relatively poorer hot performance of the UHPC could be due to its very dense structure, from which moisture escapes less readily. This has two effects: a physical effect due to reduced van der Waals forces as water expands upon heating, and a chemical effect whereby detrimental transformations can take place under hydrothermal conditions.

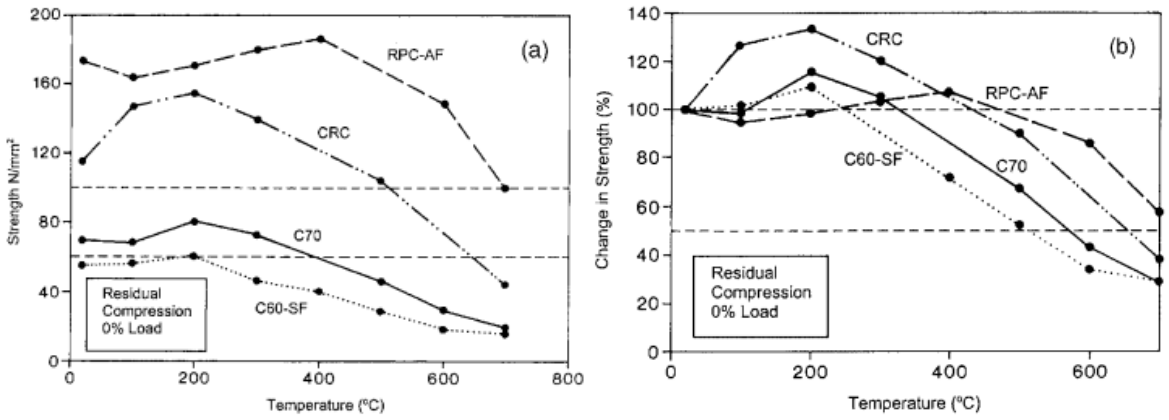

Figure 2.26: Effect of temperature upon the residual compressive strength of two high-performance concretes (C60-SF, C70) and two ultra-high-performance concretes (CRC, RPC-AF) after heat cycling without load at 2°C min^{-1}: (a) actual values; (b) percentage of initial strength at 20°C (Khoury, 2000).

This suggests that the UHPC hot strength loss could have been more pronounced had the specimens been kept for a longer time at appropriate temperatures. Normal-strength concretes and high-performance concretes microstructurally follow similar trends when heated, but ultra-high-performance concrete behaves differently, as evidenced by rate of moisture loss readings taken at constant high temperatures (Khoury, 2000).

2.3.2 TENSILE STRENGTH

The tensile strength of concrete is important because it determines the ability of concrete to face cracking. Direct measurement of concrete tensile strength is seldom made because of difficulties in gripping the specimen to apply loads and in maintain a uniform tensile stress across the section. An indication of concrete tensile strength can be obtained by the splitting-tension and flexure tests. The splitting-tension test is an indirect test for tensile strength of concrete in that a horizontal concrete cylinder is loaded in compression through bearing strips placed along two axial lines that are diametrically opposite on the specimen.

Tensile strength is reduces with increasing temperature, the reduction already taking place at 100°C. The reduction of the characteristic tensile strength of concrete is represented by the coefficient $K_{c,t}(\theta)$ which denotes the ratio between the tensile strength at room temperature and the one at elevated temperatures.

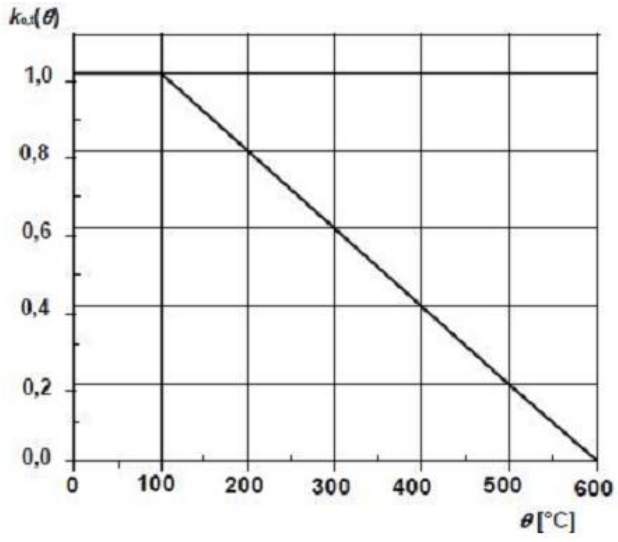

Figure 2.27: Coefficient $K_{c,t}(\theta)$ allowing for decrease of tensile strength $(f_{ck,t})$ of concrete at elevated temperatures (Eurocode EN1992-1-2).

Figure 2.28 show that the residual tensile strengths for both NSC and HSC decreased similarly and almost linearly with increasing temperature. Also, tensile strengths measured by the splitting-tension test were consistently higher than those obtained by the direct-tension test.

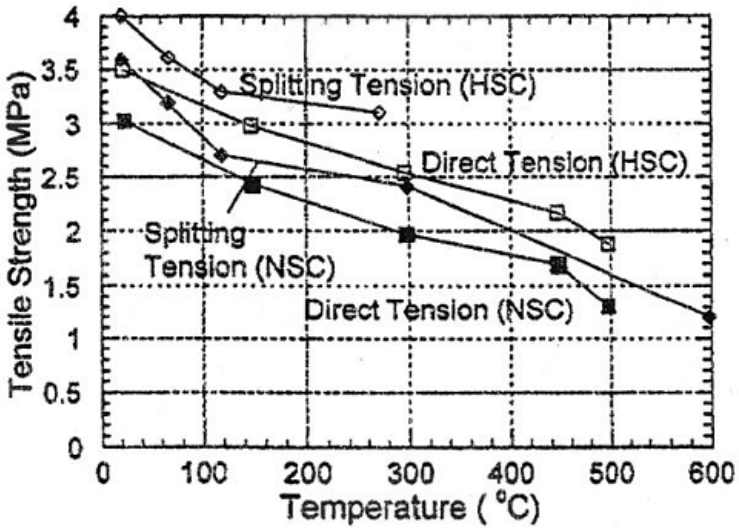

Figure 2.28: Residual tensile strengths of HSC and NSC (Noumowe et al., 1996).

High-Performance Concrete containing silica fume (fc = 60-120 MPa) is more sensitive to high temperature (T = 100-800°C) than ordinary concrete, owing to its denser cementitious matrix, with lower diffusivity, and to the greater role of the aggregate, whose thermal decay is much more harmful in HPC. To evaluate the tensile strength in direct and indirect tension, a special experiment was run in the Politecnico Di Milano, Felicetti and Gambarova, 1998. They tested two highly-siliceous concretes (fc = 72 and 95 MPa) for direct and indirect tension (3-point bending), to investigate their residual mechanical properties after a single thermal cycle at high temperature (T = 105-500°C). In analogy with the tests in compression, there are many factors that influence the results of the tests in traction at high temperature Figure 2.29.

The tensile strengths in direct and indirect tension are shown in Figure 2.29b; it appears that their ratio f_t^*/f_t increases with the temperature of the thermal cycle. Since f_t^* is related to concrete non-linear behavior (softening included), the tendency of (f_t^*/f_t) to grow, beyond 250°C, is indicative of the greater deformability of the concrete, even if the peak strength decreases dramatically. The decay of the tensile strength is shown also by the plot of the ratio f_c/f_t = compressive strength/tensile strength, Figure 2.29b, which increases with the temperature of the thermal cycle (from 16 at 20°C to more than 20 after a cycle at 400°C).

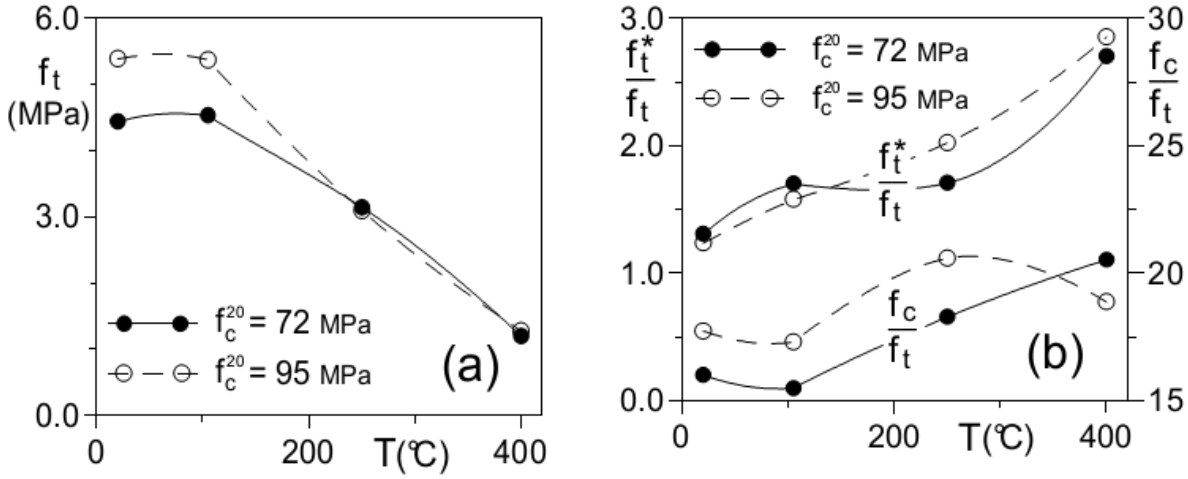

Figure 2.29: Direct tension, notched cylinders: (a) plots of the residual strength; and (b) plots of two strength ratios (f_c/f_t = compressive-to-tensile strength ratio; f_t^*/f_t = indirect-to-direct strength ratio; indirect strength = 3-point bending); Felicetti and Gambarova, 1998.

Summing up, the tensile strength tends to decrease more than the compressive strength after a cycle at high temperature, and this fact should be taken into account in R/C structures, when considering the resistant mechanisms based on the tensile strength, such as bond, bar tension-stiffening, web shear and punching shear (Felicetti and Gambarova, 1998).

From the limited tensile test data available in the literature, the aggregate type and mixture proportions have a significant effect on the tensile strength; the decrease in tensile strength of calcareous aggregate concrete is twice as high as that of siliceous aggregate concrete at 500°C; concretes with lower cement content have lower reduction in tensile strength than those with higher cement content; the heating rate has minimal effect on tensile strength at high temperature; and the residual tensile strength is somewhat lower than the tensile strength measured at elevated temperature.

2.3.3 POISSON'S RATIO

Poisson ratio is needed for conducting structural analyses of flat slabs, arch dams, tunnels, tanks, and other statically indeterminate members. At normal ambient conditions Poisson's ratio for concrete can vary from 0.11 to 0.32, but is generally in the range from 0.15 to 0.20. Under uniaxial compression loading, the beginning of matrix cracking occurs at the stress level where there is an apparent increase in the Poisson ratio value. At ambient temperature there appears to be no consistent relationship between Poisson ratio and concrete characteristics such as water-cement

ratio, curing age, and aggregate gradation, but it is generally lower in high-strength concrete and higher for saturated concrete and for dynamically-loaded concrete.

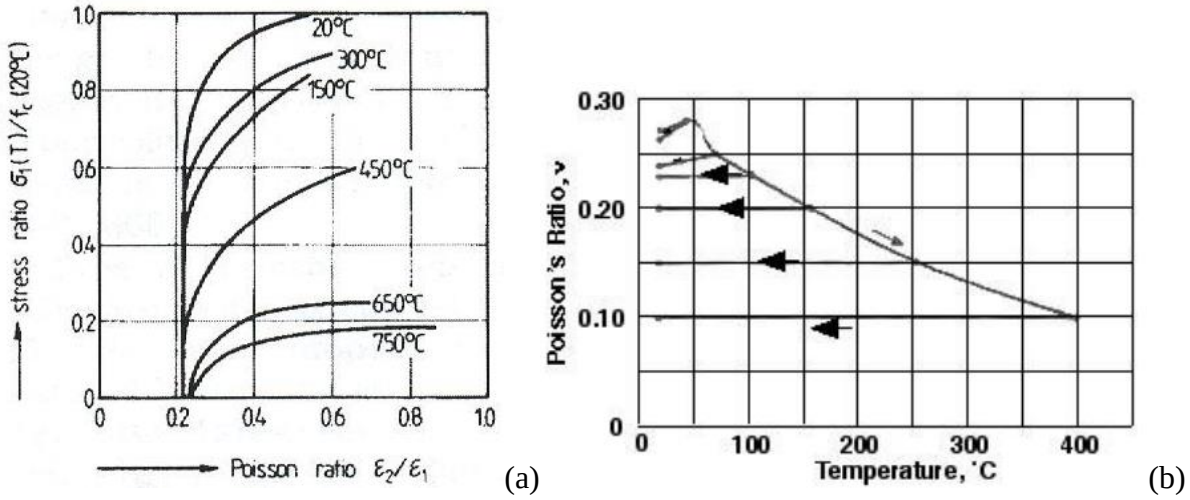

Figure 2.30: (a) Poisson ratio for uniaxially loaded concrete at high temperature (Ehm, 1985).

(b) Poisson's ratio as a function of temperature for a quartzite concrete (Marechal, 1972).

At 20˚C the Poisson ratio is constant until the load exceeds about 70% of the ultimate load, while as the temperature increases the deviation of Poisson ratio increases till in some cases it is >0.5. Figure 2.30(b) indicates that the Poisson ratio decreases with increasing temperature from about 0.2 at room temperature to about 0.1 at 400˚C. This drop was attributed to a change in state due to heating that resulted in water desorption (e.g., weakening of the microstructure caused by breakage of bonds due to heating and by microcracking). When the specimen was permitted to cool after a given change in state the variation of Poisson ratio with temperature was slight and nil when the evaporable water had been removed. In general, Poisson ratio values obtained after drying are less than before drying. In measurements on sealed cylinders the change in Poisson ratio with increasing temperature was small (e.g., 0.2 to 0.18). When the concrete is under a confining pressure as it would be in many nuclear power plant concrete structures, it has been hypothesized that Poisson ratio at elevated temperature would be about the same as at room temperature.

Figure 2.31 presents Poisson ratio results as a function of temperature for the different aggregate materials and the two nominal concrete compressive strengths. The Poisson's ratio values generally ranged from 0.11 to 0.25. Although results obtained at higher temperature were somewhat erratic and a general trend was not apparent, results did show lower Poisson's ratio values at room temperature for the higher strength concretes.

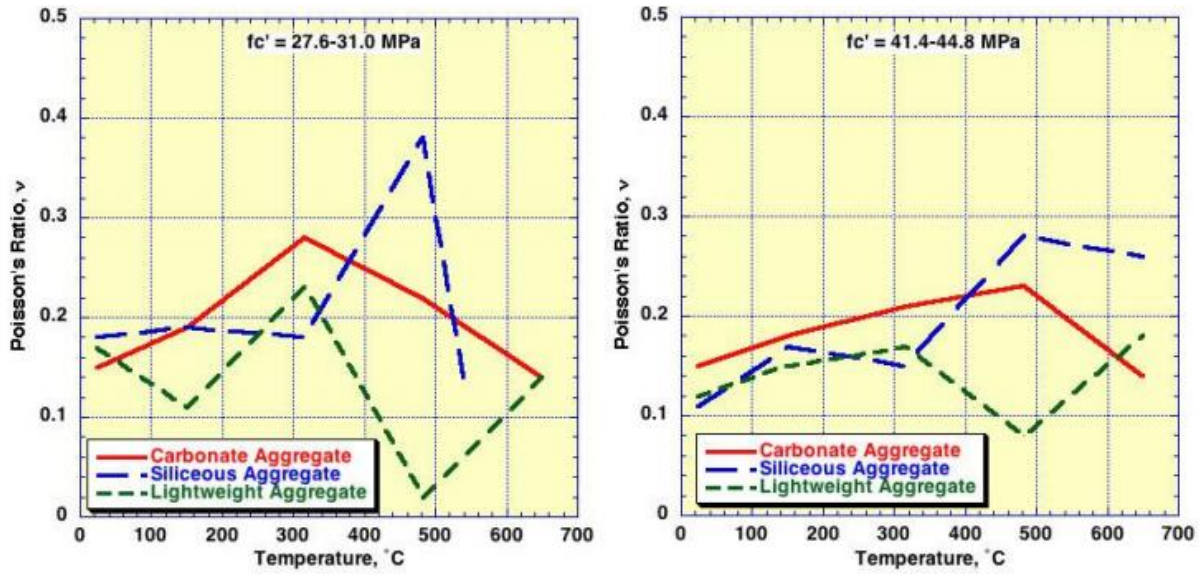

Figure 2.31: Effect of aggregate type and concrete strength on Poisson ratio (Cruz, 1966).

Elsewhere Poisson's ratio for high strength concrete has been reported to range from 0.11 at 20°C to 0.25 at 400°C, while above 400°C it increased [34]. Additional data for high strength concrete indicated that when the stress did not exceed 50% of peak value, the Poisson's ratio decreased with an increase in temperature [35].

2.3.4 MODULUS OF ELASTICITY

Studies carried out and assessed by show that modulus of elasticity depends mainly on the compressive strength of the concrete. Therefore, Young modulus is affected by the same factors as the compressive strength, like type of cement, water cement ratio, type of aggregate, loading conditions during the thermal cycle, maximum temperature reached during heating. However, besides the last parameter, only the type of aggregate and to a lesser extent the loading conditions during heating process have a sizeable influence on the elastic modulus, which is more temperature-sensitive than the compressive strength (both at high temperature and after cooling), because concrete stiffness is directly affected by thermal cracking.

As seen in Figure 2.32 siliceous aggregates (like basalt and quartzite, $E_C{}^T/E_C{}^{20}$ = 0.4-0.5 at 500°C), while light-weight aggregates are close to or better than calcareous aggregates (at 500°C, $E_C{}^T/E_C{}^{20}$ up to 0.70 - 0.75 for expanded clay).

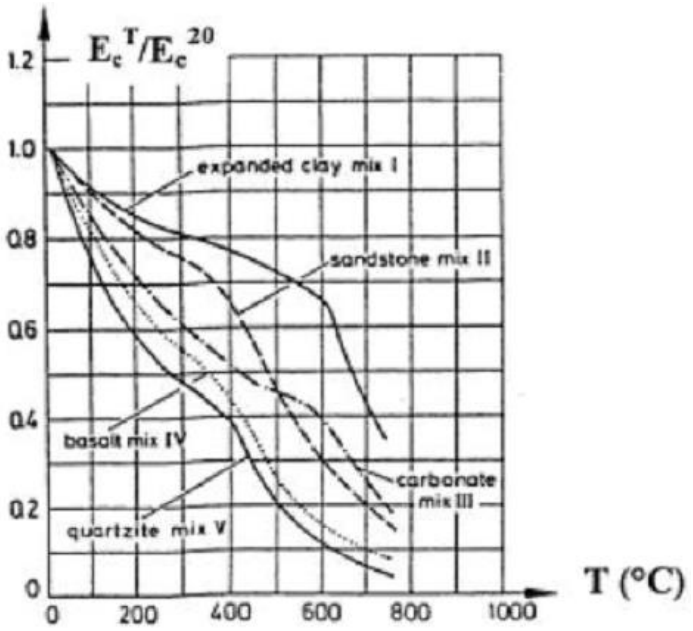

Figure 2.32: Elastic moduli of similar mixes containing different type of aggregate (du Bèton, 2008).

Figure 2.33 presents a summary of data assembled under this activity for sealed and unsealed specimens that were either tested at temperature (hot) or after cooling (cold). Generally the modulus of elasticity decreased with increasing temperature for all types of testing, further decreases in modulus occurred with an increase in number of thermal cycles and exposure time, and sealed specimens were more sensitive to these factors with decrease in modulus of elasticity becoming fairly significant at temperatures above 150˚C.

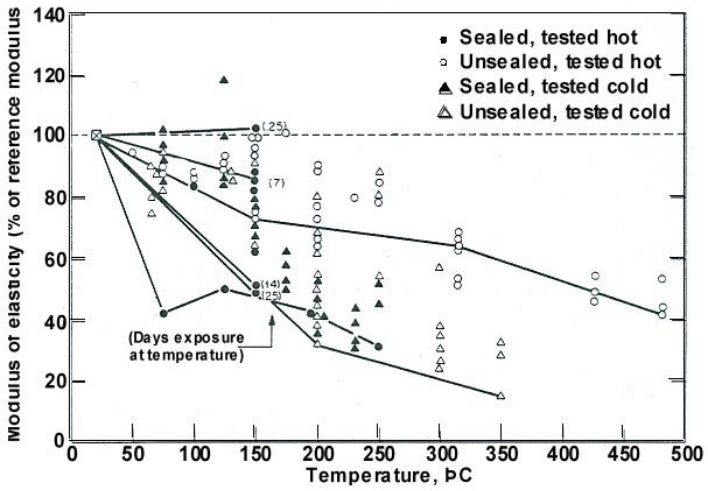

Figure 2.33: Compilation of data on modulus of elasticity vs temperature (Nanstad, 1976).

2.4 HIGH STRENGTH CONCRETE

Early research on the effects of elevated temperature on concrete properties and performance in large measure was in support of the development of prestressed concrete pressure vessels for nuclear power plant designs, tunnels and bridges. Starting in the 1980s concretes with increasing compressive strengths started to become commercially available and primarily utilized in the construction of high-rise buildings. Use of HSC offered economic advantages because concrete column size could be reduced, thus permitting lighter structures and more usable space. It also had application in the construction of prestressed girders for bridge construction and other specialized applications in which high performance (e.g., low permeability) is required. Today concretes having compressive strengths up to 140 MPa and above can be produced through use of special fabrication procedures.

HSC is produced primarily through use of a relatively low water/cementitious ratio and incorporates silica fume. Because this leads to a reduced permeability with respect to normal weight concretes, there has been a concern that the HSC may be more susceptible to explosive spalling under fire conditions due to the buildup of pore pressure in the cement paste. Because one of the primary applications of HSC has been general civil engineering building structures, most recent research on elevated-temperature effects on concrete has shifted to HSC in fire conditions. Because some of the newer generation reactor designs may incorporate HSC, or high-performance concretes, a limited discussion is provided below.

A comprehensive review of the experimental and analytical studies on the performance of concrete when exposed to short-term, rapid heating, such as occurs in fires, has been prepared. Although the report does present some information on normal-strength concretes (NSC), the emphasis of the report is on concretes having initial high compressive strengths. Based on several authors basic conclusions provided in the following:

• The material properties of HSC vary with temperature differently than those of NSC. The differences are more pronounced in the temperature range from 25°C to about 400°C, where higher strength concretes have higher rates of strength loss than lower strength concretes. These differences become less significant at temperatures above 400°C. Compressive strengths of HSC at 800°C decrease to about 30% of the original room temperature strengths.

• For unstressed and stressed tests of HSC, the variations of compressive strength with temperature are characterized by three stages: (1) an initial stage of strength loss (25°C to approximately 100°C), (2) a stage of stabilized strength and recovery (100°C to approximately 400°C), and (3) a stage above

400°C characterized by a monotonic decrease in strength with increase in temperature. HSC has a higher rate of compressive strength loss in the temperature range between 100°C and 400°C compared to NSC.

• For unstressed residual strength tests of HSC, the compressive strength vs temperature relationships are characterized by two stages: (1) an initial stage of minor strength gain or loss (25°C to 200°C), and (2) a stage above 200°C in which the strength decreases with increasing temperature.

• The strength recovery stage of higher strength concretes occurs at higher temperatures than lower strength concretes. Compressive strengths of HSC obtained from the stressed tests are higher than those obtained from the unstressed and unstressed residual strength tests in the temperature range of 25°C to 400°C. The application of preload reduces strength loss in this range of temperature. Varying the preload levels from 25 to 55% of the original compressive strength, however, does not cause significant difference in compressive strengths of HSC at elevated temperatures.

2.5 SPALLING DUE TO HIGH TEMPERATURE

Spalling is the violent or non-violent breaking off of layers or pieces of concrete from the surface of a structural element when it is exposed to high and more or less rapidly rising temperatures, as experienced in fires with heating rates typically 10–30^{o}C/min^{-1}. Spalling can be grouped into four categories: (a) aggregate spalling; (b) explosive spalling; (c) surface spalling; (d) corner/sloughing-off spalling. The first three occur during the first 20–30 min of the fire and are influenced by the heating rate, while the fourth occurs after 30–60 min influenced by the maximum temperature (Khoury, 2000).

This separation can happen in different ways, as classified by the Institution of Structural Engineers (1975):

• General or destructive spalling: This is a violent form of spalling which occurs at an early stage of heating and may result in extensive damage or complete destruction of the concrete element.

• Local spalling: This consists of sometimes violent surface spalling, aggregate splitting or corner separation. Aggregate spalling is caused by aggregate failure close to the surface and involves small pieces flying off from the surface. This type of spalling does not adversely affect the structural performance, causing only superficial damage.

• Sloughing off: This is a progressive form of breakdown which involves partial separation of material from the concrete element. Corner spalling occurs later, often in the decay stages of the fire. It is characterized by larger corner pieces falling off the concrete due to tensile cracks developing at corners and edges. Due to the late onset of this type of spalling the concrete affected is already considerably weakened from fire exposure and any exposed reinforcement is subjected to much lower temperatures. Thus corner spalling is not thought to have a significant impact on structural fire performance.

Due to the fact that explosive spalling poses the greater threat to structural stability this form will be investigated in more detail. In current design codes like [EC2-EN1992-1-2, 2005], there is not much information about spalling. It is stated that no checks for spalling are necessary if the moisture content of the member is less than 3% (Figure 2.34) or the member is designed for internal exposure and that the tabulated data is used to prescribe generic fire ratings for concrete elements (except for axis distances > 70 mm). For concrete grades 80/95 < C ≤ 90/105 spalling can occur in any situation for concrete exposed directly to the fire and four methods are recommended to be used, regarding reinforcement mesh, type of concrete, protective layers and inclusion in the concrete mix of more than 2kg/m^3 of monofilament propylene fibres.

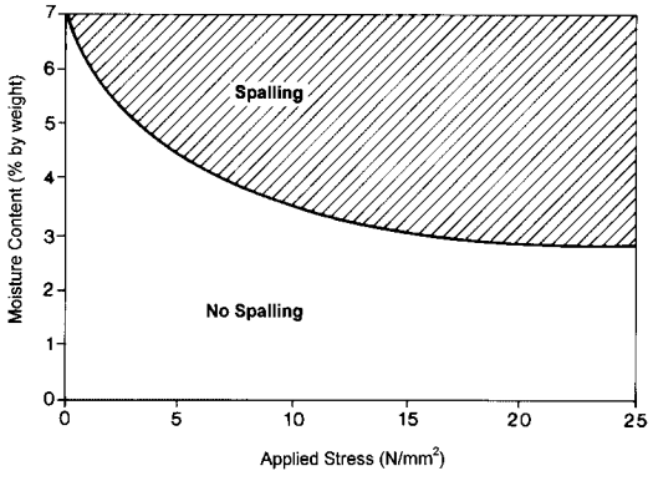

Figure 2.34: Explosive spalling empirical envelope for normal-strength concrete, showing influences of moisture content and applied stress (Khoury, 2000).

2.5.1 FACTORS INFLUENCING SPALLING

The main factors influencing concrete spalling in fire are as follows:

•Material: permeability, saturation level, aggregate size and type, presence of cracking and reinforcement.

•Geometry: section shape and size.

•Environment: heating rate, heating profile, load level.

The main factors are the heating rate, permeability of the material, pore saturation level (especially above 2–3% moisture content by weight of concrete, Figure 2.34), and the presence of reinforcement and the level of external applied load (Khoury,2000).

Low-permeability high-performance concrete (HPC) is more prone to explosively spall, and to experience multiple spalling with respect to normal-strength concrete, despite its higher tensile strength. This is because greater pore pressures build up during heating (Figure 2.35), owing to the material's low permeability. Also, the peak in pore pressure occurs nearer to the surface for HPC which explains why thinner concrete sections spall repeatedly from HPC concrete in fire.

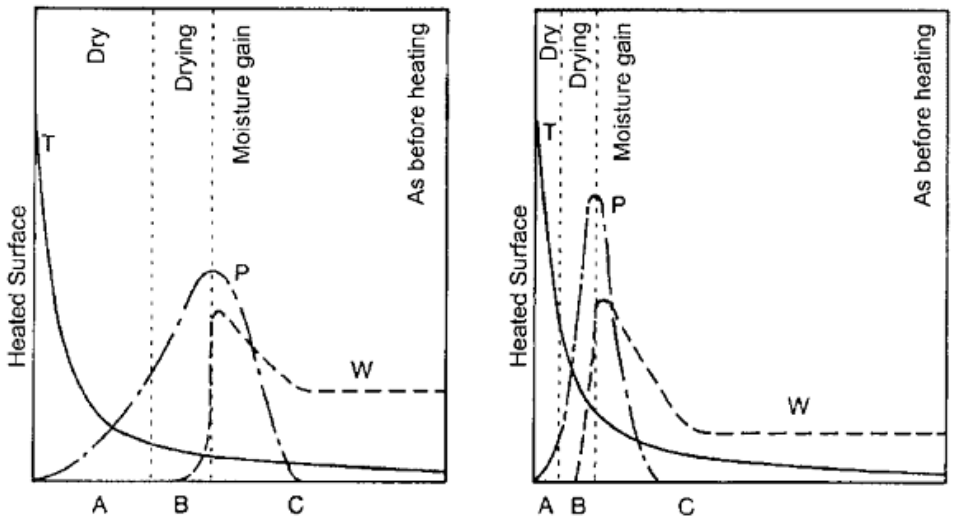

Figure 2.35: Gradients of temperature, pore pressure and moisture in normal and high-performance concrete sections during heating from one unsealed surface (Anderberg and Khoury, 2000).

2.5.2 MECHANISMS OF EXPLOSIVE SPALLING

Explosive spalling can occur through the following mechanisms: pore pressure spalling, thermal stress spalling and thermal cracking spalling.

2.5.2.1 PORE PRESSURE SPALLING

In this case, a build-up of high pore pressures and severe gradients results as a consequence of migration of air, vapor and liquid water in the porous network, as seen in Figure 2.36. While temperature increases, some part of the water is evaporated through the surface, and the other part is transferred into the interior of the element where vapor condenses again if the temperature is below the saturation vapour temperature. As a result, a quasi-saturated layer can be formed. Now the material can be divided into three zones: (1) dry and dehydrated zone, (2) drying and dehydrating zone, (3) quasi-saturated layer that acts as an impermeable wall for vapor release, and (4) unchanged zone far away from its heated surface, where the material satisfies same conditions as before fire.

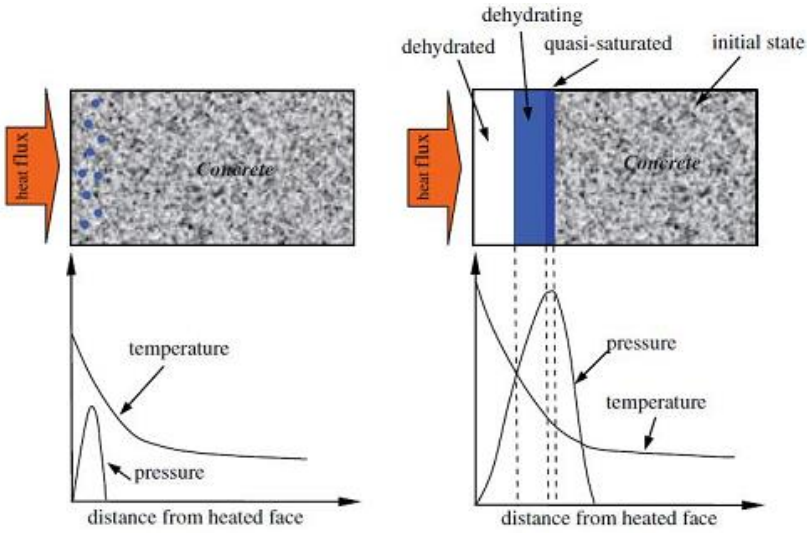

Figure 2.36: The process for the build-up of pressure (Zeiml et al., 2005).

The pressure peak is situated in the saturated layer (moisture clog). The formation of the moisture clog depends on the permeability of the material: the lower the permeability the faster the moisture clog develops and the higher the pressure is and its pressure gradient (Yufang Fu, 2010).

2.5.2.2 THERMAL STRESS SPALLING

This type of failure is due to rapid heating that generates excessive thermal stresses, and this is a proof that other factors than pore pressures may contribute to explosive spalling.

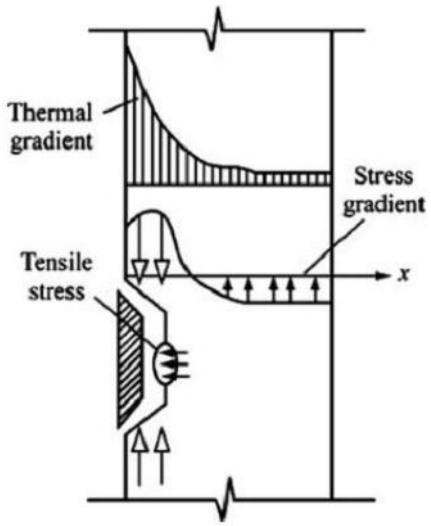

Figure 2.37: Mechanism of thermal stress spalling (Yufang Fu, 2010).

Severe thermal gradients that induce thermal shock will generate high compressive stresses close to the heated surface due to restrained thermal expansion and tensile stresses in the cooler interior regions, (Figure 2.37). With temperature increase the aggregates dilate until they degraded chemically generating tension and the cement paste shrinks as soon as water escapes generating compression of the material, this leading to strain incompatibilities (Yufang Fu, 2010).

2.5.2.3 THERMAL CRACKING SPALLING

This case takes into account the heterogeneity of the concrete. Internal cracks in concrete within high heating rate can be influenced by factors as (without taking into account any external loading): release of absorbed and chemically bound water, thermal mismatch stress between aggregates and cement paste, temperature gradient, decomposition of hydration (Yufang Fu, 2010).

Thermal cracks can be divided in three types: (a) shrinkage cracks induced by the decomposition of hydration; (b) TMS cracks (radial, tangential and aggregate cracks) induced by the thermal mismatch between the aggregate and the hardened cement paste, and (c) internal and external cracks induced by temperature gradients, (Yufang Fu, 2010).

As seen from the different spalling mechanisms presented above, it can be stated that spalling is related to the generation of pore pressures and development of cracks, which in turn are influenced by the heating rate and the heterogeneous composition of the concrete.

2.5.3 SPALLING IN DIFFERENT TYPES OF CONCRETE

2.5.3.1 HIGH PERFORMANCE CONCRETE (HPC)

According to Kalifa et al. (2000), the high compactness of HPC is the main parameter responsible for spalling at high temperatures. When comparing experimentally a normal concrete (M30, w/c = 0.5) with a HPC concrete (M100, w/c = 0.32), both with calcareous aggregates, it could be noticed that they have globally a similar thermal behaviour, related with their similar thermal properties (thermal conductivity and specific heat). The difference comes when measuring the pore pressure, up to 4 MPa in the HPC and 2 MPa in the normal concrete; as well HPC underwent higher pressure gradients than normal concrete.

It can be stated that as a consequence of lower permeabilities (to vapor and liquid water), there is a large difference in the thermodynamic conditions reached in the porous network, which results in much higher pore pressures.

Tests ran by Bastami (2011) on HSC were done on 16 samples, 12 with silica fume mixtures and 4 without. It was observed that all the mixtures specimens that were heated to temperature higher than 300^{o}C, experienced spalling and mass loss. In the tests, spalling ranged from insignificant aggregate spalling (which causes surface pitting) to, in extreme cases, large parts of the specimens being blown off with explosive force that are categorized in four types: explosive (parts larger than 1 cm), surface (parts smaller than 1 cm), aggregate and corner spalling. The tests showed that the spalling degree decreased drastically when the water to binder ratio levels increased in the mixtures containing silica fume and also that silica fume in general could control explosive spalling due to increasing tensile strength.

2.5.3.2 SELF COMPACTING CONCRETE (SCC)

Tests ran by Mathew (2011) on SCC concluded that explosive spalling occurs in both vibrated concrete and SCC in the inside temperature range between 350^{o}C and 580^{o}C. On the other hand, no spalling was observed in any of the LSCC (Laterized Self Compacting Concrete) specimen tested. No

crack was found in LSCC up to 600°C. Surface cracks were found on the specimens only at 800°C and the number of cracks was more in water cooled specimen.

As an overview of the experimental results on different types of concrete, it can be stated that the main factor contributing to spalling are the aggregate/binder mix and water to cement ratio. Addition of silica fume can be a parameter that controls the likelihood of spalling due to increasing of tensile strength of concrete. Great results of using Laterized Self Compacting Concrete show that this replacement of the traditional aggregates could be considered as a substitute fire protection material for conventional concrete.

It is interesting to analyze the results when it comes to water to binder ratio on HSC. It is stated that low water to binder ratios bring in greater susceptibility to spalling because of the very dense concrete matrix obtained with silica fume as a partly cement replacement. Even though low ratio implies higher strength and lower porosity, this will lead to higher pressures in the material. This is the opposite as for the normal concrete, where it is considered that spalling will not occur for moisture content lower than 3%.

It is clear that there is a large difference between normal concrete and the newly developed concretes because of the thermodynamic conditions met in the porous network of the latter, which results in a much high pore pressure that increases the changes of spalling occurrence.

For a better understanding of the features that can induce spalling, one should have knowledge about concrete characteristics at high temperatures. Resent research shows that the addition of polypropylene (pp) fibres to the concrete is one way to limit or avoid spalling under fire conditions.

2.6 ROLE OF POLYPROPYLENE FIBRE AT HIGH TEMPERATURE

One of the well-known methods of reducing the risk of explosive spalling is the addition of polypropylene fibres (pp-fibres) to the concrete mix. This approach works on the basis that the pp-fibres have different thermal characteristics from those of normal concrete. The mechanism underlying the positive effects of application of pp-fibres is that, when concrete containing pp-fibres is exposed to elevated temperatures or to fire, the pp-fibres undergo two main effects, which ultimately reduce damage due to explosive spalling (Bayasi and Dhaheri, 2002; Hannant, 1998; Tatnall, 2002; Segre et al., 1998; Kalifa et. al., 2000).

First of all, the fibres expand at a different rate than the matrix, causing small fissures or openings to be formed between the cement paste matrix and the fibres. Research work shows that these fissures are enough to allow some relief of the vapor pressure that builds up in the pores of the

concrete. Secondly, as the heating continues and the temperature of the fibres reaches the range of 165°C to 171°C, the fibres melt. From 360°C, the fibres evaporate. Disappearance of the fibres provides passage ways or channels along which water vapour can dissipate, so avoiding build-up of pressure. These two effects enhance the relief of the stresses that are suddenly developed by the vapour pressure build-up, which subsequently reduce explosive spalling.

CHAPTER - 3

LITERATURE REVIEW

The aim of this chapter is to give a brief overview of the works made by other authors in order to understand the main parameters controlling pore pressure spalling and to plan a new experimental campaign able to give answer to problems still open. The most significant aspects related to mass loss, thermal and hygrometric behaviour of concrete subjected to heating, with the aim at testing related to the phenomenon of spalling. Also brief discussion of spalling influence by water/cement ratio, water content, heating rate and type of aggregate. As regards the aspects mentioned above, reference articles are discussed below:

• Dal Pont S., Dupas A., Ehrlacher A., and Colina H. "An Experimental Relationship between Complete Liquid Saturation and Violent Damage in Concrete Submitted to High Temperature", Magazine of Concrete Research, 57.8, pp. 455-61, 2005.

• Kalifa P., Menneteau F.D., and Quenard D. "Spalling and Pore Pressure in HPC at High Temperatures", Cement and Concrete Research, 30, pp. 1915-1927, 2000.

• Kalifa P., Chènè G., and Gallè C. "High-Temperature Behaviour of HPC with Polypropylene Fibres: From Spalling to Microstructure", Cement and Concrete Research, 31, pp. 1487-1499, 2001.

• Mindeguia, J. C., Pierre Pimienta., Carre H., La Borderie Ch. "Experimental Study on the Contribution of Pore Vapour Pressure to the Thermal Instability Risk of Concrete". 1st International Workshop on Concrete Spalling due to Fire Exposure, Liepzing, German, pp.150-167,3-5 September 2009.

• Mindeguia, J. C., Pimienta P., Noumowè A., and Kanema M. "Temperature, Pore Pressure and Mass Variation of Concrete Subjected to High Temperature - Experimental and Numerical Discussion on Spalling Risk", Cement and Concrete Research, 40, pp. 477-487, 2010.

• Mindeguia, J. C., Pimienta P., Hager I., and Carrè H. "Influence of Water Content on Gas Pore Pressure in Concretes at High Temperature", 2nd International RILEM Workshop on Concrete Spalling due to Fire Exposure, Delf, The Netharlands, pp. 113-121, 5-7 October, 2011.

• Mindeguia, J. C., Pimienta P., Carrè H., and Borderie C. L. "Experimental Analysis of Concrete Spalling due to Fire Exposure", European Journal of Environmental and Civil Engineering, 2013.

• Bangi M.R. and Horiguchi T. "Study on Pore Pressure Spalling in Hybrid Fibre- Reinforced High Strength Concrete at Elevated Temperatures", Cement and Concrete research, 41, pp. 1150-1156, 2011.

• Felicetti R., Monte F. L., and Pimienta P. "The Influence of Pore Pressure on the Apparent Tensile Strength of Concrete", 7th International Conference on Structures in Fire, Zurich, Switzerland, June 6-8, 2012.

3.1 GENERAL DESCRIPTION OF THE TEST METHODS

A better understanding of the results obtained by different authors requires a brief explanation of the different set-up of the tests carried out, together with a description of the heating mode and characteristics of concrete under examination.

Dal Pont et al., 2005: The experimental work carried out by Dal Pont et al. (2005) is aimed at measure the gas pressure and temperature in a concrete specimen (discs of diameter 150 mm and 50 mm thickness) heated on one face at about 280°C, with a heating rate of 1.5°Cmin^{-1}. The lateral surface has been insulated to guarantee a unilateral flux and avoiding thermal dispersions. Each specimen has been equipped with a J type thermocouple and a pressure sensor. The gauges are made of a steel tube, stuck into concrete by means of high-resistance glue, at 20–25 mm from the heated face. Pressure gauge (able to measure pressures up to about 1.5 MPa) has been also stuck on the free tube end (Figure3.1).

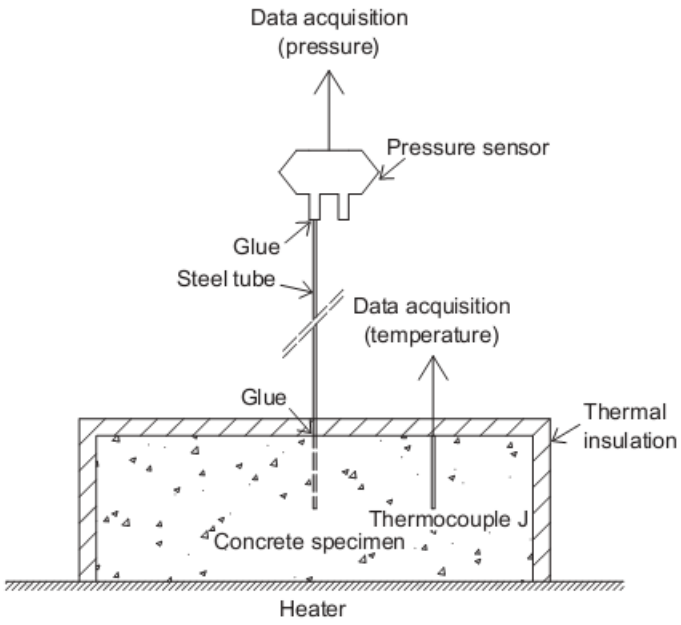

Figure 3.1: Scheme of the experimental set-up (Dal Pont et al., 2005).

The use of high thermal resistance glue allowed a perfect seal, and no leak was observed during the tests. The tests were performed on a high-performance concrete M100, characterized by a water to cement ratio w/c = 0.33 and use of limestone aggregates. The main mechanical characteristics are represented by the compressive strength f_c = 109 MPa, the tensile strength f_t = 6 MPa and the modulus of elasticity E = 36.70 GPa.

Kalifa et al., 2000: The device was designed in order to make simultaneous measurements of pressure, temperature at various positions in a concrete specimen and the thermal load is applied on one face of a prismatic concrete specimen (30 X 30 X 12 cm^3), whereas the lateral faces of the specimen are heat-insulated with porous ceramic blocks. Heating is provided by means of a radiant heater (up to 5 kW and 800°C) that covers the surface of the specimen, placed 3 cm above it (Figure 3.2).

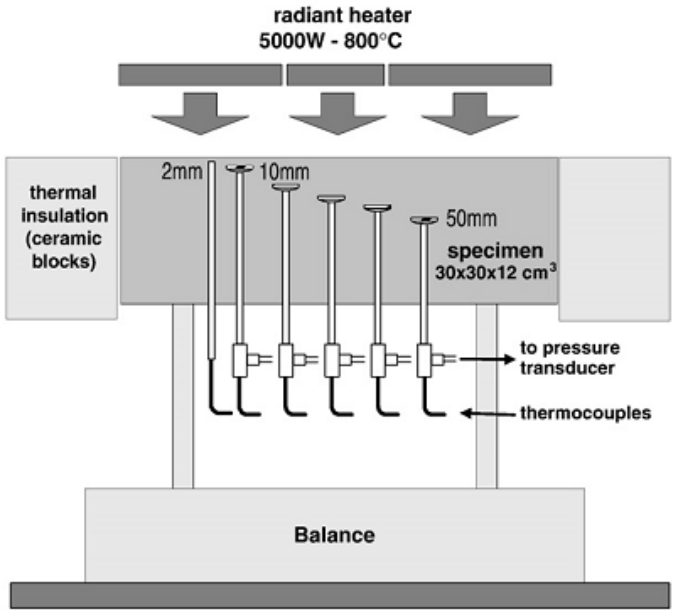

Figure 3.2: The experimental set-up (Kalifa et al., 2000).

The specimen is placed on a balance in order to monitor its mass during heating. A retention tray is placed between the specimen and the balance for retaining water that may come out from the rear face of the specimen. The specimens were instrumented with six gauges placed at casting, for simultaneous pressure and temperature measurements. These gauges are made of a sintered metal round plate (Ø12 X 1 mm) crimped in a metal cup. The latter is brazed to a thin metal tube (inner

diameter 1.6 mm), which comes out of the rear face of the specimen. At the time of testing, a tight connector is placed at the free end of the tube. It firstly connects the gauge to a piezoelectric pressure transducer through a flexible tube filled with silicone oil. Secondly, a thermocouple (Ø 1.5 mm) is inserted in the tube through the connector down to the metal plate. The free volume of the gauge is around 250 mm^3. This alters slightly the measured pressure values.

Five gauges were placed in the central square zone of 10 x 10 cm^2, at 10, 20, 30, 40 and 50 mm from the heated surface, respectively (Figure 3.2). The sixth gauge is made of a plain tube, the end of which is located at 2 mm from the heated surface for measuring its temperature. Both thermocouples and pressure tubes are very loose so that they do not disturb mass measurements.

The tests were carried out on two mixes: an ordinary concrete (M30, w/c = 0.5, f_c = 34.9 MPa) and a HPC (M100, w/ c = 0.32, f_c = 91.8 MPa), both made with calcareous aggregates. The tests were performed in a temperature range where spalling may occur: the temperature of the radiant heater was 450°C, 600°C and 800°C, respectively.

Mindeguia et al., 2009: The specimens are instrumented with the same type of experimental set-up used in Kalifa et al., 2000 in Figure 3.2.

This article describes three different modes of the testing, namely:

•Slow heating on cylindrical samples: three gauges are placed along the radius of the sample (at the mid-height cross section of the sample) according to the, Figure 3.3. Ø 160 mm x h 320 mm cylindrical samples are heated in an electrical sample at 1°C/min. When temperature reaches around 600°C in the furnace, test is stopped.

•Moderate and rapid heating on prismatic samples: the test consists in applying a thermal load to one face of a prismatic sample (30 x 30 x 12 cm^3) using a radiant heater placed 3 cm above it. Samples are equipped with six gauges. One of them consists in a single plain tube in which one end is placed at 2 mm of the heated surface for only temperature measurement. In order to measure internal temperature and pressure, the other five gauges were placed at 10, 20, 30, 40 and 50 mm of the heated surface (Figure 3.4).

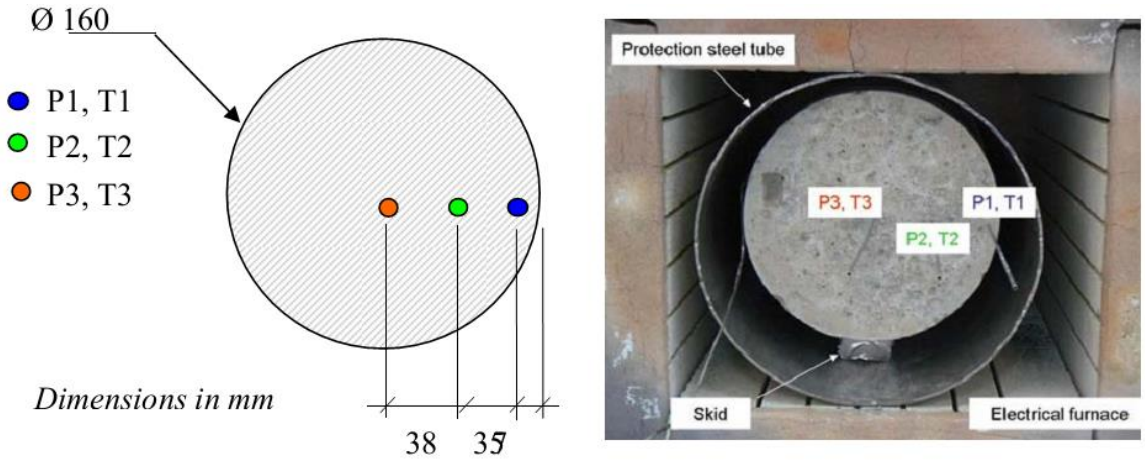

Figure 3.3: Slow heating test on cylindrical sample: position of the three pressure gauges (the three gauges are in the same cross section, i.e. at mid-height of the sample, Mindeguia et al., 2009).

The six gauges are placed at the centre of the heated surface, in a 10 x 10 cm² square (Figure 3.4).

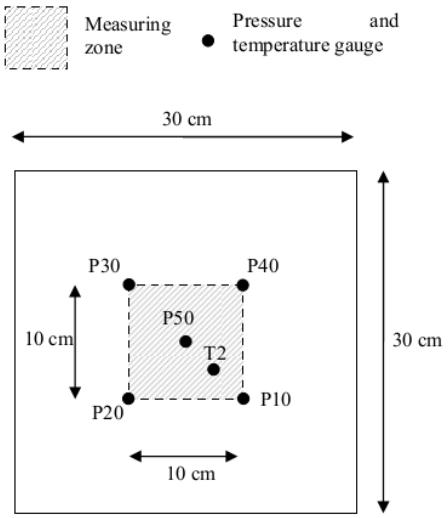

Figure 3.4: Moderate and rapid heating on prismatic samples: position of the temperature and pore vapor pressure measuring zone (Mindeguia et al., 2009).

In the moderate heating the radiant heater was controlled in such a way that its temperature rapidly reaches 600°C (after around 5 minutes). The power was then maintained constant during 6 hours. At last, samples were naturally cooled down. Rapid heating on prismatic samples: this test is almost the same than the moderate heating. The only difference is that the radiant heater is controlled in such a way that its temperature rapidly reaches 800°C.

•ISO fire on mid-size slabs: The total surface of the slab is 700 x 600 mm² and its exposed surface is 600 x 420 mm². Its thickness is 150 mm. Two concrete slabs were tested under ISO-834 fire during 1 h for each configuration. The first slab was equipped with three pressure gauges (at 10, 20 and 30 mm from the exposed surface) while the second one was only equipped with two pressure gauges (at 10 and 30 mm from the exposed surface). For both slabs, gauges were placed at the centre of the slab, in a zone where we can assume that heating flow and fluids movement are unidirectional (Figure 3.5).

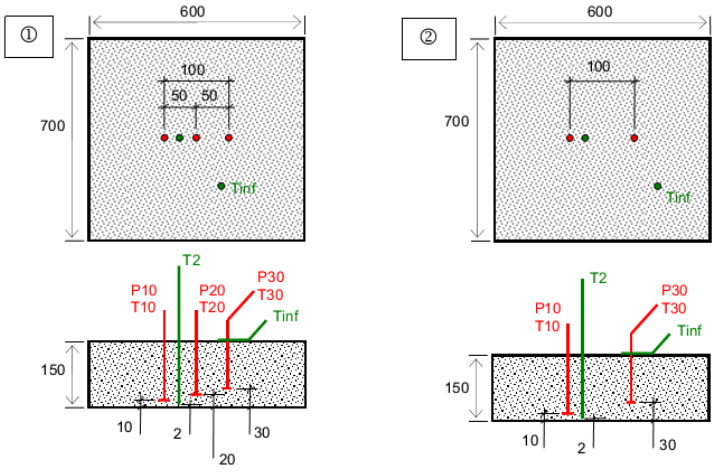

Figure 3.5: ISO fire and moderate heating on slabs: position of the temperature and pore vapour pressure measuring zone (one [(1)]-type slab and one [(2)]-type slab for each testing configuration).

The Figure 3.6 presents, for all the different heating procedures, the evolution with time of the temperature in the furnace and the temperature that is measured at 10 mm from the exposed surface in the concrete sample.

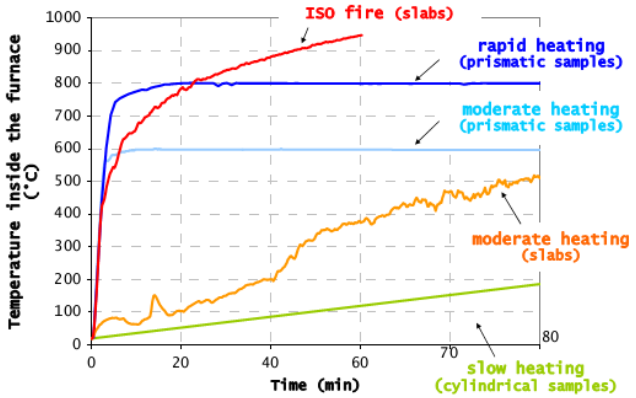

Figure 3.6: Evolution with time of the temperature in the furnace (Mindeguia et al., 2009).

The types of tested concrete are:

•B40: concrete with water to cement ratio, w/c = 0.54 and compressive strength f_c = 37MPa, with limestone aggregates;

•B40F2: concrete with water to cement ratio, w/c = 0.54 and compressive strength f_c = 29MPa, with limestone aggregates and the addition of 1.98 Kg/m^3 polypropylene fibers having a diameter, Ø = 18 microns, length L = 12 mm and a melting point of about 170^{o}C;

• B40SC: concrete with water to cement ratio, w/ c = 0.54 and compressive strength f_c = 43 MPa, siliceous and calcareous 4/20 gravel (in particular flint);

• B60: concrete with water to cement ratio, w/c = 0.30 and compressive strength f_c = 61 MPa, with limestone aggregates;

• B60F2: concrete with water to cement ratio, w/c = 0.30 and compressive strength f_c = 70 MPa, with limestone aggregates and the addition of 1.84 Kg/m^3 of polypropylene fibers.

Mindeguia et al., 2010: In this article the experimental set-up was used same as reported in Kalifa et al. (2000). The tests are carried out on five different concrete mixtures, all with siliceous aggregates, of which shows the salient features:

•B325: concrete with water to cement ratio, w/c = 0.62 and compressive strength after 28 days equal to fc = 35MPa;

•B350: concrete with water to cement ratio, w/c = 0.55 and compressive strength after 28 days equal to fc = 36MPa;

•B400: concrete with water to cement ratio, w/c = 0.44 and compressive strength after 28 days equal to fc = 53MPa;

•B450: concrete with water to cement ratio, w/c = 0.36 and compressive strength after 28 days equal to fc = 62MPa;

•B500: concrete with water to cement ratio, w/c = 0.29 and compressive strength after 28 days equal to fc = 76MPa.

Two tests were carried out for each concrete mixture. The radiant heater was controlled in such a way that its temperature rapidly reaches 600°C (after around 5 min). The power was then maintained constant during 6 h.

Mindeguia et al., 2013: In this article the experimental set-up was used same as reported in Kalifa et al. (2000). The tests were carried out on six different concrete mixtures, all with siliceous aggregates, of which shows the salient features:

•B40: concrete with water to cement ratio, w/c = 0.54 and compressive strength after 28 days equal to fc = 37MPa, with calcareous gravel;

•B40F2: concrete with water to cement ratio, w/c = 0.54 and compressive strength after 28 days equal to fc = 29MPa, with calcareous gravel and addition of 2Kg/m^3 polypropylene fibres.;

•B40SC: concrete with water to cement ratio, w/c = 0.54 and compressive strength after 28 days equal to fc = 43MPa, with silico-calcareous gravel;

•B40SCF2: concrete with water to cement ratio, w/c = 0.54 and compressive strength after 28 days equal to fc = 46MPa, with silico-calcareous gravel and addition of 2Kg/m^3 polypropylene fibres;

•B60: concrete with water to cement ratio, w/c = 0.30 and compressive strength after 28 days equal to fc = 61MPa,with calcareous gravel;

•B60F2: concrete with water to cement ratio, w/c = 0.30 and compressive strength after 28 days equal to fc = 70MPa, with calcareous gravel and addition of 2Kg/m^3 polypropylene fibres.

Samples were heated up to 120, 250, 400 and 600°C, temperature evolves under a heat flow rate of 1°C/min, and the temperature is stabilized around the fixed value during 6 h. Tested samples at room temperature were in fact previously dried at 80°C.

3.2 MEASUREMENT OF PRESSURE

From the experimental point of view, several authors (Zeiml at al., 2008; Kalifa et al., 2001; Mindeguia et al., 2010; Jansson and Bostrom, 2010) have directly measured the local pressure in concrete specimens subjected to thermal transients. In most cases this was performed by embedding thin stainless steel pipes provided with external electronic sensors. Possible alternatives (Bangi, 2011) come from the adoption of a porous sensing head (to measure the mean pressure of rather high volumes) and filling the pipe with thermally stable silicon oil (to prevent any moisture leakage). It has to be noted that the pressure measured in this way results from the equilibrium reached by the probe inside cement matrix because of the gas pressure (vapour + air) in the pores. Nonetheless, consistent results are generally obtained in different test conditions (concrete grade, moisture content, heating rate) and values as high as 5 MPa have been reported in case of HPC (Bangi, 2011); lower values are reported for Normal Strength Concrete (Mindeguia et al., 2010).

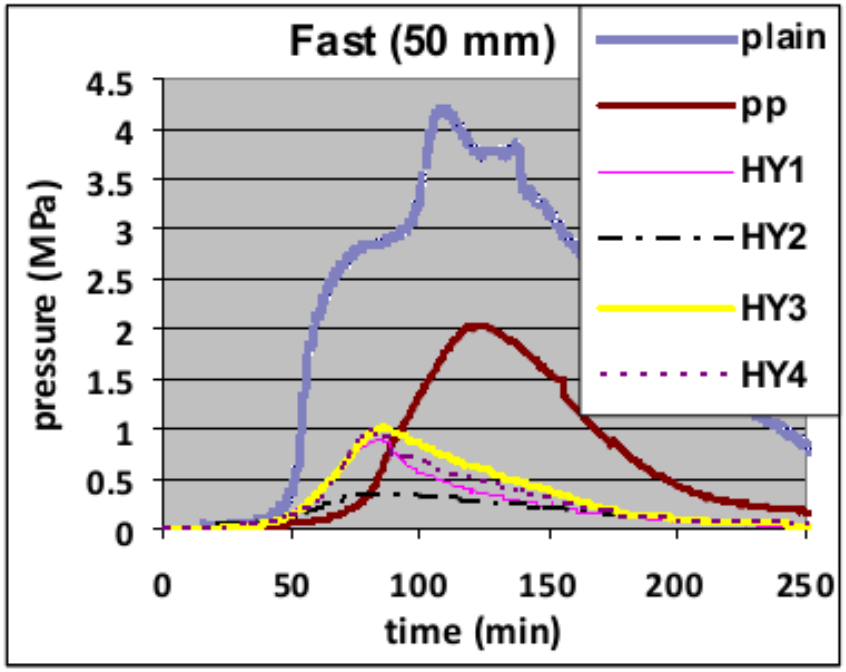

Figure 3.7: Build – up of pressure with time under fast heating (Bangi, 2011).

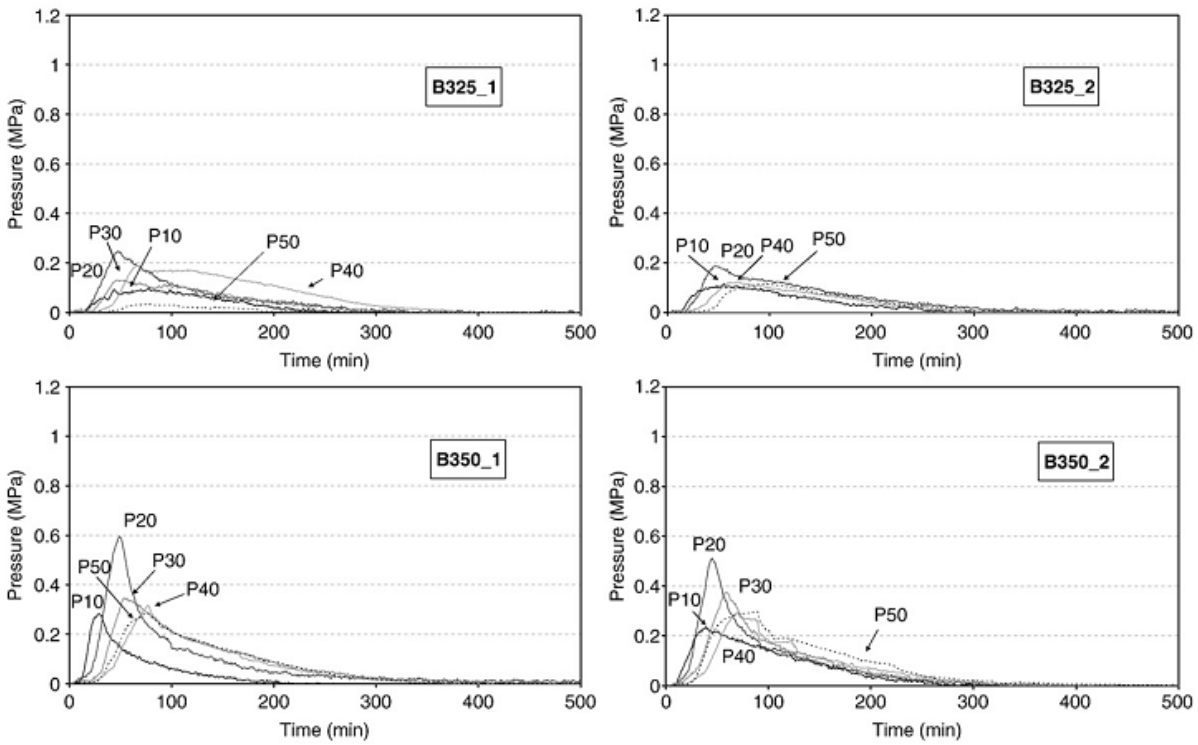

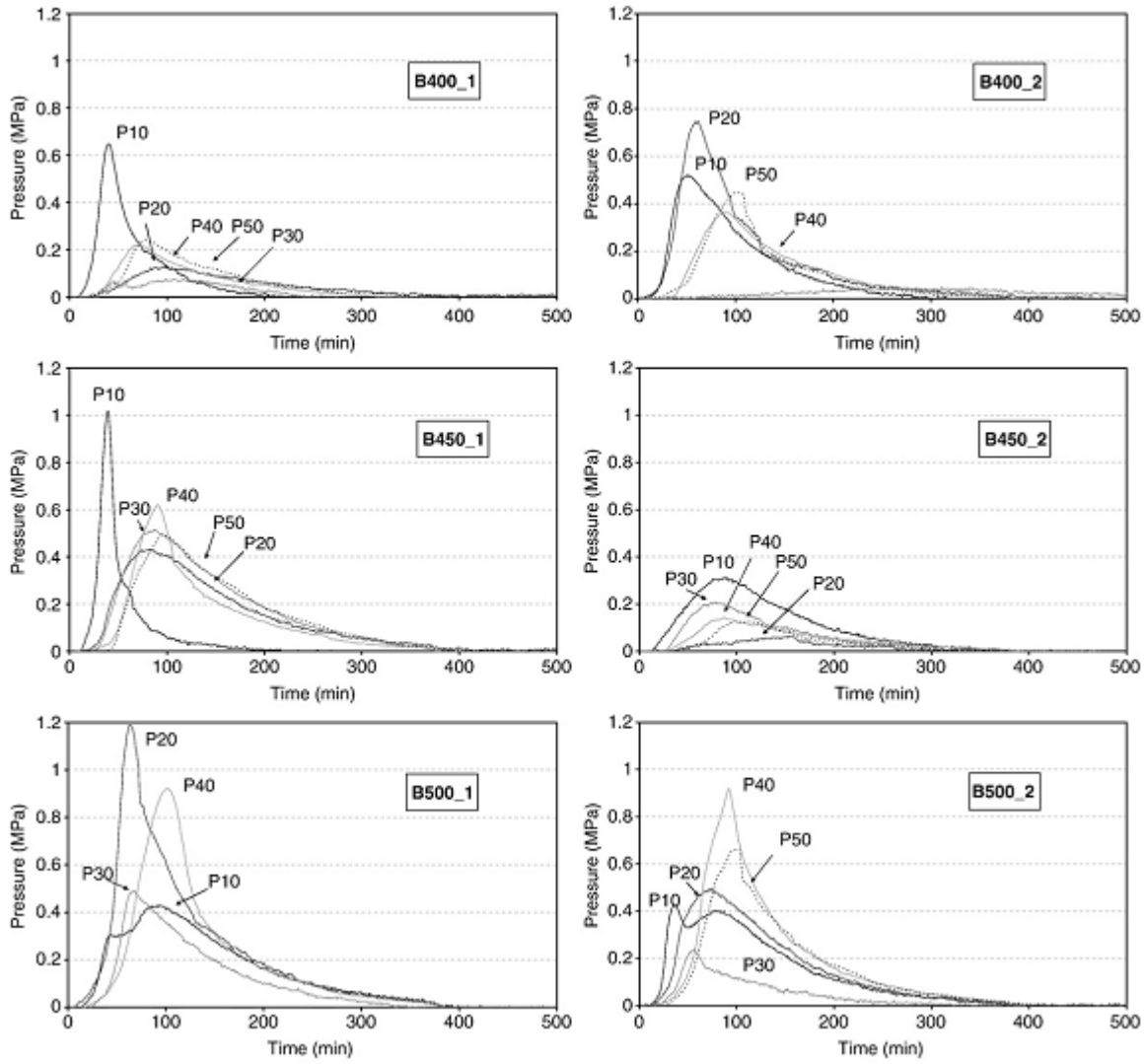

Figure 3.8: Pressure as a function of time for all the tested concrete mixtures (the number after P is the distance in mm from the heated surface) (Mindeguia et al., 2010).

Few authors have investigated the influence of several parameters on both spalling amount and pore gas pressure. Their studies covered a wide range of experimental results (from no spalling to large amount of spalling and from low to high values of pore pressure; Mindeguia et al., 2009; 2010). Despite pore pressure is surely a spalling driving force; Jansson and Boström (2010) concluded that, for the considered cases, a direct relationship between the spalling severity and the measured values of pore pressure wasn't evident. Some specimens spalled with measured pore pressures lower than 0.5 MPa, while other specimens didn't spalled even with pressure higher than 3 MPa. Hence, Jansson and Boström (2010) proposed a new spalling mechanism based on the concept of

moisture clog (spalling is fostered by high pore liquid pressure and by the lower strength of the hot and water-saturated concrete layer).

It is probable that pore gas pressure cannot be the only physical origin for concrete spalling; it can be evaluated with both pore gas pressure built-up and the thermo-mechanical process. It is worth noting that it is still difficult to distinguish the contribution of the thermo-mechanical and the hygro-thermal mechanisms for explaining concrete spalling. Indeed, both mechanisms are coupled and influence on each other.

However, the other research trend is based on numerical models simulating the heat and mass transfer taking place in concrete exposed to high temperature. This involves the solution of a complex set of coupled differential equations and several approaches, based on different simplifying assumptions, have been proposed in the last thirty years (Gawin et al., 2011b). Their consistency is often tested against the ability to fit the temperature and pressure values obtained in experimental tests. In these models, one critical problem in assessing the risk of concrete spalling is the mutual interaction between pore pressure and the mechanical response of the material. As commonly done in multi-phase porous media, the total stress $\mathrm{t}^{\mathrm{tot}}$ is split into the effective stress $\mathrm{t}^{\mathrm{eff}}$, borne by the solid skeleton and the solid phase pressure p^{s} exerted by the pore fluids (Gray and Schrefler, 2007):

$$\mathrm{t}^{\mathrm{tot}} = \mathrm{t}^{\mathrm{eff}} - \mathrm{p}^{\mathrm{s}}.\mathrm{I} \tag{3.1}$$

Where I is the unit tensor (tensile stress and relative pressure are assumed to be positive).

The solid pressure can be expressed as a combination of the gas and capillary pressures and different expressions have been proposed in the literature (Gray and Schrefler, 2001). In some models only the gas phase is considered, with different weight coefficients. One option, according to Biot's theory for compressible fluids inside a stiff skeleton, is to introduce the bare gradients of the gas pressure into the equilibrium equations (Tenchez and Purnell, 2005). Another, and opposite, option is to assume that gas pressure is exerted inside the pores and should be multiplied by the material porosity (Dwaikat and Kodur, 2009).

Intermediate values (Ichikawa and England, 2004) are obtained by considering the elastic solution for the stress intensification around a spherical cavity (Timoshenko, 1970). More sophisticated models take the capillary pressure into account as well (Gray and Schrefler, 2001; Gawin et al., 2011a; Gawin et al., 2011b), this pressure being multiplied by the fraction of skeleton area in contact with liquid water. Nonetheless, the role of capillary pressure is not critical neither in fast thermal and

moisture transients (Davie et al., 2006), nor in increasing significantly the mechanical damage (Gawin et al., 2006), to the point that the combined action of the restrained thermal strain is often considered as the most likely factor in triggering explosive spalling in concrete structures exposed to fire. Also the thermal dilation of liquid water inside the fully saturated pores may initiate the microcracking of cement paste (Dal Pont et al., 2005).

According to Dal Pont et al. (2005), a mechanical effect due to thermal dilation gradients and a hydro-thermal effect leads to a build-up of pore pressure. Differential thermal dilation and tensile stresses are induced in concrete by heating. This phenomenon is amplified in concrete due to the different thermal dilation of cement paste and aggregates. Moreover, dehydration shrinks cement paste while aggregates expand. Dehydration is also associated with the release of free liquid water inside concrete which transforms into vapor. Liquid water and gas (composed of dry air and water vapor) are in equilibrium inside the porous network of concrete.

The equilibrium equation is given by means of the well-known Laplace equation:

$$p^{gw} + p^{ga} - p^{w} = 2\sigma(T)\chi \tag{3.2}$$

Where χ represents the curvature of the interface between the capillary water and the gas phase inside the pores of the medium, p^{gw}, p^{ga}, p^{w} are respectively vapor water, dry air and liquid water pressures and $\sigma(T)$ is the water surface tension.

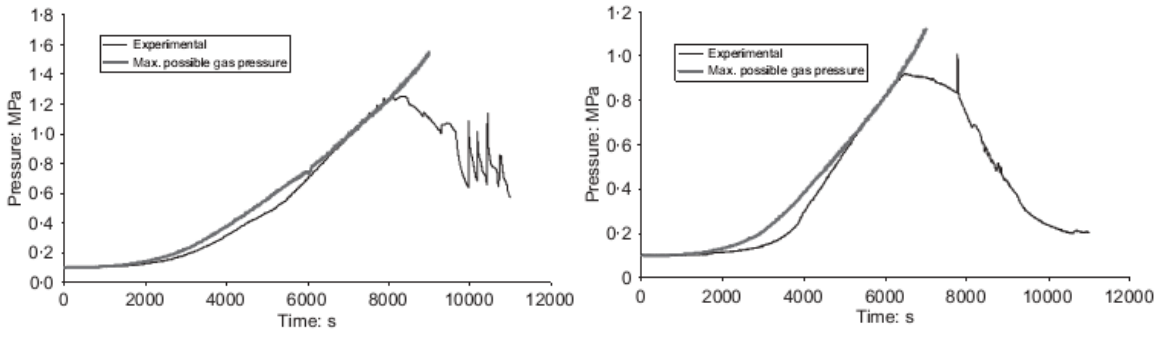

(a) (b)

Figure 3.9: Development of the pore pressure as a function of the time (Dal Pont et al., 2005).

Figure 3.9 (a, and b) showed that the cracking mechanism can basically occur in two ways.

•In Figure 3.9 (a) small peaks in the pressure, nearly tangent to the maximal possible gas pressure curve are present. These small peaks can be interpreted as the consequence of the formation of

microcracks in concrete paste, which are not large enough to let free moisture escape in a sudden way (Dal Pont et al., 2005).

• On the other hand, Figure 3.9(b) shows a sudden cracking that increases concrete permeability and leads to a rapid decrease of gas pressure, which means that moisture can rapidly escape the concrete. It is interesting to observe a cracking mechanism that is moisture escapes after the formation of the second microcracks (Dal Pont et al., 2005).

Exceeding the tensile strength is in itself the macroscopic result of unstable flaw propagation through the same porous network where fluid pressure is exerted. Considering the influence of pressure in this internal instability would be a more consistent way to understand the role played by water (liquid and vapour) in triggering spalling. Hence, in Felicetti et al. (2012) a splitting test was performed on cubic specimens when maximum pore pressure was reached. The results shows that the pore pressures influence the tensile strength of concrete see detail in section 4.2.

3.3 FACTORS INFLUENCING PORE PRESSURE

Pore pressure of the concrete can be influence by the water to cement ratio (w/c), water content, heating rate, type of aggregates and presence of fibres content in the mix. All the influence factors are explained below with respect to the research reported:

3.3.1 WATER TO CEMENT RATIO (w/c)

The water to cement ratio can significantly influence on the concrete permeability: reduction of w/c ratios leads to greater compactness of the cementitious matrix, therefore leading to a lower permeability of the material.

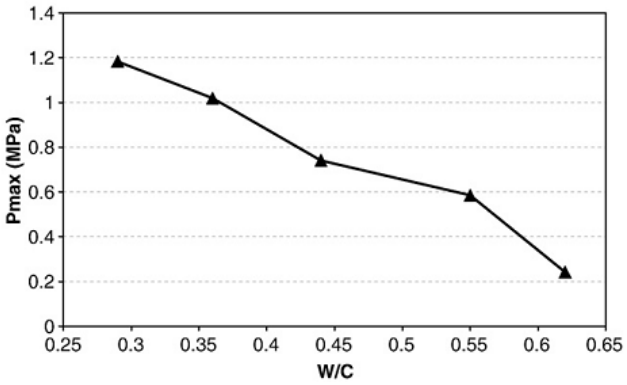

Figure 3.10: Maximum pressure as a function of w/c ratio (Mindeguia et al., 2010).

Low permeability involves a less mass transfer which leads to higher values of pore pressure in the system. Figure 3.10, shows that the higher the w/c ratio, the lower the pore pressure. This underlines the role of the concrete transport properties (porosity, permeability) on the thermo-hygral behaviour of the material, and in particular on the build-up of pore pressures.

Mindeguia et al. (2013) point out how the w/c ratio effects the damage of concrete (damaged areas larger and deeper) given by spalling, as shown in Figure 3.11 for concretes mix B40 (w/c = 0.54) and B60 (w/c = 0.30).

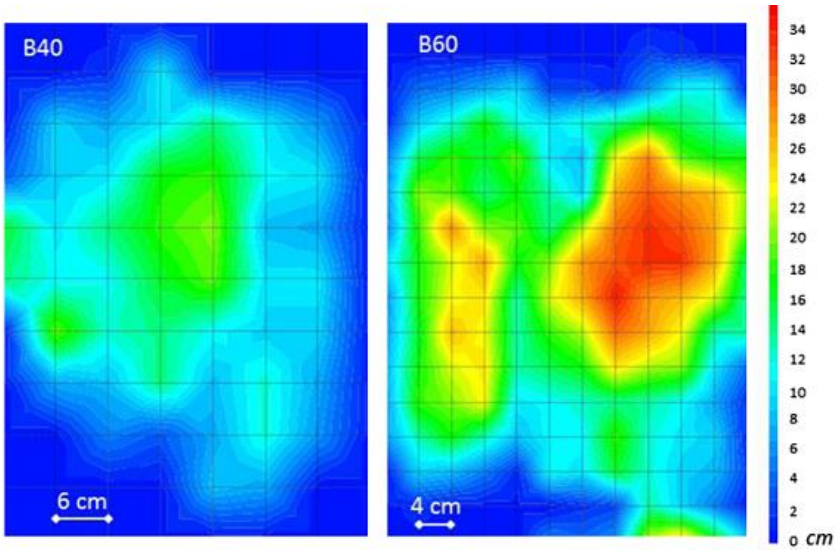

Figure 3.11: Surface mapping of spalling after one hour of ISO fire test. B40 slab on the left, B60 slab on the right (Mindeguia et al., 2013).

3.3.2 HEATING RATE

The influence of the heating rate on the pore pressure of concrete was analyzed by Mindeguia et al. (2009), (2010), (2013) and Felicetti et al. (2012). From these analyzes it is clear that the increase in the thermal loading severity, in terms of heating rate and maximum reached temperature, allows the pore gas pressure to be greatly reduced (Figure 3.12), Mindeguia et al. (2013).

The more severe the heating has the lower the measured gas pore pressures. These differences were attributed to the larger network of cracks in samples submitted to higher heating rates. Large vertical cracks on the sample lateral sides were observed. It was assumed that more severe heating rates lead to higher damage of samples because higher thermal gradients inducing compression-

tensile stresses and higher thermal incompatibilities between cement paste and aggregates. This thermal damage generates higher permeability allowing then gas pressure reduction. Interestingly, significant traces of moisture were observed around the lateral cracks, indicating the creation of drains for water in heated concrete. It was also observed that the total weight loss and the rate of weight loss were higher in the case of concrete specimen heated at higher heating rates which confirms the hypothesis of a higher permeability. It is important to note that after the tests done with moderate heating, no similar cracks were observed on the samples, Mindeguia et al. (2011).

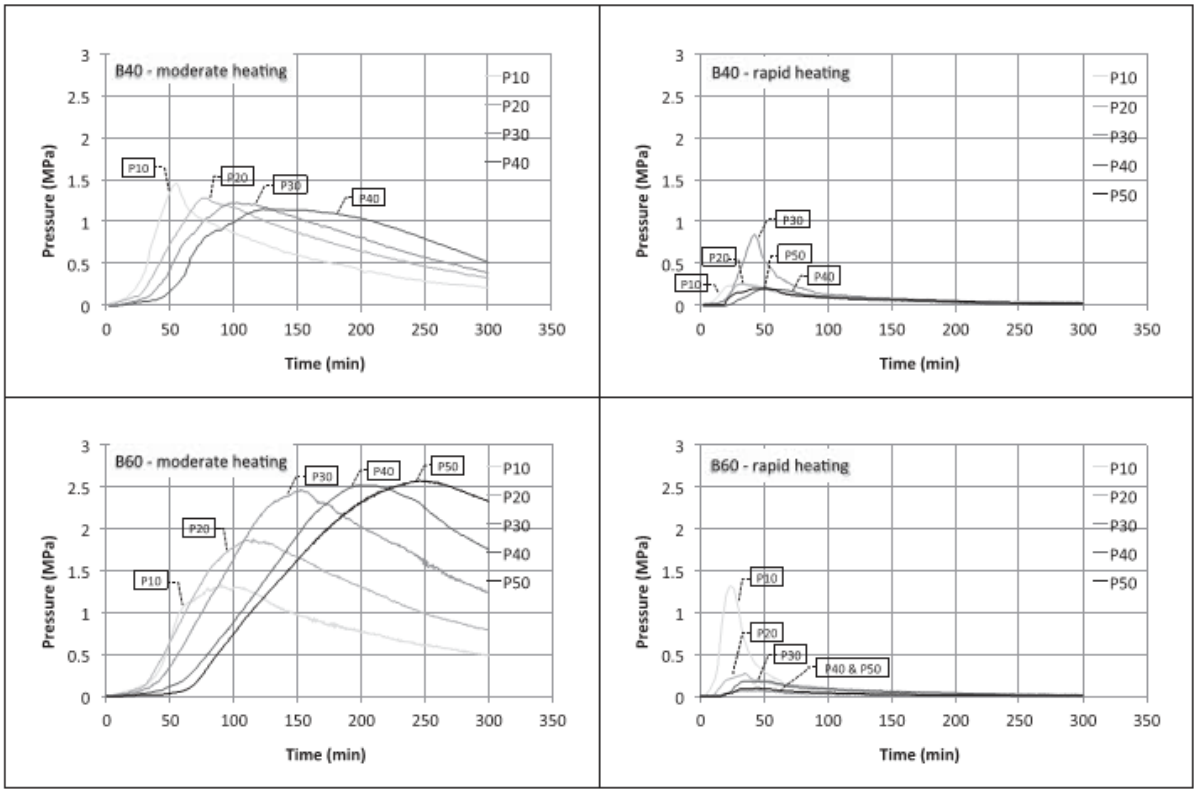

Figure 3.12: Temporal evolution of pore gas pressure for the B40 and the B60 depending on the temperature curve (moderate heating on the left, rapid heating on the right); at the top, B40; at the bottom, B60 (Mindeguia et al., 2013).

3.3.3 WATER CONTENT

Mindeguia et al. (2011) have performed the test on the influence of water content on gas pore pressure in ordinary concrete (B40, w/c = 0.54 and compressive strength = 37 MPa) and high performance concrete (60, w/c = 0.3 and compressive strength = 61 MPa) at high temperature. The samples of B40 and B60 were conditioned as follows: in air (designation B40_Air), dried at 80°C

(B40_Dried) and immersed in water until the mass of the specimen could be considered constant (B40_Water). The results of gas pore pressure and temperature evolution obtained on pre-dried and water immersed concrete specimens were compared with those stored in air (20°C and 50 % R.H.). All above tests were done with the radiant heater target temperature of 600°C. Figure 3.13, 3.14 and 3.15, the comparisons of pore pressure, temperature and weight loss curves recorded during the heating cycle for the air stored, dried, and stored in water concretes are presented.

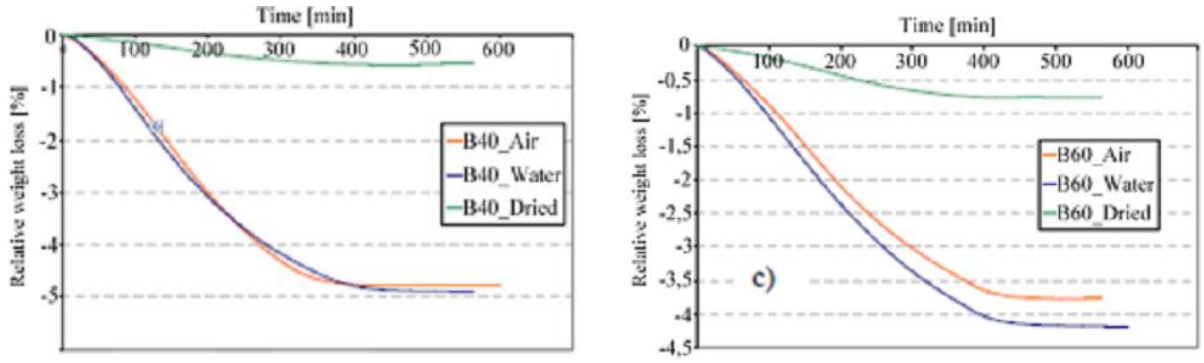

Figure 3.13: Evolution of the weight loss vs. time for B40 and B60 for different storage conditions (Mindeguia et al., 2011).

During heating there were many micro-cracks opening near the heated surface, facilitating in this way the vapour transport. It can be concluded that, for B60_Water, the gas pore pressures are released faster than in B60_Air. It may happen due to approximate amount of free and bounded water released during heating. The free water content of B40 is greater because of the greater amount of water in the mixture (188 kg/m^3 for B40 concrete against 165 kg/m^3 for B60). In contrast, the bounded water content is higher in the B60; probably because of its greater cement content 550 kg/m^3 for B60 concrete against 350 kg/m^3 for the B40. No significant difference between weight loss of B40_Air and B40_Water specimens was observed.

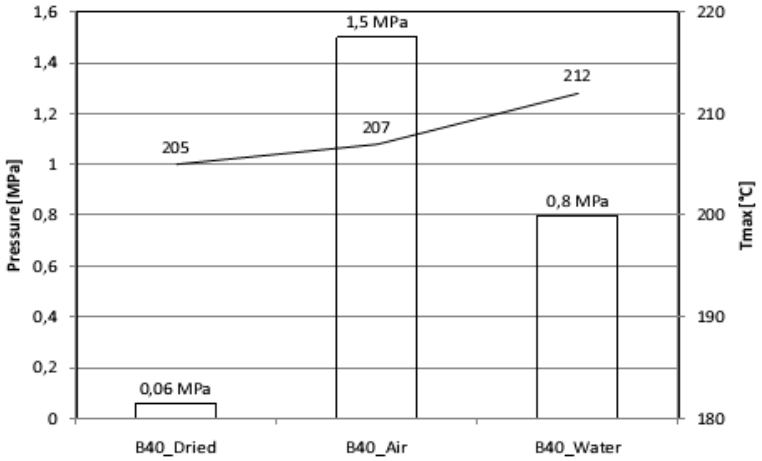

Figure 3.14: Maximum value of gas pore pressure and temperature for B40 for different storage conditions (Mindeguia et al., 2011).

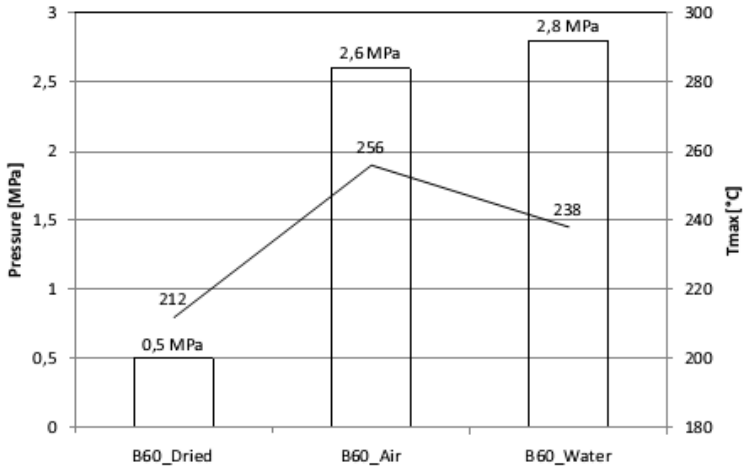

Figure 3.15: Maximum value of gas pore pressure and temperature for B60 for different storage conditions (Mindeguia et al., 2011).

Why concrete with saturated pores does not present significant higher gas pore pressures?

This phenomenon could be attributed to the higher damage level that is induced by heating during tests on water-immersed samples. The water that fills the pores of the sample expands. The high value of the water thermal expansion may induce tensile stresses and then crack development within the material. As a consequence, these cracks can increase the transport properties of concrete (gas permeability in particular). By this means the reduction of gas pore pressure can be observed. This hypothesis is supported by a particular behaviour of concrete samples (B40_Water

and B60_Water) that was observed during the tests. During the heating, the cracking of the surface was quite audible between the tenth and twentieth minute of the test. Such sounds were not audible in the other tests.

3.3.4 AGGREGATES TYPE

The test results from different authors are inconsistent, it can generally be concluded that the likelihood of thermal stress explosive spalling is less for concrete containing a low thermal expansion aggregate. Kalifa et al. (2000), found that the thermal dilation of the aggregates plays an important role in damage and varies significantly with its nature and calcareous aggregates dilate less than siliceous ones.

According to Mindeguia et al. (2010), the experiment had done with siliceous aggregates and observed that the water drops and vapor flow escaping from the samples. Moreover, severe damage of the samples was observed. Figure 3.16 the cracking and the aggregate surface spalling of a sample after a test. This important damage (i.e. cracking and aggregate spalling) can be explained by the instable behaviour at high temperature of the flint aggregates used in the concrete mixtures. Complementary high temperature tests were carried out on flint aggregates (without cement paste).

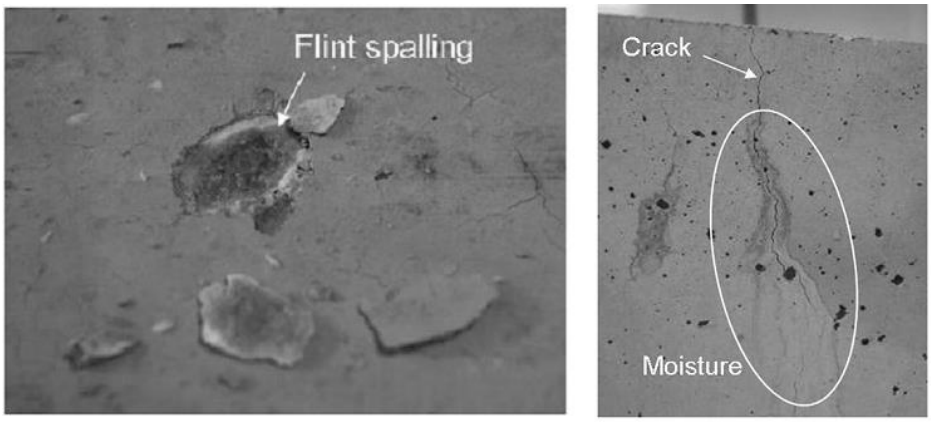

Figure 3.16: Aggregate (flint) spalling on the heated surface (a). Cracking and moisture marks on the lateral face (b) (Mindeguia et al., 2010).

They confirmed the fact that the flint aggregates used in the concrete mixtures are thermally unstable from 120°C to 200°C. This behaviour is explained by the high temperature cleavage of flint, which can be due to high vapor pressures that build up into the own laminar microstructure of the aggregate (Mindeguia et al., 2010).

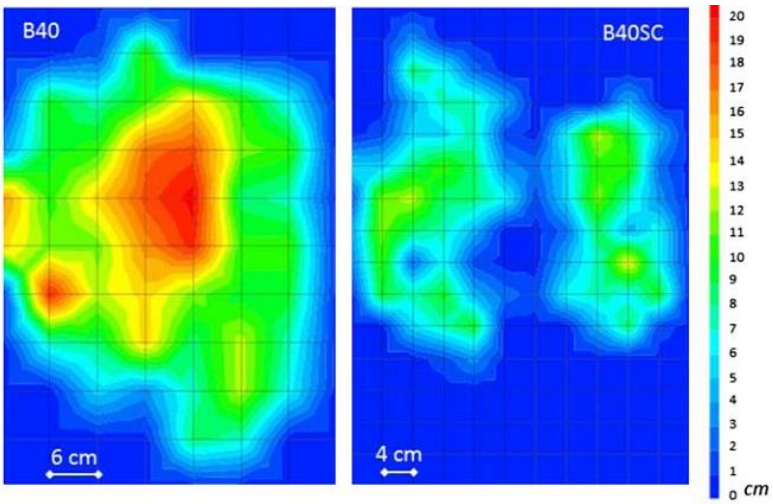

Figure 3.17: Surface mapping of spalling after one hour of ISO fire test. B40 (calcareous gravel) slab on the left, B40SC (silico-calcareous gravel) slab on the right (Mindeguia et al., 2013).

Mindeguia et al. (2013), found that the amount of spalling for the concrete made with silico-calcareous aggregates with flint (B40SC) is lower than the concrete made with purely calcareous (limestone) aggregates (B40). Figure 3.17 compares, with the same scale, the mappings of the measured spalling on a B40 slab and on the B40SC slab that showed spalling. This result was not expected. Indeed, previous research has shown that spalling of corners of columns exposed to the standard fire curve ISO 834-1 was higher in concrete containing flint compared to concrete made with calcareous aggregates (Pimienta et al., 2010). Here, we observe that a certain type of instable aggregates (flint) may reduce the slabs spalling. However, it is necessary to emphasize the importance of taking into account the cracking and then the material damage caused by the presence of aggregates thermally unstable, in order to provide a reliable assessment of the risk of spalling.

3.3.5 PRESENCE OF POLYPROPYLENE FIBRES

A major recent development in the prevention of explosive spalling has been in the discovery of the beneficial effect arising from the inclusion of Polypropylene fibres in the concrete mix. According to Kalifa et al. (2001) pp-fibres melt at 170^{o}C, turn into vapor at 341^{o}C, and the burning point 457^{o}C as shown on the thermo gravimetric (TGA) and differential thermal analyses (DTA) reported in Figure. 3.18.

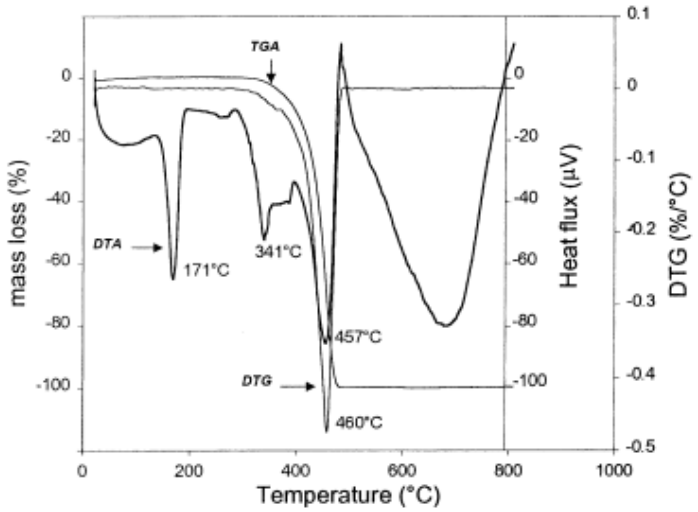

Figure 3.18: DTA, TGA, and differential thermo gravimetric analysis (DTG) of pp-fibre (Kalifa et al., 2001).

When pp melted and partially absorbed by the cement matrix, the fibres leave a pathway for gas. So they contribute to the creation of a network more permeable than the matrix, which allows the outward migration of gas and results in the reduction of pore pressure. The tests were performed on concrete average strength 105–110 MPa and the fibre dosage ranged between 0 and 3 kg/m^3. It was shown that fibres had a good efficiency against spalling even at dosages as low as 0.9 kg/m^{3}in the tested conditions.

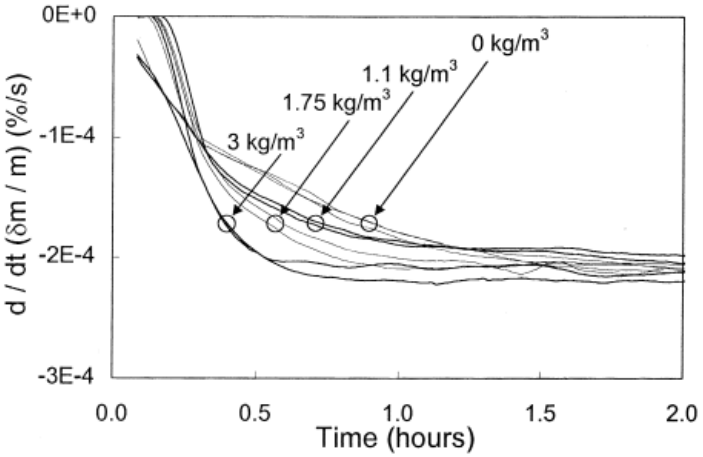

Figure 3.19: Rate of mass loss versus time for various fibres dosages (Kalifa et al., 2001).

Figure 3.19 shows that the rate of mass loss increases with increasing fibre dosage. This effect is significant although it is largely attenuated by the fact that at a given time, the thickness of the zone affected by the drying–dehydrating process is low (typically 20 mm) with respect to that of the specimen (120 mm). The increase in the rate of mass loss with fibre dosage brings to light the contribution of the fibres in the creation of a connected network for the outward transfer of water.
However, the global temperature rise does not depend on fibre dosage. The temperature rise exhibits a plateau-like disturbance that starts above 100°C and ends between 160°C and 200°C, which is close to the melting point of the fibres. In the plain concrete, this disturbance ends around 250°C Figure 3.20 (left) (Kalifa et al., 2001).

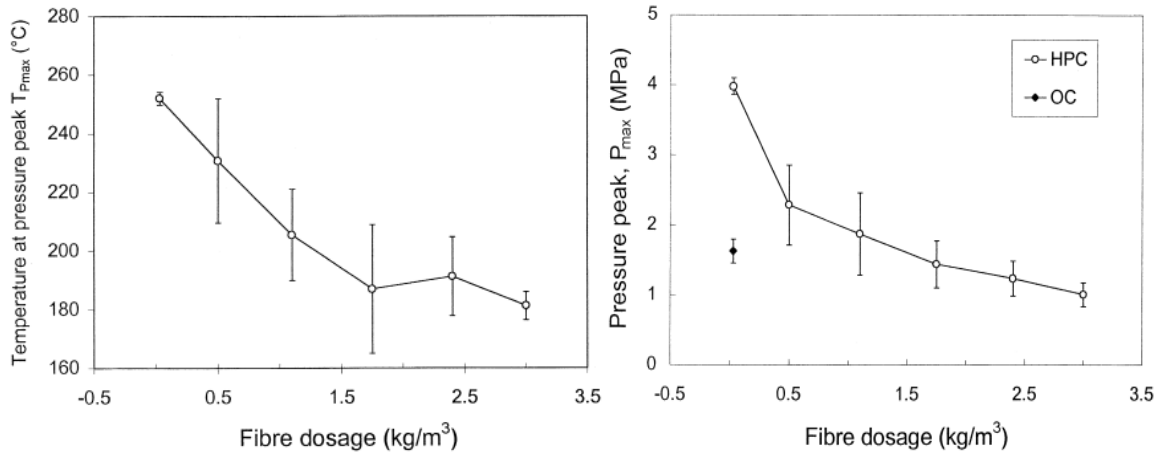

Figure 3.20: Temperature at pressure peak versus fibre dosage (left) and pressure peaks versus fibre dosage (right) (Kalifa et al., 2001).

The peak pressure decreases with increasing of fibre dosage, (Figure 3.20 (right)) and the pressures peaks appear at a temperature close to the melting temperature of pp (171°C) and far below its temperature of vaporization (341°C). It was mentioned earlier that pp dilates by about 10% when melting; this reduces the volume available for the transfer of gas and fluid. It is very unlikely that fibres can be evacuated from the specimen before the pressure peak, except for those with an end in contact with a free surface of the specimen. However, fibres appeared to be prevented from spalling at dosages as low as 0.9 kg/m^3, which is far from the percolation threshold. Also, the distribution of fibres in the concrete may not be very homogeneous, so that the effective percolation threshold is probably reached at a fibre dosage higher than the theoretical value.
The most interesting and surprising aspect of these observations stems from the comparison between the two concretes at 400°C: the fibre concrete exhibits a much higher crack density than

the plain concrete, as shown on Figure 3.21. In the fibre concrete, cracks are very thin (close to 1 μm) and form a dense network between and around the sand and aggregate skeleton. On the other hand, in the plain concrete, cracks are thicker (around 10 μm) and cover a large distance by linking the bigger aggregates.

On the other hand the behaviour of fibres after melting observation with a scanning electron microscope (SEM) were done on polished surfaces taken from the core of 5 X 5 X 10 cm^3 concrete specimens that were exposed to a temperature ranging between 160°C and 200°C for at least 6 h. These observations showed that as soon as temperature exceeds the fibre melting point (171°C) the fibres are not visible anymore in their initial bed (Figure 3.22). This brings out that the polymer was absorbed by the porous network despite the large size of the molecules compared to pore diameter.

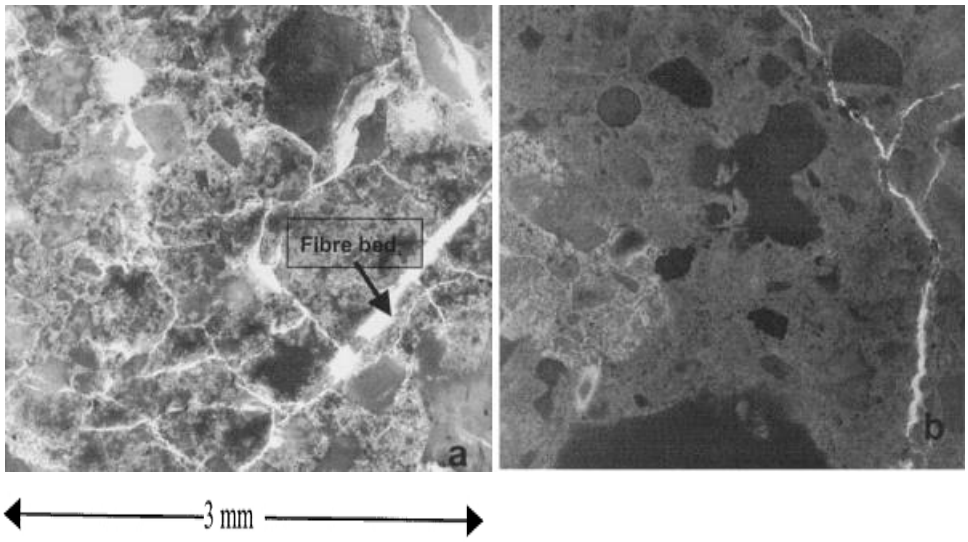

Figure 3.21: (a) Fibre concrete (α_f = 3 kg/m^3) and (b) plain concrete after 400°C treatment. The images represent a polished surface impregnated with fluorescent resin and observed under blue and polarized light. Cracks and fibres filled with the resin appear in white (Kalifa et al., 2001).

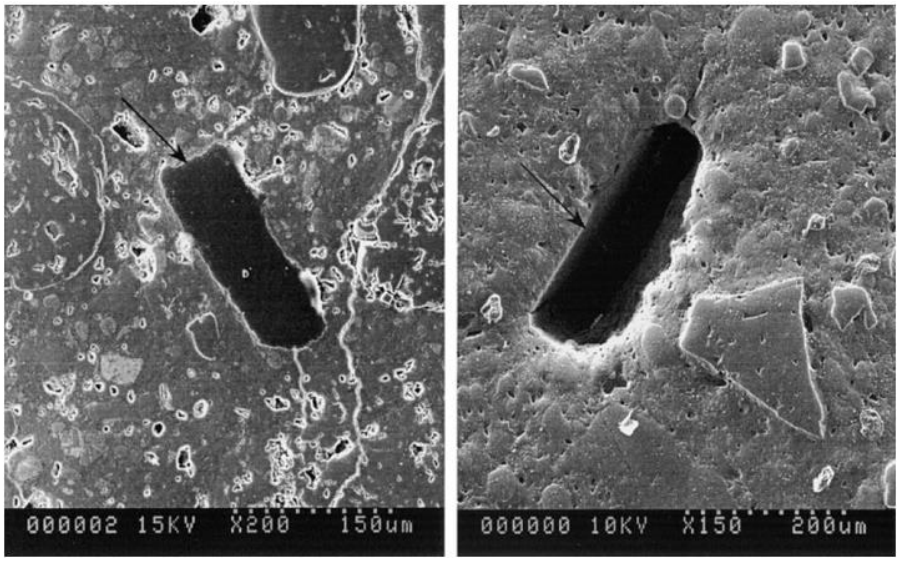

Figure 3.22: Cross-section of a fibre observed through an SEM. The fibre is visible at initial state (left) but the polymer disappeared after a 200°C treatment (right) and only the fibre bed is visible (Kalifa et al., 2001).

Finally, on the fact that pp fibres have been used in HPC constructions at a dosage of 2 kg/m^3 with the intention of reducing the concrete spalling sensitivity. Besides, fire tests carried out on columns and reported elsewhere showed that fibres had a significant effect at dosages as low as 0.9 kg/m^3, which is far below the theoretical percolation threshold. Also, PTM (Pressure Temperature Measurement) tests carried out on fibre HPCs showed that fibres have a striking effect on the pressure fields that built up in the porous network during heating: as fibre dosage increased from 0 to 3 kg/m^3, pressure peaks were reduced by a factor of 4 and pressure gradients were reduced by a factor of 2. These effects were mostly pronounced between 0 and 1.75 kg/m^{3}and less pronounced between 1.75 and 3 kg/m^3 (Kalifa et al., 2001). Considering the theoretical work by Garboczi et al., (1995), this change in fibre effect around 1.75 kg/m^3 may be related to the fact that fibres have reached the percolation threshold at that dosage. Finally, pressure measurements as well as permeability measurements suggest that a dosage around 1 kg/m^3 should be sufficient for this type of concrete (average strength 105–110 MPa) and this range of heat solicitation. This may not apply to other types of concrete, with other aggregate size distribution or with greater pore refinement, as in UHPC, in which the percolation threshold is probably at a minimum.

CHAPTER - 4

EXPERIMENTAL CAMPAIGN

Concrete members exposed to fire undergo high thermal gradients, due to concrete low thermal diffusivity, and pressure build-ups, because of the gradual evaporation of water in the pores. The latter is the main driving force for mass transfer, leading to both progressive drying close to the surface and vapour migration toward the cold core of the member. As a result, a quasi-saturated layer is formed where pressure peak develops, because of reduced gas permeability (Kalifa et al., 2000). This phenomenon is even more severe along symmetry planes, where moisture transport is impossible. Examples are concrete cylinders and spheres, whose higher sensitivity to spalling comes also from the curved shape of the isostatics (Debicki et al., 2011). Another example is the thin web in precast I-beam (Figure 4.1), which may exhibit delamination's and even through holes after a fire, in spite of the limited time required to dry. This latter example is the starting point of the approach adopted in the following (Felicetti et al., 2012): the mono-dimensional thermo-hygral transient occurring in a thin web (Figure 4.1b) can be re-created by properly heating concrete cubes (Figure 4.1c), to check concrete fracture response along the symmetry plane. This scheme involves the problem of heating two opposite faces and to prevent any thermal and mass flow through the lateral faces, as will be discussed.

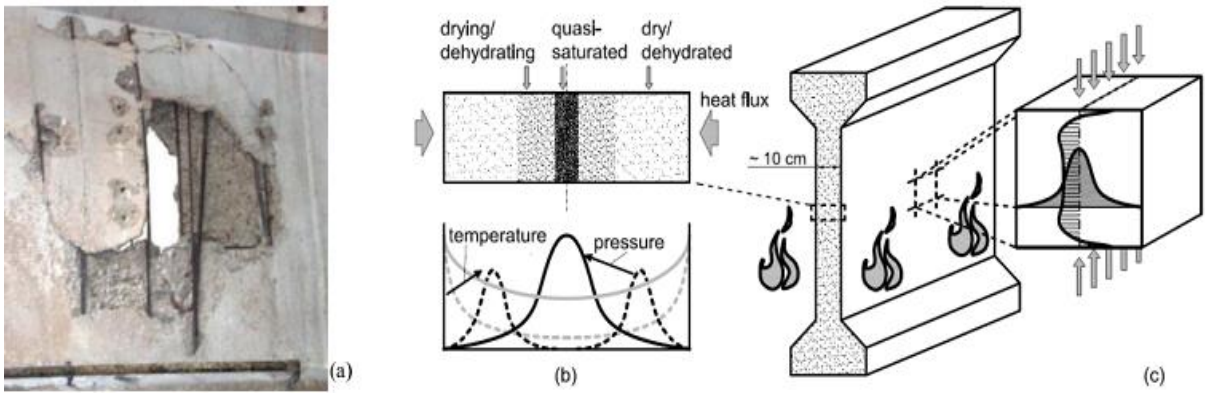

Figure 4.1: Thin web in a fire-exposed I-beam: (a) through hole, (b) temperature, pressure and moisture plots in the web during the heating process and (c) specimen philosophy.

On the contrary, the significant thermal stress which develops in the actual structure is substantially smoothed down in the proposed test, to limit the investigation to the role that pore pressure has in reducing the apparent tensile strength of heated concrete. Testing in tension is performed by splitting (according to UNI EN 12390-6, 2000), which requires a rather simple test setup and can be easily implemented in the case of hot specimens; contrary to bending tests, this technique brings in far less structural effects, with an almost constant ratio between the indirect tensile strength and the true tensile strength (Bamonte and Felicetti, 2007).

4.1 EXPERIMENTAL SET-UP (PORE PRESSURE MEASUREMENT AND SPLITTING TEST)

In this experimental campaign, we proposed the description of the individual components and experimental procedures implemented in order to evaluate the influence of pore pressure on the apparent tensile strength of the high performance concrete (Plain concrete: 95-S, 70-S and Fibre concrete: 70-S-Pm with pp-fibre dosages of 0.5, 1 and 2 Kg/m^3) being examined.

4.1.1 MATERIALS AND CONCRETE MIX DESIGNS

This experimental campaign includes 5 concrete mixes, differing for their compressive strength; type and content of fibres. The cement type and class were selected in order to keep the volumetric fraction of the cementitious matrix as constant as possible. CEM I, 42.5 R was used in combination with Ground Granulated Blast Furnace Slag (GGBS), as shown in Table 4.1 (Rossino et al., 2013). Two concrete grades are considered with $f_{cm,cube}$≥ 70 and 95 MPa (determined at 28 days on 100 mm-side cubes), whose mix design includes silico-calcareous (SC) aggregate (Mixes 70-S, 95-S). For the intermediate strength class ($f_{cm,\ cube}$ ≥ 70 MPa), pp fibers have been added. Polypropylene fibers are monofilament fibers (mnf, L = 12 mm; $\varnothing_{eq}$ = 20 µm, extruded straight fibers treated with a surfactant agent), designed specifically to prevent concrete spalling [46,47]. Monofilament fibers come in three contents: 0.5, 1.0 and 2.0 kg/m^3 (Mixes 70-S-Pm 0.5, 70-S-Pm 1 and 70-S-Pm 2, respectively). The aggregate-type is silico-calcareous. The 5 mixes and their properties at the fresh state, as well as their compressive strength at 28 days, are reported in Table 4.1 (see [48, 49, and 50] for the testing procedures). In the mix designs, the binder is a combination of CEM I and GGBS. The surfactant agent covering the monofilament pp fibers is responsible for the decrease of the density at increasing values of the fiber content (see Table 4.1). Cubes with 100 mm-sides were cast to investigate the microstructure and to measure pore pressure, while cylinders (Ø = 150 mm, h = 300 or 50 mm) were

used to evaluate the compressive strength at 28 days or to measure vapor permeability.

Table 4.1: Mix designs and mechanical properties of the concretes.

Mix No	1	2	3	4	5
Mix designation	95-S	70-S	70-S-Pm 0.5	70-S-Pm 1	70-S-Pm 2
CEM I (kg/m^3)	480	400	400	400	400
GGBS (kg/m^3)	300	200	200	200	200
SC gravel^ (kg/m^3)	821	860	860	860	860
SC aggr^^ (kg/m^3)	667	699	699	699	699
pp mnf (kg/m^3)	-	-	0.5	1	2
sp (kg/m^3)	12.79	2.76	2.76	2.76	2.76
w/b ratio	0.24	0.36	0.36	0.36	0.36
$\rho_{fresh\ state}$ (kg/m^3)	2440	2390	2380	2370	2350
$f_{cm,,cyl}/f_{cm,\ cube}$ (MPa)	90/99	62/72	63/70	60/70	60/69

Note : sp = acrylic superplasticizer; w = water; b = binder; ρ = density; (^) d_a = 0-8 mm; (^^) d_a = 8-16 mm; $f_{cm,\ cyl}/f_{cm,\ cube}$ = concrete compressive strength on cylinders/cubes at 28 days.

All specimens were cured in water for 28 days according to [44]. The cubes were later kept at 10°C for further 28 days, in order to slow down the hydration process.

4.1.2 EXPERIMENTAL PLAN

To better understand the experimental plan of this research work on HPC, detail description of the plan is given in Table 4.2.

Table 4.2: Experimental plan for the measurement of pore pressure.

	Mix	Mass loss	Tensile strength (virgin)	Pressure Measurement		Heating rate (^{o}C/min)
				Prove with sealing	Prove without sealing (dry at temp. 50^o C)	
Plane concrete (PC)	95-S	2	3	7	2	0.5 with 9
	70-S	2	3	9	3	2 with 3 1 with 1 0.5 with 8
pp Fibre Concrete	70-S-Pm 0.5	2	3	7	3	0.5 with 10
	70-S-Pm 1	2	3	6	3	2 with 1 0.5 with 8
	70-S-Pm 2	2	3	7	3	1 with 2 0.5 with 8

4.1.3 HEATING SYSTEM

The heating system consists of two radiant panels (Figure 4.2a) placed on two opposite faces of the concrete cubes (Figures 4.2b and 4.2c), in order to guarantee the symmetry heating with respect to the mid-plane of the specimen. Radiant panels allowed to obtain a variety of heating rates (up to 120°C/min) thanks to the built-in thermocouples connected to separate controllers. Though the significance of the internal heater temperature is debatable, this allows repeatable testing conditions. For measuring the pore pressure of cubes during heating silicon oil was used inside the capillary steel pipe and it allow better transmission of pore pressure. But silicon oil can enter the probe through the capillary steel pipe during heating and create perturbation to measure the pore pressure. So to avoid the problem related to measuring of pore pressure, the capillary steel pipe was filled with half of silicon oil on the T-connector side and half of air on the probe side (inside the concrete Figure 4.2c,d).

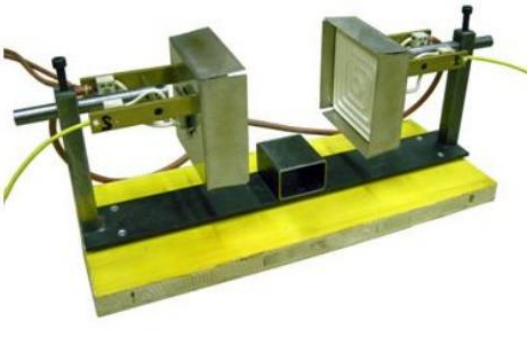

(a)

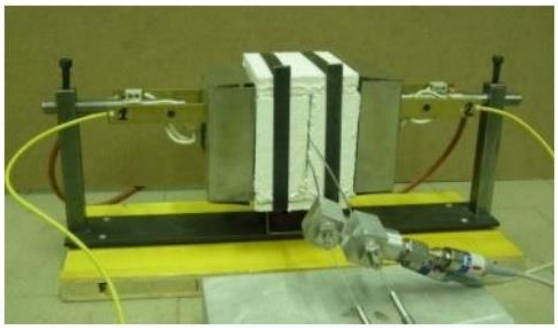

(b)

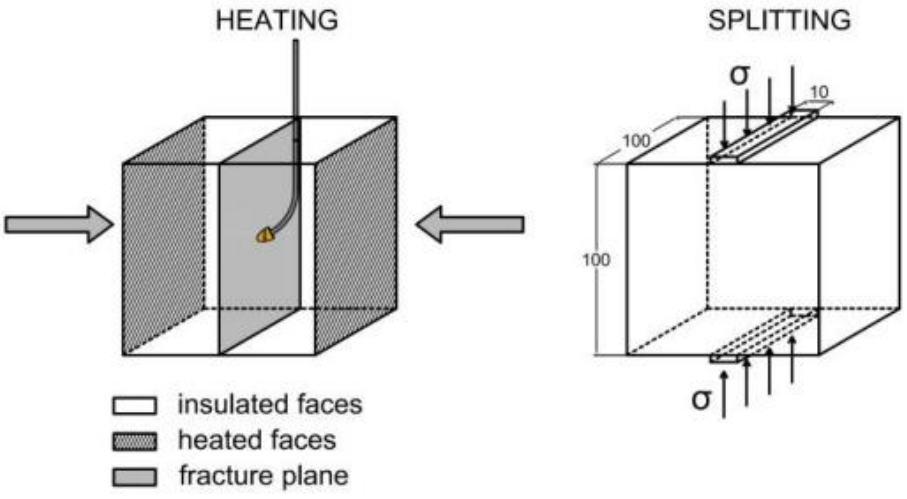

(c)

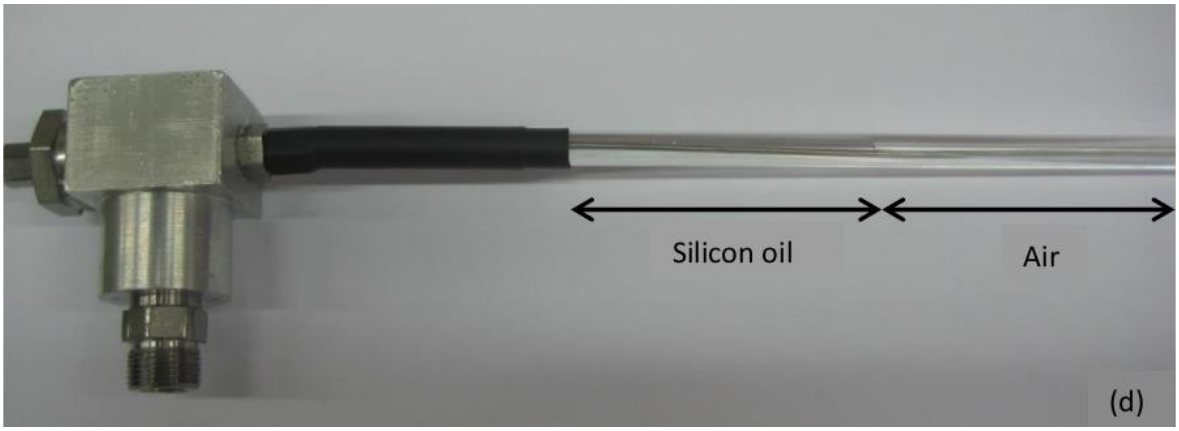

Figure 4.2: (a) Heating system, (b) insulated specimen during heating, (c) scheme of heating and splitting, and (d) separation of silicon oil and air.

4.1.4 SEALING

Sealing is fundamental in creating a mono-dimensional hygral flux, by preventing the specimen from drying through the lateral faces. To seal the specimen epoxy resin (DP 760 by 3M) with aluminium foils was used. In this method epoxy glue smeared was placed on aluminium foils papers to avoid the formation of air bubbles during heating that may be caused by vapour pressure acting on specimen surfaces. The aluminium foils on opposite two faces were cut in the splitting plane, to prevent any contribution to the tensile strength of the cube, Figure 4.3a; then the thin cuts were sealed with silicon, Figure 4.3b.

(a)

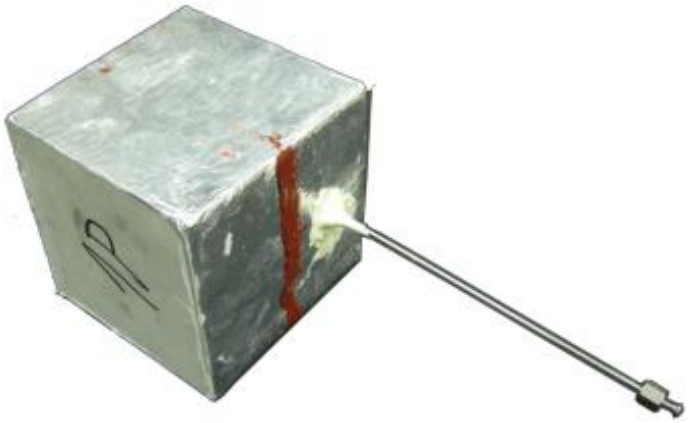

(b)

Figure 4.3: Cut of aluminium foils (a) and sealed with red silicon glue (b).

4.1.5 INSULATION

Thermal insulation is necessary to create a mono-dimensional heat flux; hence, the four cold faces were covered with 20 mm-thick insulating layer of ceramic fibre material (Figure 4.4).

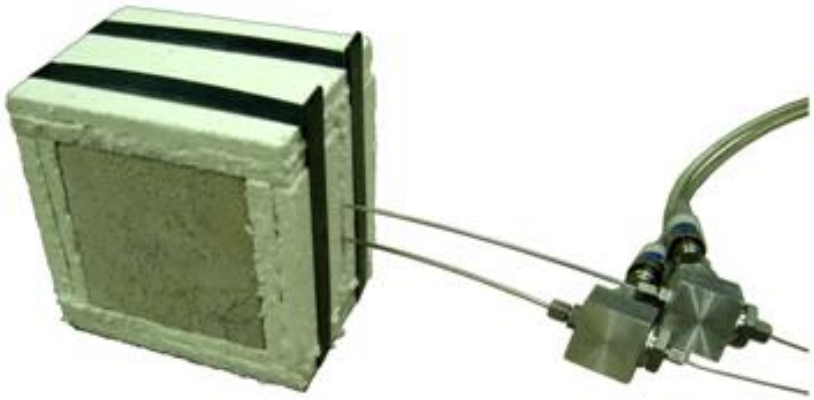

Figure 4.4: Sealed and insulated specimen ready for heating.

4.1.6 HEATING RATE

The choice of the heating rate is quite critical: very high heating rates cause severe damage (i.e. microcracks) in the concrete due to thermal stresses (hence, low values of pore pressure, the vapour being free to escape through the microcracks), while very low heating rates cause significant drying (leading, again, to low values of pore pressure). In order to understand the effect that the heating rate has on high performance concrete with regard to pore pressure and thermal stresses, some preliminary experiments (to understand the order of magnitude of pore pressure) were performed.
To investigate the role played by heating rate in concrete hot behaviour, three different heating rates were applied: a slow heating (0.5 and 1°C/min) and intermediate heating rates (2°C/min). After that the external temperature reached 600°C, the temperature was kept constant.

4.1.7 MEASUREMENT OF PORE PRESSURE AND TEMPERATURE

The specimens were instrumented with a single gauge placed at the centred of the cube, for simultaneous pressure and temperature measurements, Figure 4.3b. The measurement of the pore pressure and temperature were performed by using capillary steel pipes (inner diameter 1.5 mm), fitted with sintered metal heads, Figure 4.5. Great attention was paid to the shape of both the head

and the pipe, in order to affect in the least possible way concrete mechanical response. Aggregate-shaped heads and curved steel pipes were used, in order to prevent the probes from lying in the mid-plane of the cube (that is the fracture plane in the splitting test, Figure 4.2c). The pipes were filled with silicon oil and had a thermocouple inside (diameter 1.0 mm). Hence, both pressure and temperature inside the head of the probe were measured. The system target temperature was decided to be 600^{o}C and the controlling device was set accordingly.

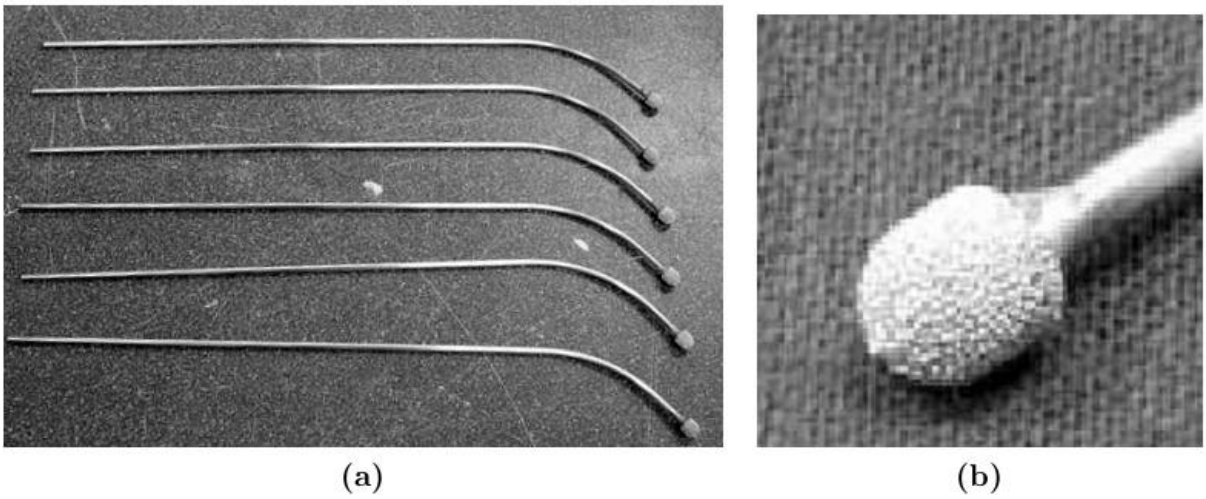

Figure 4.5: Probes for pressure measuring: (a) capillary steel pipe and sintered metal head, (b) detail of sintered metal head.

4.1.8 COLD TESTS

In order to define the reference tensile strength in virgin condition, splitting test were performed on unheated specimens (6 plains- and 9 fibres-concrete).

4.1.9 HOT TESTS

A total of 50 specimens (21 plain- and 29 fibre-concrete) were tested, by applying 3 different heating rates:(a) 0.5°C/min (17 plain-concrete and 26 fibre-concrete), (b) 1°C/min (1 plain- and 2 fibre-concrete), and (c) 2°C/min (3 plain- and 1 fibre-concrete).

During heating, both pressure and temperature were monitored in the centroid of the cubic specimen; when the maximum pore pressure was reached, the specimen was brought (in about two minutes) under the press for the splitting test, while continuously measuring pressure and temperature. The data acquisition was achieved by using two different software, where first one is

for measuring temperature and pore pressure and the second one is for splitting test to measure the pore pressure and the failure load. As for positioning, the specimens were placed centrally in the loading frame with regards to the marks and the packing strips had been already stacked by using adhesive tape. Samples mounted on the loading frame were arranged in a way that the loading direction was perpendicular to the casting direction, Figure 4.6. The loading rate was determined according to UNI EN 12390-6, 2010. As a result, the tensile splitting test strength of specimen was calculated by Equation:

$$f_{ct} = \frac{2*F}{L*d*\pi} \tag{4.1}$$

Where,

f_{ct} is tensile splitting strength in MPa, L is the length of specimen in mm, d is designated dimension of specimen in mm, and F is the maximum load in N.

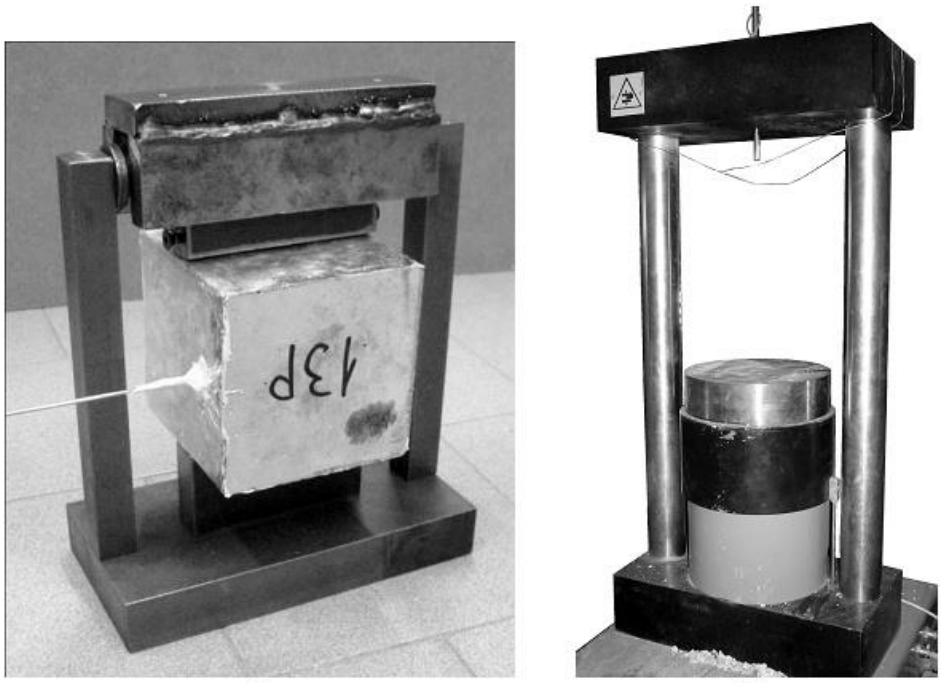

(a) (b)

Figure 4.6: System for the splitting test: (a) the specimen placed on the supporting frame and (b) hydraulic press used for the imposition of the load.

4.2 MICROSTRUCTURE AND THERMAL PROPERTIES ANALYSIS

The phisyco-mechanical processes triggering concrete explosive spalling are related to the heat-induced micro- and meso-structural changes. To have new information on concrete properties at the microstructural level, as well as on how concrete spalling sensitivity is affected by polypropylene fibres, ordinary and high-performance concretes were investigated in an external laboratory, after being heated to different temperatures. In this study, also another mix (normal strength concrete, 45-S) was investigated. The study was focused on the relationship among porosity, vapor permeability, thermal diffusivity, pore pressure and microcracking inside the cementitious matrix. The same mixes above discussed are involved. The mix design of HPC was discussed in the section 4.1.1, the materials and mix design of normal strength concrete (45-S) are given in Table 4.3.

Table 4.3: Mix design of normal strength concrete

CEM I (kg/m^3)	400
calc. Filler (kg/m^3)	200
SC gravel^ (kg/m^3)	883
SC aggr^^ (kg/m^3)	610
sp (kg/m^3)	1.8
w/c ratio	0.56
$\rho_{fresh\ state}$ (kg/m^3)	2340
$f_{cm,,cyl}/f_{cm,\ cube}$ (MPa)	40/47

Note : sp = acrylic superplasticizer; w = water; c = binder; ρ = density; (^) d_a = 0-8 mm; (^^) d_a = 8-16 mm; $f_{cm,\ cyl}/f_{cm,\ cube}$ = concrete compressive strength on cylinders/cubes at 28 days.

4.2.1 EXPERIMENTAL TECHNIQUES

In order to characterize the mixes from the microstructural point of view and to investigate heat-induced effects, several experimental techniques were used:

• Scanning Electron Microscopy (SEM): both polished sections and fractured surfaces were examined by means of a Zeiss EVO MA15 (thermoionic source in Lanthanum hexaboride LaB_6);

• Mercury Intrusion Porosimetry (MIP) by means of Pascal 140 and 240 porosimeters (Mercury intrusion rate = 5 and extrusion rate = 6);

First of all, small cylinders (Ø = 20 mm, h = 100 mm) suitable for microstructural analysis were cored from a number of concrete cubes. The tests were performed in residual conditions considering five target temperatures: 20 (reference temperature), 105, 250, 500 and 750°C. The specimens were heated inside an electric furnace (heating rate = 1°C/min); once the target temperature was reached, that temperature was kept constant for 2 hours, followed by the cooling phase (cooling rate = -0.25°C/min down to 200°C and then natural cooling inside the closed furnace). So far, the tests had been performed on Mixes 45-S, 70-S, 70-S-Pm1, 70-S-Pm2 and 95-S.

On the other hand concrete samples were characterized from the physico-mechanical point of view by measuring pore pressure and permeability on virgin specimens (20°C, at 28 days, according to [40]).

4.2.2 DIFFUSIVITY TEST

The proposed test method is to analyse the temperature differentials induced by a slow heating ramp within a slender concrete cylinder (Ø= 100 mm - L/Ø= 3). This length to diameter ratio guarantees a negligible effect of the specimen ends on the temperature field of the central cross-section, which can be assumed to be a function of just the radial distance from central axis. The specimen is instrumented with two thin shielded thermocouples, placed at the centre and at 5 mm from the lateral surface (Figure 4.7). These small sensors are preliminarily tied to the mould with nylon wire and after casting they remain embedded in the concrete, giving no significant disturbance to the thermo-hygral response of the material. The test is performed in a common electric furnace regulated by a ramp generator and a closed-loop controller. In order to harmonize the boundary condition with the axisymmetry of the problem, the specimen is positioned into a cylindrical steel sleeve, which levels any difference in the radiation from the heating elements. A more accurate time response of the system may be obtained by fitting the sleeve with one further thermocouple, to be connected to the furnace controller.

The test is run by slowly heating the furnace at constant rate (R = 1.0°C/min for Ø = 100 mm). This value comes from the compromise between the two conflicting requirements of measuring a sizeable temperature differential between the embedded thermocouples (usually 20-30°C) while being still able to assign a reference temperature to the material sample at each stage during the test. In case of a different specimen size, the temperature differential is expected to rise with the diameter squared and then the heating rate should be adjusted accordingly.

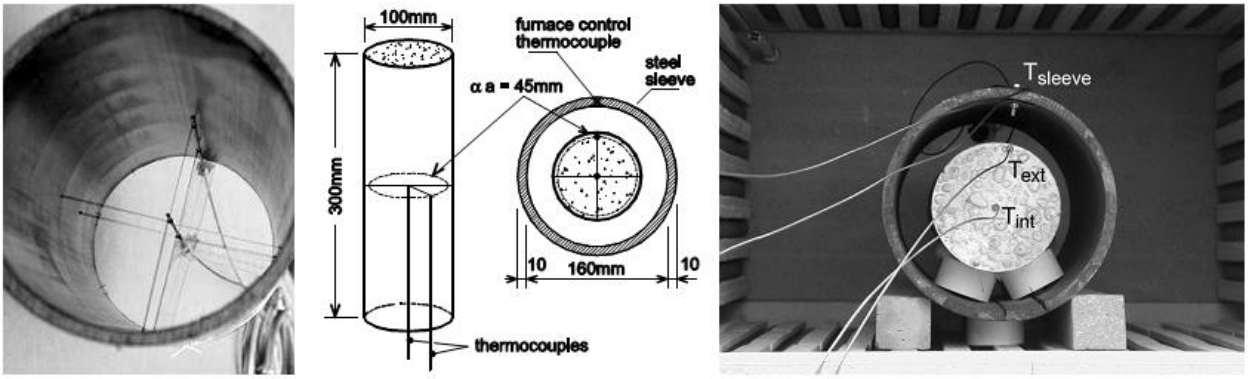

Figure 4.7: Cylindrical mould fitted with two thermocouples, specimen geometry and test setup for the measurement of the temperature transient in the cylinder.

The main outcome of the experimental test is a time plot of the temperature difference T_{ext} - T_{int} between the two thermocouples embedded in the concrete specimen. For the interpretation of the results, the axisymmetric problem of an infinitely-long cylinder, with no internal heat sources or sinks, is considered. In this case, the differential equation governing the transient heat conduction is the following:

$$\rho c.r\ \frac{\partial T}{\partial t} = \frac{\partial}{\partial r}\left(\lambda.r\frac{\partial T}{\partial r}\right) \cong\ \lambda.\left(\frac{\partial T}{\partial r} + r\frac{\partial^2 T}{\partial r^2}\right) \tag{4.2}$$

where the material properties (ρ = density, c = specific heat, and λ = thermal conductivity) may be combined in a single parameter (namely the thermal diffusivity D = λ/ρc) under the reasonable assumption of spatially invariant (or smoothly changing) thermal conductivity. In the case of constant D, if the outer surface of radius a is heated at constant rate R starting at time t = 0, the closed-form solution for the temperature difference ΔT between two measuring points located on the central axis and at a radial distance α·a is:

$$\Delta T(t) = T_{ext} - T_{int} = \frac{Ra^2}{4D}.\left(\alpha^2 - 8.\sum_{i=1}^{N}\frac{1-J_0(\alpha z_i)}{z_i^3.J_1(z_i)}.e^{-D\left(\frac{z_i}{a}\right)^2.t}\right) \tag{4.3}$$

where J_0 and J_1 are the Bessel function of the first kind and z_i are the zeroes of J_0. Two separate components can be recognized in brackets in Equation 4.3: a steady state parabolic temperature distribution, ruled by the dimensionless radius α, and a start-up transient which can be neglected for sufficiently high values of the dimensionless Fourier's time F_o= D t /a^2 (F_o>0.5, i.e. t> 30 min for

a = 50 mm). If only the first term is considered, the thermal diffusivity can be worked out from the experimentally measured temperature difference ΔT:

$$D(T_m) \cong R\,(\alpha \cdot a)^2 / 4\Delta T\ ,\ \ T_m = (T_{int} + T_{ext}) / 2 = \text{mean temperature in the cylinder} \qquad (4.4)$$

The heating rate of the specimen surface cannot be strictly regarded as a constant and the nominal setting value of the furnace controller cannot be used in the analysis of the results. For this reason, the actual instantaneous heating rate R_{eff} should be determined from the time-history recorded at the two measuring points:

$$R_{eff} = \beta \cdot \dot{T}_{ext} + (1-\beta) \cdot \dot{T}_{int} \quad \text{, where } \beta \cong 1/4 \qquad (4.5)$$

4.3 PRELIMINARY EXPERIMENTAL CAMPAIGN

Under this campaign the influence of pore pressure on the apparent tensile strength of concrete experimental and numerical tests were performed on several concrete mixes with different heating rate. To better understand and to link with the present experiment on HPC, the experimental and numerical results are discussed below.

4.3.1 EXPERIMENTAL DESCRIPTION

The experimental work was performed in Milan in 2011 (see Felicetti et al., 2012). The concrete type B40, thoroughly investigated by Mindeguia et al. (2009), was used; the mix design is reported in Table 4.4. This concrete has a mechanical behaviour close to NSC, meaning that spalling is unlikely to occur. Two batches were cast: the former without and the second with monofilament polypropylene fibres (pp fibres; 2 kg/m^3, Table 4.5).

Table 4.4. Mix design.

Constituent	**Quantity [kg/m^3]**
Cement	347
8/12.5 Calc.	327
12.5/20 Calc.	714
0/2 Sand	838
Water	186
Additive [a/c]	Up to 1%
Fibre content	2 kg/m^3

Table 4.5. Fibre characteristics.

Monofilament Polypropylene Fibres	
diameter [μm]	18
length [mm]	12
melting temp. [°C]	170
vapour.temp. [°C]	340

Before heating the specimen sealing was done by three components which are epoxy glue, aluminum foils paper and silicon, see detail in section 4.1.4.

To investigate the role played by heating rate in concrete hot behaviour, four different heating rates were applied: a slow heating (1°C/min), two intermediate heating rates (2 and 10°C/min) and a fast heating (120°C/min, equal to the mean heating rate in the former four minutes of Standard Fire). In order to define the reference tensile strength in virgin condition, splitting tests were performed on unheated specimens (4 plain- and 6 fibre-concrete); moreover further six specimens (3 plain- and 3 fibre-concrete), previously dried in oven at 120°C for 16 days (weight loss ≈ 4 - 4.5%), were tested. Observing the results (Table 4.6), it is worth noting that, in terms of strength, there is no difference between plain-concrete and fibre-concrete in both virgin and dried conditions; on the contrary, drying process leads to a significant decrease in the splitting tensile strength (about 23% less).

Table 4.6: Reference tensile strength in virgin and dried specimens.

	Virgin specimens			**Dried specimens**		
	All	Plain	pp fibre	All	Plain	pp fibre
Mean [MPa]	3.60	3.66	3.56	2.76	3.66	3.56
Norm. st. dev. [%]	7.5	6.3	8.6	11.4	6.3	8.6

For the measurement of pressure, 22 specimens (16 plain-concrete and 6 fibre-concrete) were tested, by applying 4 different heating rates: (a) 1°C/min (2 plain-concrete), (b) 2°C/min (4 plain-concrete and 2 fibre-concrete), (c) 10°C/min (4 plain-concrete and 4 fibre-concrete) and, (d) 120°C/min (6 plain-concrete).

4.3.1.1 PORE PRESSURE TRENDS AT INCREASING TEMPERATURE

The experimental results of 22 tests for the 4 heating are shown in terms of temperature-time (Figure 4.8a) and pressure-time (Figure 4.8b) curves, while in Figures 4.9a-d the results are reported in terms of pressure-temperature together with the saturation vapour pressure curve, P_{SV} (Buck et al., 1981). The results confirm the pore pressure values obtained by Mindeguia et al. (2009).

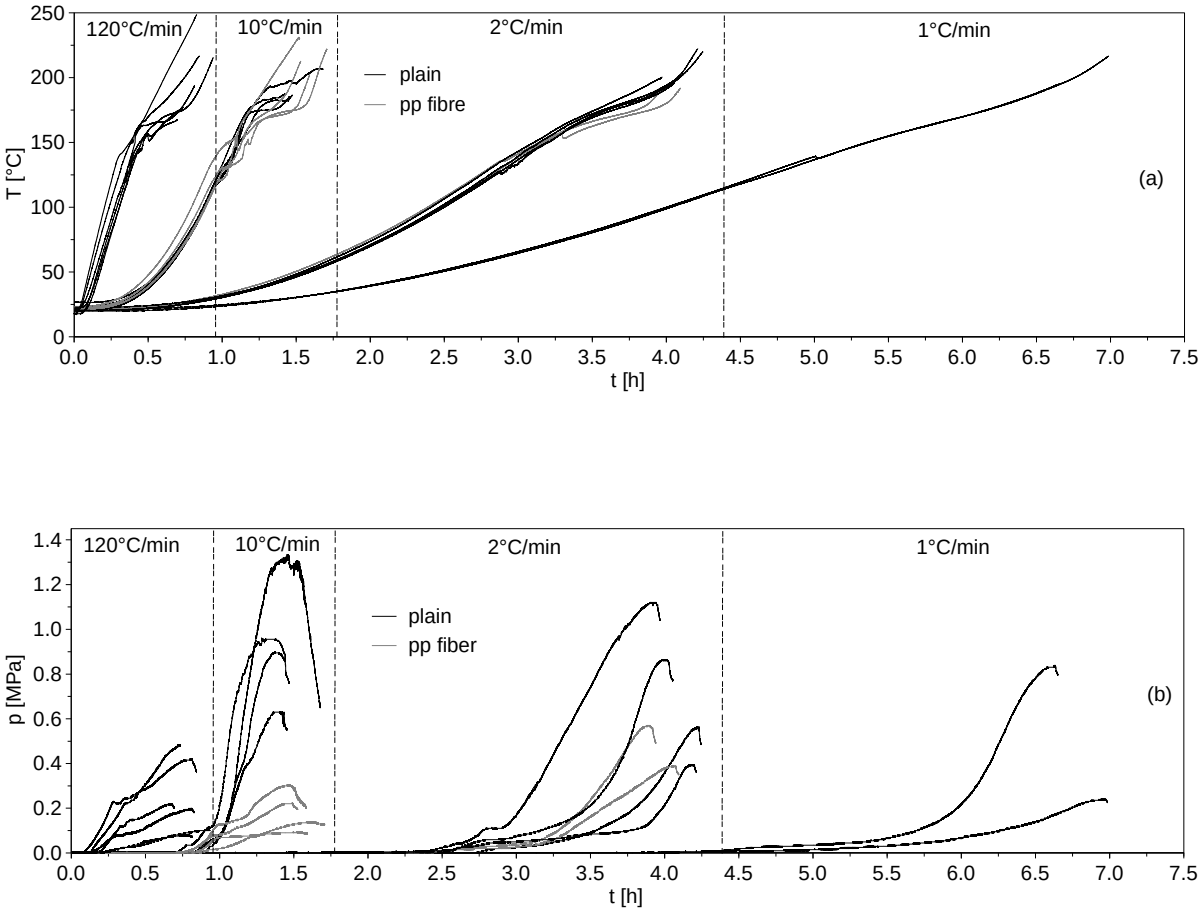

Figure 4.8: (a) Temperature development and (b) pressure development in the centroid as a function of time.

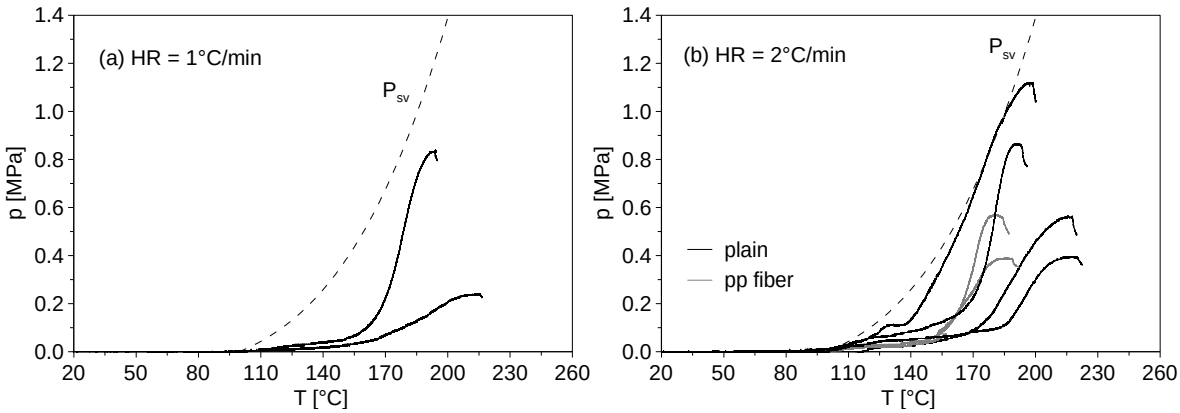

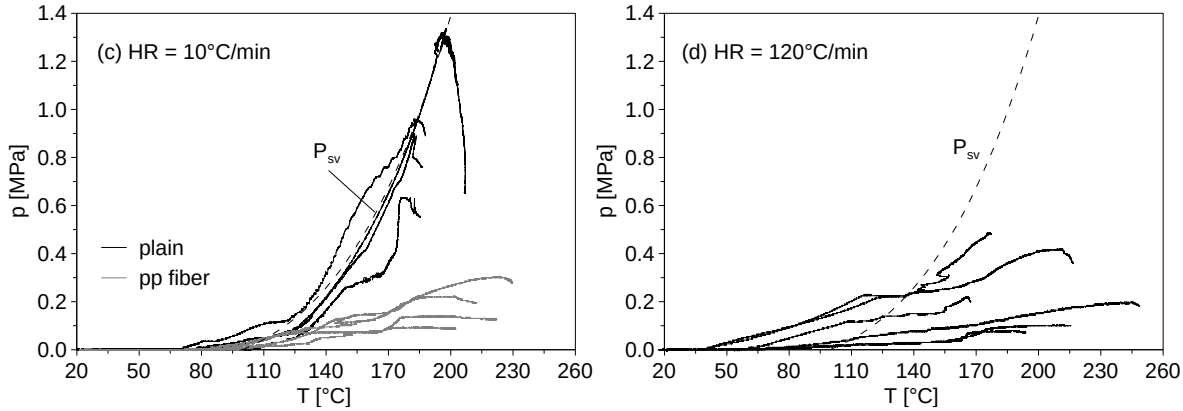

Figure 4.9: Saturation vapour pressure curve (P_{SV}) and pore pressure-temperature curves for the different heating rates: (a) 1°C/min, (b) 2°C/min, (c) 10°C/min and, (d) 120°C/min.

Experimental results underline four aspects:

•the qualitative development of pore pressure is similar for all the tests: the dramatic pressure rise occurs almost at the beginning of a plateau in the time-temperature curve (that corresponds to the beginning of water vaporization) and the peak is achieved at the end of this plateau;

•the irregular shape of the pressure-temperature curves for HR = 120°C/min (Figures 4.8b and 4.9d) seems to suggest concrete cracking, probably due to the thermal stresses (this is substantiates by the numerical results, see Section 4.3.2);

•intermediate heating rates (2 and 10°C/min) cause pore pressure plots to lie close to the saturation vapour pressure curve, whereas significant gaps were observed for slow and high heating rates (1 and 120°C/min), probably due to a more pronounced drying and cracking, respectively;

•fibre-concrete leads to lower pressures than plain-concrete (even more than 75% less);

•in the initial stage, there is a not-negligible overpressure caused by the partial pressure of the dry air in the pores media (this overpressure induced pore pressure to be higher than P_{SV}; Mindeguia et al., 2009).

The dispersion of the pressure peaks at the same nominal testing conditions can be ascribed to some variability among specimens in the effectiveness of the sealing system or in the moisture content. Nonetheless, this is functional for performing the fracture test under the same thermo-mechanical conditions but different pressures.

4.3.1.2 INFLUENCE OF PORE PRESSURE ON THE SPLITTING TENSILE STRENGTH

As mentioned before, splitting test was performed when maximum pore pressure was reached; this means that experiments had not been performed at a specific temperature.

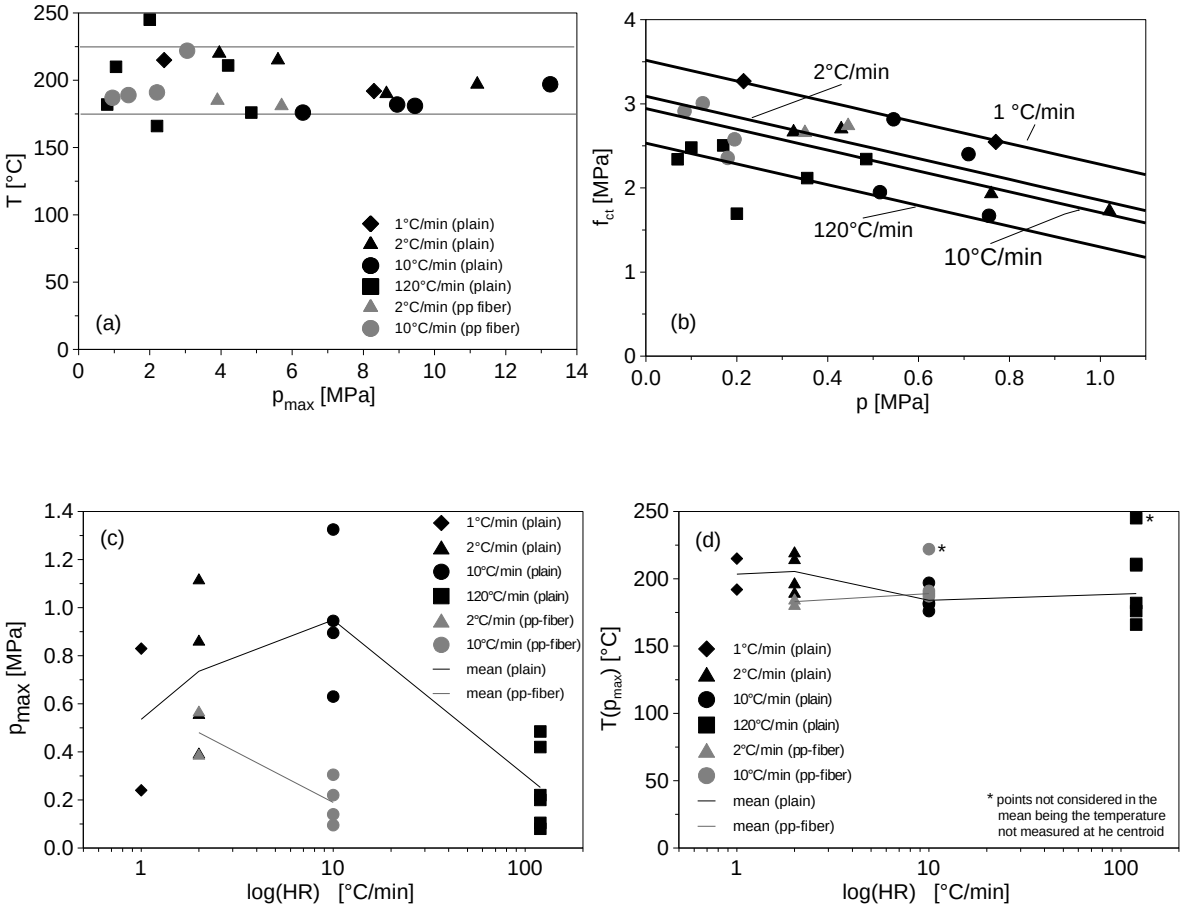

Figure 4.10: (a) Temperature at the peak pore pressure; (b) tensile strength-pore pressure plot; (c) peak pore pressure and (d) corresponding temperature as functions of the heating rate (HR).

However, peak pressures were achieved in a narrow range of temperature (175°C to 225°C), as shown in Figure 4.10a,d. Then, the possible chemo-physical decay of concrete may be assumed uniform in the whole set of specimens. The results obtained from the splitting tests are reported in Figure 4.10b as a function of the pressure measured during the test.

Considering only the data belonging to 2°C/min and 10°C/min a linear regression has been performed, obtaining a negative slope k = -1.24. The choice of considering only the two mentioned

heating rates for the linear regression was suggested by the large range of pressures covered by them with respect to the other heating rates. Then, for each heating rate, the barycentre of the data distribution $(p^{AV}, f_{ct}^{AV})_{HR}$ was evaluated and four straight lines with a slope equal to k and passing through these average points are plotted in Figure 4.10b.

The comparison between the values of tensile strength obtained experimentally, f_{ct}^{ex}, and theoretically, f_{ct}^{th}, by applying the linear model (four lines) is shown in Table 4.7. Mean value and standard deviation of the normalized error $(f_{ct}^{ex} - f_{ct}^{th})/f_{ct}^{ex}$ are 1.4 ± 12.8 % considering all the data (while are 0.1 ± 0.9, 0.9 ± 6.9, 1.9 ± 15.2 and 1.7 ± 17.8 % considering separately 1, 2, 10 and 120°C/min, respectively). These values are of the same order of magnitude of the standard deviation of the tensile strength measured in virgin condition (Table 4.6), underlining the reliability of the proposed linear model. Hence, it can be inferred that the detrimental effect of pore pressure on the indirect tensile strength is almost independent on the heating rate and it revealed to be linear and proportional to a value close to k = 1.24.

Table 4.7: Experimental and theoretical tensile strength (f_{ct}^{ex} and f_{ct}^{th}, respectively) at the pressure p measured during the splitting test, for the different heating rates; in particular: (a) 1°C/min, (b) 2°C/min, (c) 10°C/min and, (d) 120°C/min.

Spec./HR	p [MPa]	f_{ct}^{ex} [MPa]	f_{ct}^{th} [MPa]	Spec./HR	p [MPa]	f_{ct}^{ex} [MPa]	f_{ct}^{th} [MPa]
23 P/(a)	0.22	3.27	3.25	9 P/(c)	0.52	1.95	2.30
20 P/(a)	0.77	2.55	2.56	35 Fi/(c)	0.18	2.36	2.72
15 P/(b)	0.76	1.93	2.15	31 Fi/(c)	0.13	3.01	2.79
26 P/(b)	1.02	1.73	1.83	38 Fi/(c)	0.20	2.58	2.70
10 P/(b)	0.43	2.70	2.56	37 Fi/(c)	0.09	2.91	2.84
19 P/(b)	0.33	2.66	2.69	22 P/(d)	0.20	1.69	2.28
41 Fi/(b)	0.45	2.74	2.54	17 P/(d)	0.07	2.34	2.44
40 Fi/(b)	0.35	2.66	2.66	16 P/(d)	0.49	2.34	1.93
7 P/(c)	0.55	2.82	2.27	18 P/(d)	0.36	2.12	2.09
8 P/(c)	0.71	2.40	2.06	21 P/(d)	0.17	2.50	2.32
6 P/(c)	0.76	1.67	2.01	25 P/(d)	0.10	2.48	2.41

On the other hand, the intercept of the lines strongly depends on the heating rate (see Table 4.8). This is the combined effect of the possible internal deterioration due to heating and the influence of thermal stresses induced by temperature gradients. At the slowest heating rate (1°C/min) the intercept is 3.5 MPa, namely 98% of the tensile strength in virgin cubes; this indicates that the material decay up to 220-230°C is negligible. Increasing the heating rate, up to 120°C/min, a sizeable reduction of the tensile strength at zero pressure becomes evident, leading to a decay of about 30%.

These results are consistent with the thermal stress peaks and damage induced, as shown by numerical analyses (see Section 4.3.2).

Heating and splitting tests were numerically simulated according to Section 4.3.2, completely neglecting moisture flow and fluid phase changes, hence considering null the pore pressure. In Table 4.8 the numerical values of splitting tensile strength are compared with the intercept of the four straight lines; there is a good agreement, stressing the effectiveness of the theoretical model just discussed.

It is worth noting that concrete strength has been evaluated through an indirect tensile test that, as is well known, generally gives higher values with respect to direct tensile tests. It has been shown (Bamonte and Felicetti, 2007) that for no thermal damage, the direct tensile strength over indirect tensile strength ratio is 1.12 – 1.25 and can reach value close to 1.70 for severe thermal damage. Hence, it is reasonable to infer that the linear relation between pore pressure and direct tensile strength is proportional to a value close to -1, as will be substantiated in the following, on the basis of fracture mechanics (Section 4.3.4).

It is interesting to study in deep the role of the heating rate on the values of peak pressure (see Figure 4.10c) and the relative values of temperature (Figure 4.10d).

From the experimental results it is clear that the highest values of pore pressure are obtained for an intermediate heating rate (10°C/min), while for high (due to micro-cracking) and for slow heating rate (due to drying) pore pressure was definitively lower; on the other hand, the heating rate for which pore pressure reaches higher values move towards slower heating rates going from plain-concrete to fibre-concrete. This is probably due to the fact that in fibre-concrete, microcracking during heating is favoured by the notch-effect induced by the canals left free by the melted fibres (Tsimbrovska, 1997; Pistol, 2011). Heating rate seems, instead, to play a marginal role on the temperature measured when peak pressure is reached.

4.3.2 NUMERICAL ANALYSIS

The numerical analyses were performed by Davide Sciancalepore and Alessandro Simonini in 2012. Thermo-mechanical numerical analyses were performed by means of ABAQUS FE code, by modelling an eighth of the insulated cube (Figure 4.11a). Mechanical behaviour was simulated through Concrete Damaged Plasticity Model, implemented in ABAQUS according to the well-known model developed by Lubliner et al. (1989) and modified by Lee and Fenves (1998).

The curves suggested by the EC2-Fire Design (2004) were used for the variation with the temperature of both concrete density and conductivity (lower limit was adopted), while the specific

heat was evaluated through back analysis of the experimental values of temperature measured in the centroid of the specimens. It should be underlined, in fact, that the peak of specific heat suggested by EC2 in the range 100-200°C (to take into account implicitly the moisture migration and evaporation inside concrete) is optimized for heating according to Standard Fire; when the thermal load is defined differently (as in the present case) the peak in the specific heat changes significantly in shape and intensity.

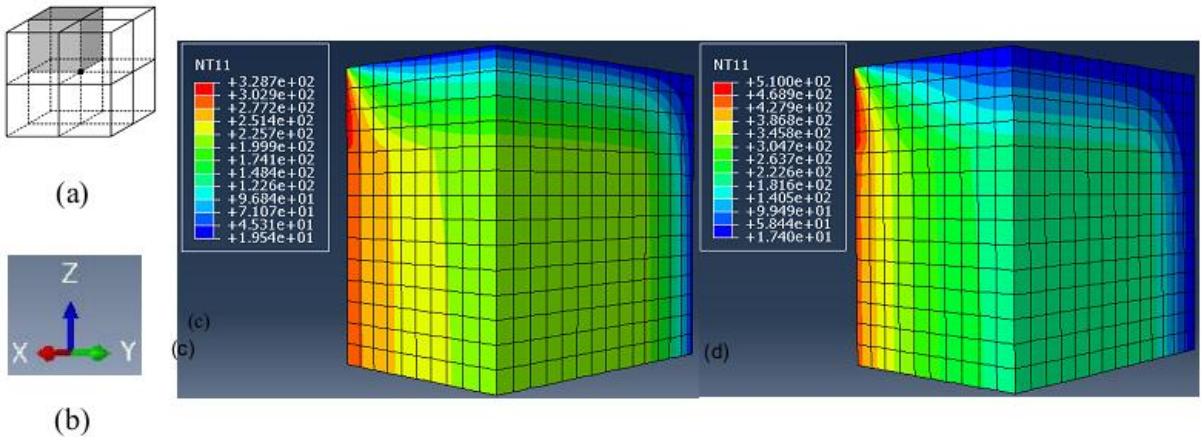

Figure 4.11: Numerical analyses results: (a) modelled eight of the specimen, (b) reference system – y, longitudinal direction, distribution of the temperature just before splitting test was performed for HR = 1°C/min (c) and HR = 120°C/min (d).

The curve suggested by EC2 was used also for the decay of the compressive strength (calcareous concrete, Figure 4.12a) with the temperature; on the other hand the decay of the tensile strength was obtained from the curve given by EC2 enlarging the range in which tensile behaviour is constant (from 20 to 230°C, Figure 4.12a) on the basis of the experimental results (for slow heating rate, hot splitting tensile strength – T ≈ 230°C - showed to be equal to the virgin one).

In order to define concrete stiffness $E_c(T)$ (see Figure 4.12a) and thermal dilation $\varepsilon_{th}(T)$ (see Figure 4.12b), the data given by Mindeguia et al. (2009) on B40 concrete (nominally equal to that used in the present work) were considered. Concrete stiffness was evaluated as the initial stiffness of the stress-load induced strain law (Figure 4.12c), where the load-induced strain $\varepsilon_{\sigma,tr,cr}(\sigma,T,t)$ is the sum of three contributions, namely instantaneous stress-related strain $\varepsilon_{\sigma}(\sigma,T)$, transient strain $\varepsilon_{tr}(\sigma,T)$ and creep strain $\varepsilon_{cr}(\sigma,T,t)$.

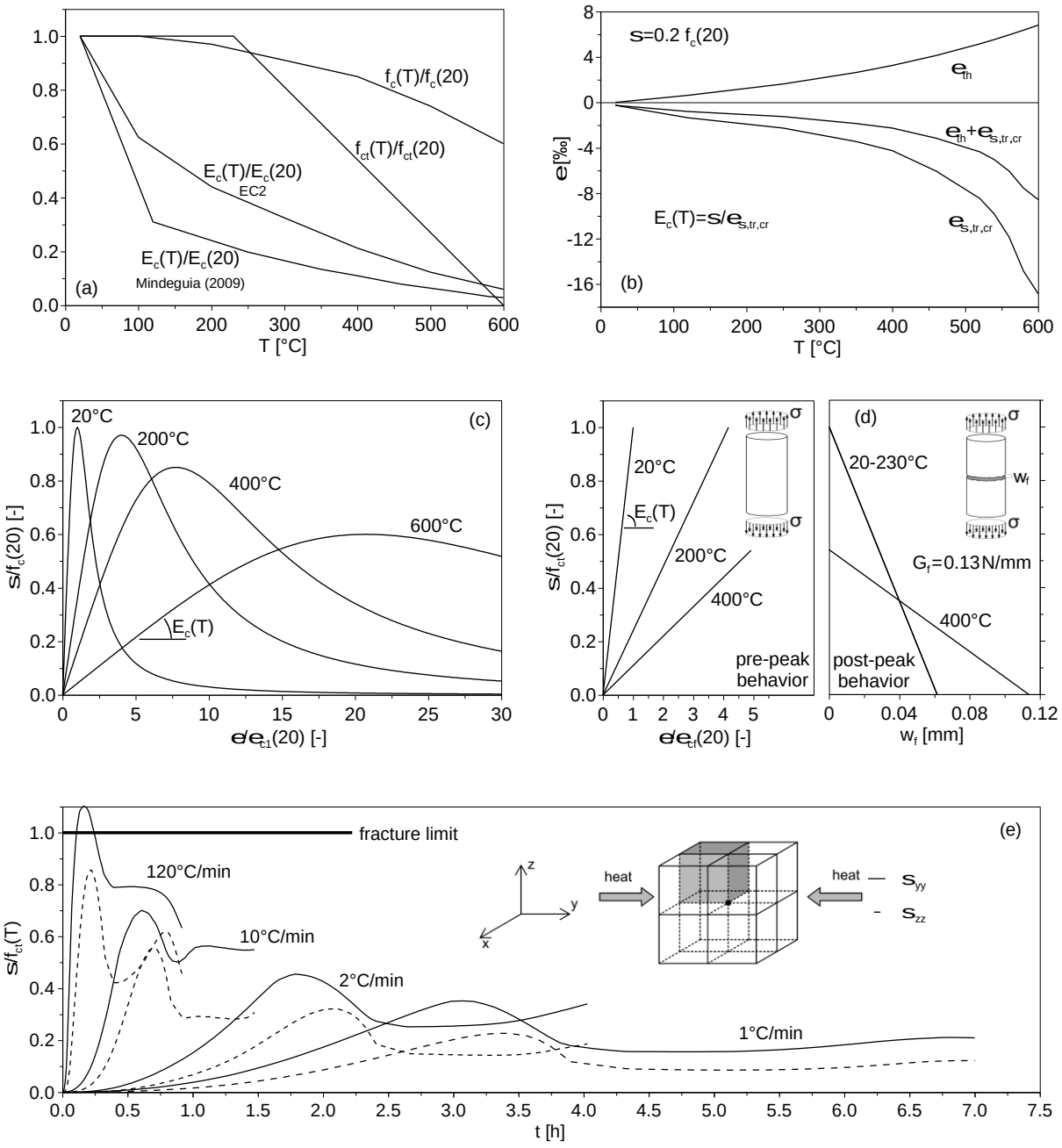

Figure 4.12: Decay of concrete compressive and tensile strength and stiffness as a functions of the temperature (a); strain components during heating (Mindeguia et al., 2009) (b); stress-load induced strain law in compression (c) and in tension (d) at different temperatures; and thermal stresses in the centroid of the specimen for the four heating rates according to numerical analyses (d).

Given the values of the different components of strain as a functions of the temperature (Figure 4.12b) for a particular level of stress $\alpha(T) = \sigma/f_c(T)$, concrete stiffness is evaluated as the ratio

$\sigma/\varepsilon_{\sigma,tr,cr}(\sigma,T,t)$. (The calculated stiffness can be considered as the initial one if $\alpha(T) \leq 0.5\text{-}0.6$, being the stress-load induced strain law rather linear for these range of stresses).

The relationship between stress and load-induced strain was described through the curve suggested by EC2 (Equation 4.6, Figure 4.12c):

$$\frac{\sigma(T)}{f_{c,T}} = \frac{3\left(\varepsilon_\sigma/\varepsilon_{c1,T}\right)}{\varepsilon_{c1,T}\left[2+\left(\varepsilon_\sigma/\varepsilon_{c1,T}\right)^3\right]} \qquad (4.6)$$

The initial stiffness of such a curve is $E_c(T) = 1.5 \cdot f_{c,T}/\varepsilon_{c1,T}$; hence, once given $E_c(T)$ and $f_{c,T}$, $\varepsilon_{c1,T}$ can be evaluated as $1.5 \cdot f_{c,T}/ E_c(T)$.

In tension, a bilinear model has been considered (Figure 4.12d); fracture energy G_f was evaluated according to CEB – fip Model Code 90 (1993) and kept constant with the temperature.

Numerical analyses were performed to simulate both the heating and the following splitting test. The temperature distributions just before the splitting test (showed in Figure 4.11c, d for HR = 1 and 120°C/min, respectively) prove the effectiveness of the insulation layer in creating a mono-dimensional heat flux. In Figure 4.12e the tensile stresses in the centroid of the specimen during heating are shown as a function of time for all the investigated heating rates (1, 2, 10 and 120°C/min). As expected, fast heating induces much higher thermal stresses than slow heating. However, only 120°C/min causes concrete microcracks because of thermal stresses (this results seems to justify the irregular growth of the measured pore pressure during the experimental tests for HR = 120°C/min); this is clear shown in Figure 4.12e where the ratio $\sigma/f_{ct}(T)$ becomes larger than 1 (this means that tensile strength is exceeded).

Table 4.8: Apparent tensile strength for null pore pressure evaluated according to the linear model f_{ct}^{th} (intercepts of the four straight lines) and numerically f_{ct}^{num} (according to Section 5) for the different heating rates. f_{ct}^{20} = 3.6 MPa.

HR [°C/min]	f_{ct}^{th} [MPa]	f_{ct}^{th}/f_{ct}^{20}	f_{ct}^{num} [MPa]	f_{ct}^{num}/f_{ct}^{20}
1	3.51	0.98	3.31	0.92
2	3.09	0.86	3.21	0.89
10	2.94	0.82	2.95	0.82
120	2.53	0.70	2.68	0.74

In Figure 4.13 the numerical values of splitting tensile strength for the different heating rates are reported together with the intercept of the four lines, as a functions of the heating rate; the agreement between numerical and experimental is satisfactory.

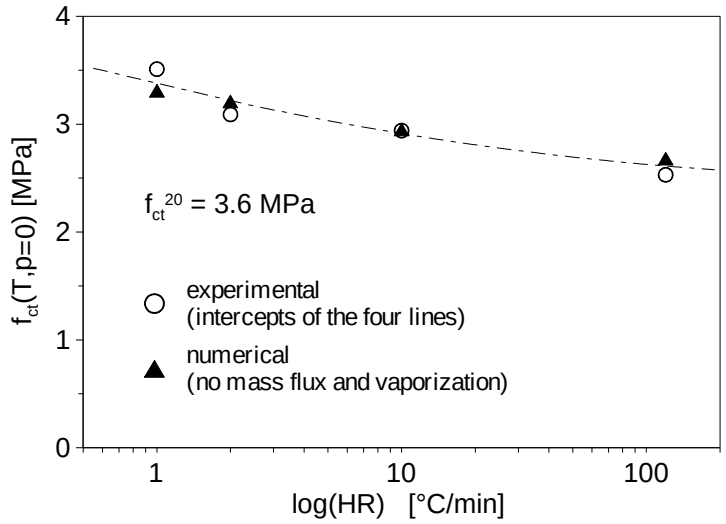

Figure 4.13: Apparent tensile strength for null pore pressure evaluated according to the linear model and numerically, as a functions of HR.

4.3.3 INTERPRETATION OF THE EXPERIMENTAL RESULTS

As discussed, the apparent tensile strength f_{ct}^{app} measured in the experimental tests resulted to be a function of: (a) the real material strength $f_{ct}(T)$ (including only the effect of thermo-physical transformation occurring at the temperature T), (b) the pore pressure p_{gas} developed in the pores and, (c) the detrimental effect $\Delta f_{ct}(T,HR)$ of thermal stress due to the inhomogeneous heating:

$$f_{ct}^{app}(p,T,HR) = f_{ct}(T) - p_{gas}(HR) - \Delta f_{ct}(T,HR) \quad (4.7)$$

where, the latter term proved to be negligible in case of slow heating rate HR (up to 1°C/min in our tests).
This finding seems to confirm the approach based on the effective stress (Equation 3.1) in case the Biot's coefficient is assumed equal to 1 (Tenchev and Purnell, 2005) and the role of the capillary pressure (Gawin et al., 2011; Gray and Schrefler, 2007) is neglected.
One alternative approach to explain this role of gas pressure is based on fracture mechanics and on the stability of the inherent material defects.

4.3.4 FRACTURE MECHANICS MODEL

The tensile behaviour of concrete may be interpreted as the global effect of many micro defects, which reach an unstable propagation when a critical level of stress is reached, according to fracture mechanics approach.

The local stress concentration around a defect is governed by the stress intensity factor, K_I, which is a function of both load level and boundary conditions. The defects propagate when K_I reaches a critical value K_{Ic}, which is a property of the material - $K_{Ic} = f(E_c, G_f)$, where E_c and G_f are the elastic modulus and the fracture energy, respectively

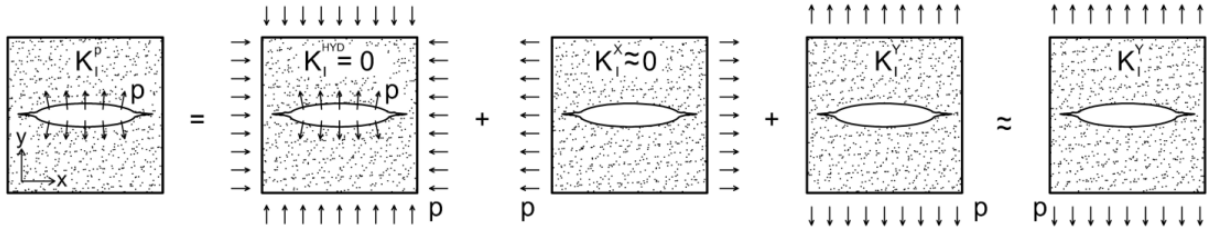

Figure 4.14: Square part of concrete with one defect.

Let us consider a concrete element including a defect which governs the material tensile response on y direction (Figure 4.14). A pressure p, exerted inside the defect, can be equivalently considered as the summation of three loading cases: hydrostatic pressure all around the boundaries, external tensile stress in both x and y directions. Hydrostatic pressure has no effect in fracture propagation ($K_I^{HYD} = 0$); moreover, for sharp-shaped defects, the stress intensification due to parallel loading ($K_I^X \approx 0$) is negligible compared to the effect of transverse loading (K_I^Y). This means that pressure inside defects (pores) is equivalent, from the fracture mechanics point of view, to an intensification of the tensile stress by the same value. This conclusion complies with the experimental results.

CHAPTER - 5

EXPERIMENTAL RESULTS

The objective of the present research project is to evaluate the effect of pore pressure on the fracture behaviour of high performance concrete, with particular attention the role played by the pp-fibres. To this purpose, several tests have been performed according to the experimental procedure discussed in Chapter 4. In this experimental campaign, 5 different concrete mixes were considered, 2 plain and 3 polypropylene fibers concrete. 50 specimens were tested: 21 were plain concrete and 29 were polypropylene fiber concrete with different fibre contents. Among all the specimens 43 were tested with heating rate = 0.5^{o}C/min, 3 specimens with 1^{o}C/min and 4 specimens with 2^{o}C/min. 14 specimens were partially dried in oven (T = 50^{o}C for one month). An overview of the tests performed is provided in Table 4.2. Dry specimens were tested in order to study the influence of low values of pore pressure on the tensile strength of concrete. On the other hand thermal properties and microstructure analyses were performed in an external laboratory to relate microstructure and thermo-mechanical behavior at high temperature.

As a result of these tests, density, mass loss, time-temperature, time-pressure, temperature-pressure, pressure-tensile strength curves were obtained for the 5 different mixes. The results are discussed in the following.

5.1 PORE PRESSURE MEASUREMENT AND SPLITTING TEST

In order to determine the content of free water, two samples for each mixture were subjected to drying in oven at the temperature of 105^{o}C, until constant value of the mass. Figure 5.1 shows that the absolute value of density loss is around 100 Kg/m^3 in the mixes 95-S and 70-S. This can ascribed due to higher amount of ground granulated blast furnace slag (300 Kg/m^3 in Mix 95-S and 200 Kg/m^3 in Mix 70-S) was used in Mix 95-S, so more free water is available due to slow hydration process. On the other hand lower relative mass loss was found in Mix 95-S (around 4 % in the Mix 95-S and 5.5 % in Mix 70-S), because of its lower permeability and greater density. However, the presence of fibre seems to have a not-negligible role, because pp fibre has higher mass loss rate due to its higher permeability. Same mass loss was found in Mix 70-S and Mix 70-S-Pm (1 and 2 Kg/m^3) (around 5.5 %).

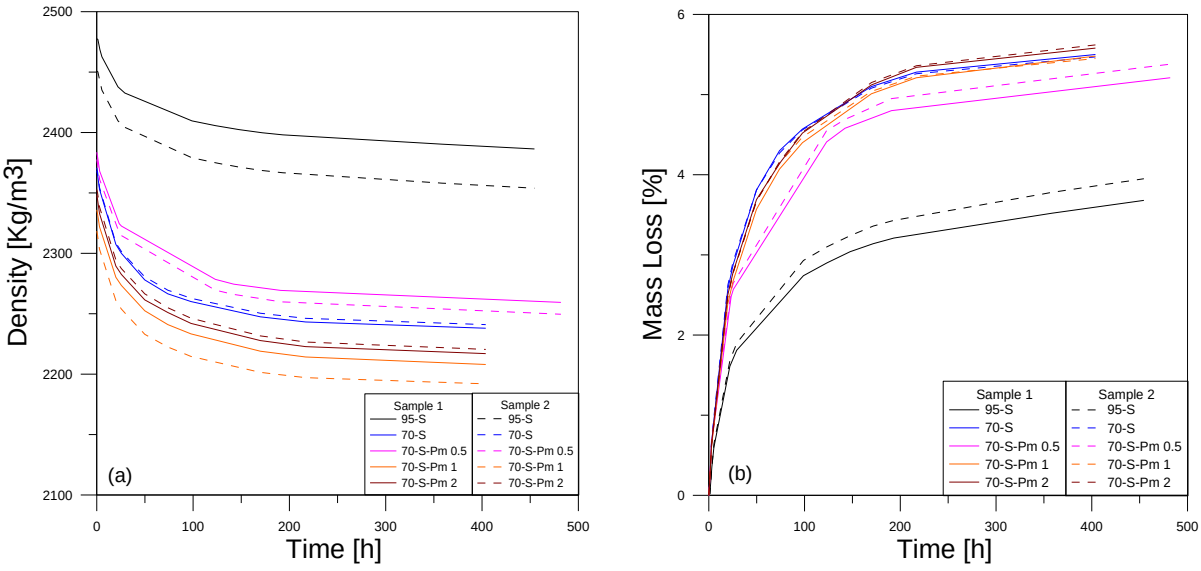

Figure 5.1: Drying in oven at T = 105°C: (a) density and (b) mass loss as a function of time.

We note that the rate of water escape increases with the increase of w/c ratio. Indeed, the low compactness of the concrete with high w/c ratio induces a higher fluid permeability and then makes easier the water transport.

Figure 5.2 shows that all time-temperature curves have similar trend for a given heating rate (0.5, 1 or 2°C/min) and a slight plateau were found in all the mixes. Plateau indicates the water phase change (vaporization). This transformation is endothermic and then consumes a great part of the energy that is brought by heating.

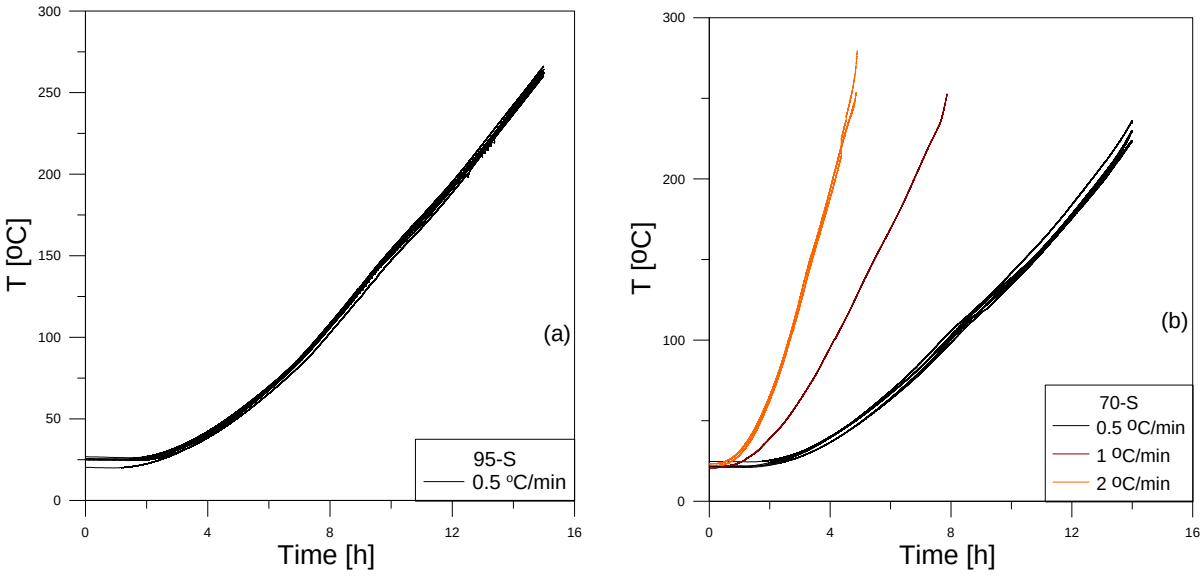

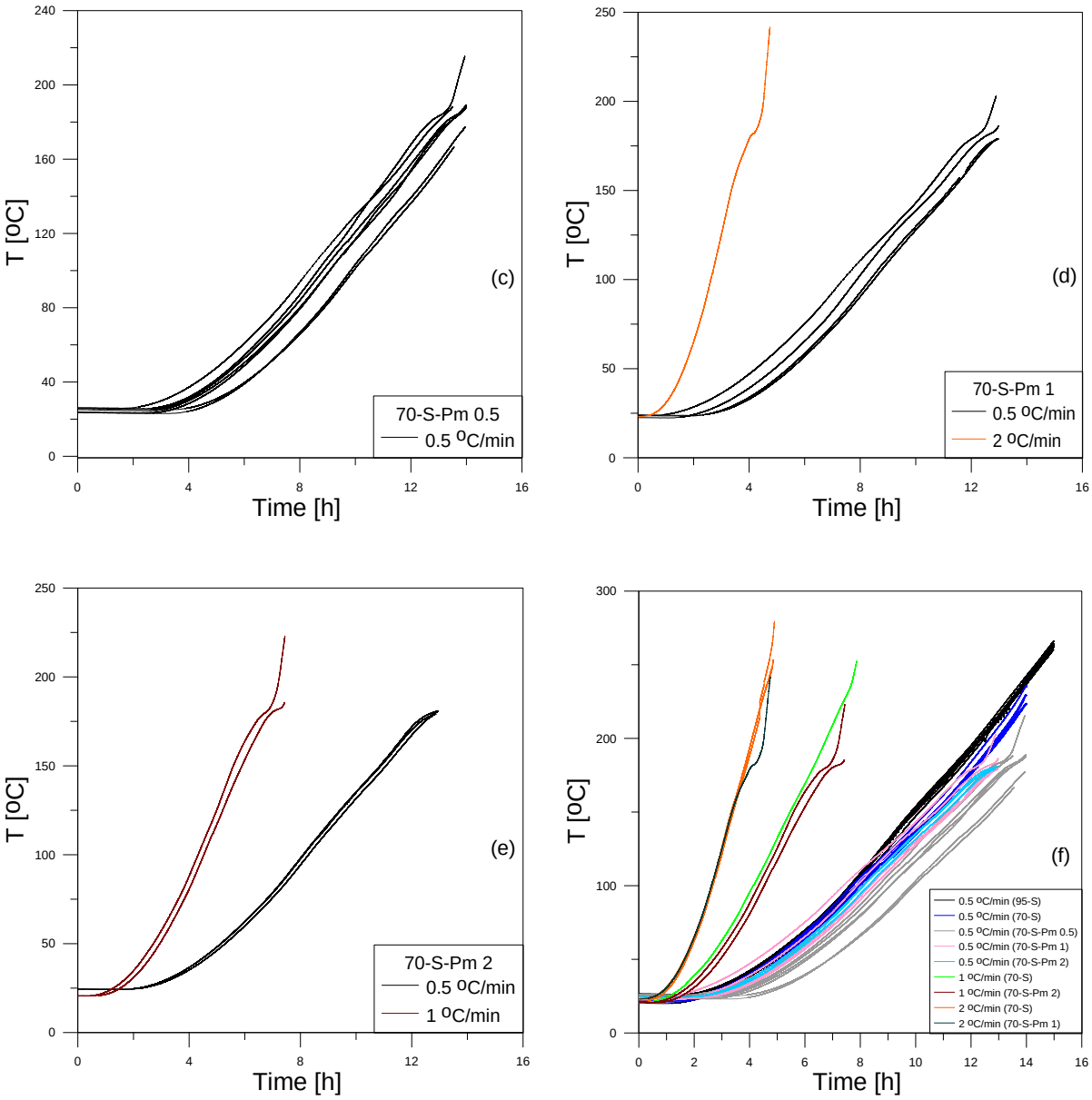

Figure 5.2: Temperature development in the centroid of the specimen as a function of time: (a) Mix 95-S, (b) Mix 70-S, (c) Mix 70-S-Pm 0.5, (d) Mix 70-S-Pm 1, (e) Mix 70-S-Pm 2 and (f) all the 5 mixes.

As a consequence, the temperature rise of concrete sample is slowed down and it can emphasize that the water vaporization can induce additional temperature gradients (Mindeguia et al., 2010). A plateau of the series of 70-S mixes were found in temperature between: 220-250°C for Mix 70-S, 160-185°C for Mix 70-S-Pm 0.5 and 150-180°C for Mix 70-S-Pm 1 and Mix 70-S-Pm 2; Mix 95-S behaves differently due to its high compactness and less permeability. The higher the fibre content has the higher the permeability and shows that the lower temperature to reach a steady vaporization.

It was also observed that the temperature plateau depends on the concrete compactness. In Mix 95-S the temperature at which plateau starts is 40°C higher than in Mix 70-S and in average around 100°C higher with respect to the pp fibre mixes (Mixes 70-S-Pm 0.5, 70-S-Pm 1 and 70-S-Pm 2). This behaviour is strictly related to the development of pressure: the higher the pressure, the higher the temperature necessary to evaporate water. Moreover, the steepness of this plateau depends on the heating rate. For heating rate = 2°C/min, a more evident plateau was obtained. In fact, the plateau is expected to be strictly horizontal in the case of steady state flux of water and this situation is far from very low heating rate (0.5°C/min), because drying during heating became significant (hence, the plateau is less evident).

Figure 5.3 presents the pore pressure measured into the samples for all the tests. The development of pore pressure seems to differentiate according to the different heating rates. The maximum values of pore pressure are: 4.6 MPa for Mix 95-S, 2.4 MPa for Mix 70-S and in average 0.9 MPa in pp fibre concrete mixes (series of Mix 70-S-Pm), with heating rate = 0.5°C/min. Pore pressure is higher in more compact concrete, because of lower permeability and porosity and higher initial water saturation. Low pore pressure was found in pp fibre concrete because of pp fibre melting and consequent release of vapour; results proved also that the decrease of w/c increases the pore pressure. This result is consistent with previous research by Kalifa et al. (2001) and Bangi (2011). In the case of intermediate heating rate (2°C/min) very low pore pressure (less than 0.5 MPa) was found for all the mixes due to the problem create for measurement of pore pressure.

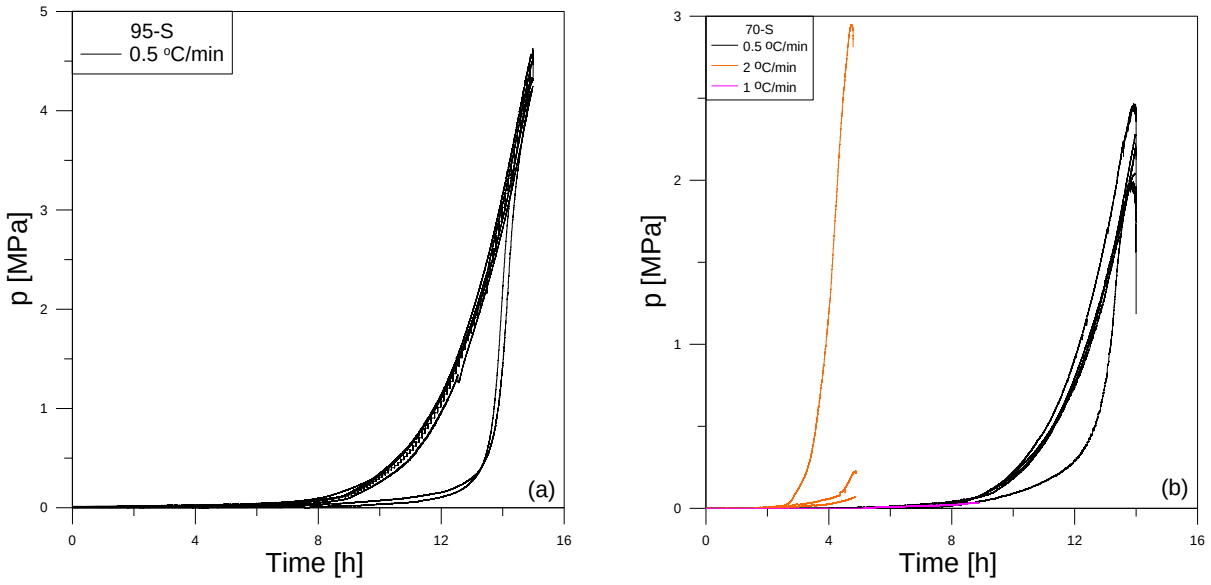

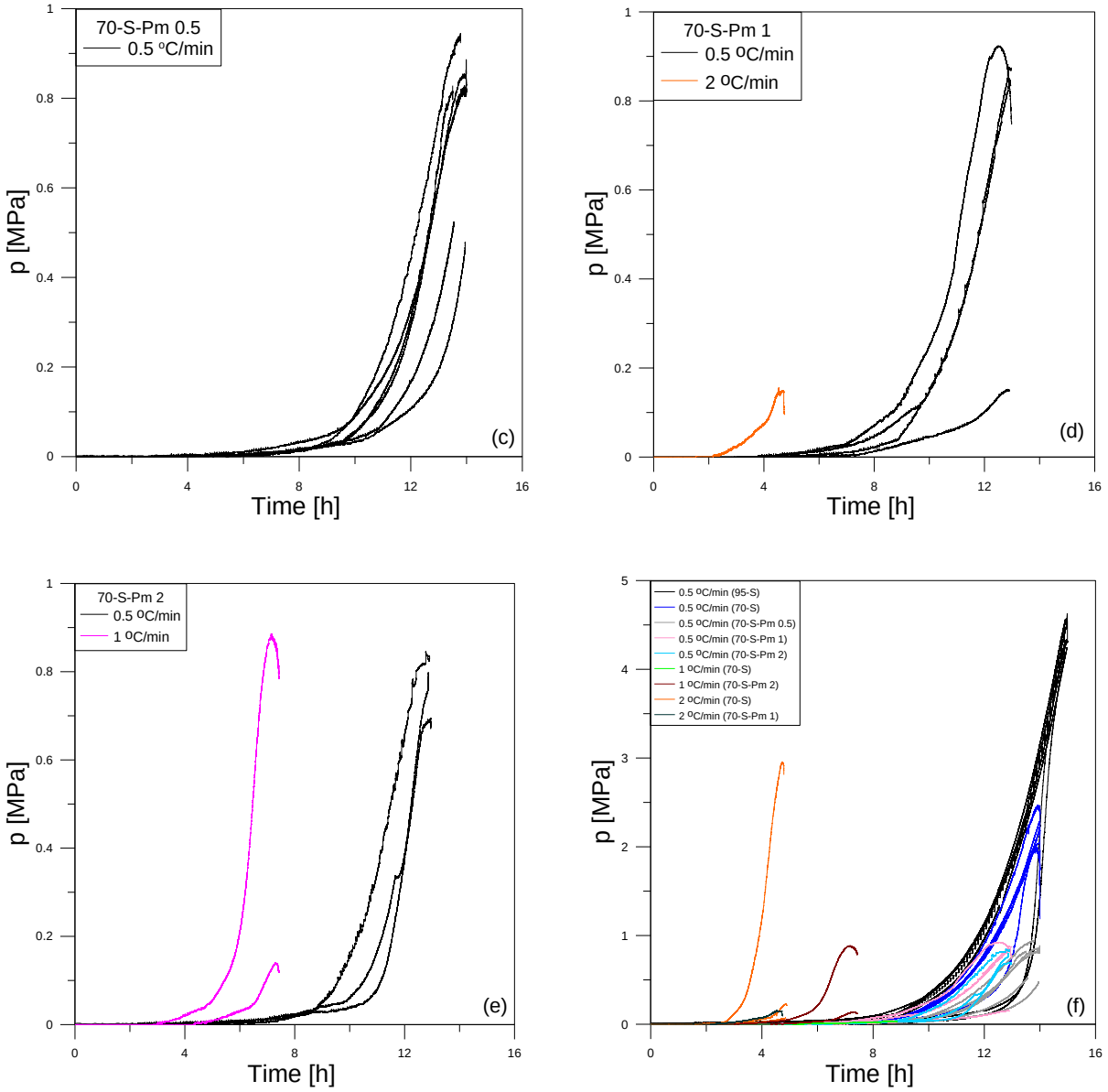

Figure 5.3: Pressure development in the centroid of the specimen as a function of time: (a) Mix 95-S, (b) Mix 70-S, (c) Mix 70-S-Pm 0.5, (d) Mix 70-S-Pm 1, (e) Mix 70-S-Pm 2 and (f) all the 5 mixes.

In Figure 5.3f, it is observed that the development of pore pressure in plain and fiber concrete have the same trend for the heating rate = 0.5°C/min. Plain concrete tends to achieve higher pore pressure (in the case of Mix 70-S, almost 3-4 times that of pp fibre concrete). The temperature at which the peak pressure was reached is lower for fibre concrete with respect to plain concrete; this is caused by the fact that the further porosity induced by fibres increases the moisture transport, hence decreasing the values of pore pressure. Obviously, the lower the pore pressure, the lower the evaporating temperature of the free water. Before the peak the vaporization rate exceeds the

vapour migration in the porous network. At the peak the two phenomena are balanced. This point is anticipated in porous concrete due to the higher vapour flow.

Figure 5.4 represents the evolution of temperature and pressure as a function of time for the five different mixes. Almost the same trend was found with the heating rate 0.5°C/min for all the mixes. The dramatic pressure rise occurs almost at the beginning of the plateau (Figure 5.4) and pressure peaks are achieved at the end of the plateau. Indeed, the beginning of plateau is the point at which phase transformation of water occurs (vaporization). At this point water always vaporizes, the rate is governs by temperature (vapour pressure), latent heat and boundary conditions. After that water is totally transformed into vapor, plateau is left and the pressure starts to decrease.

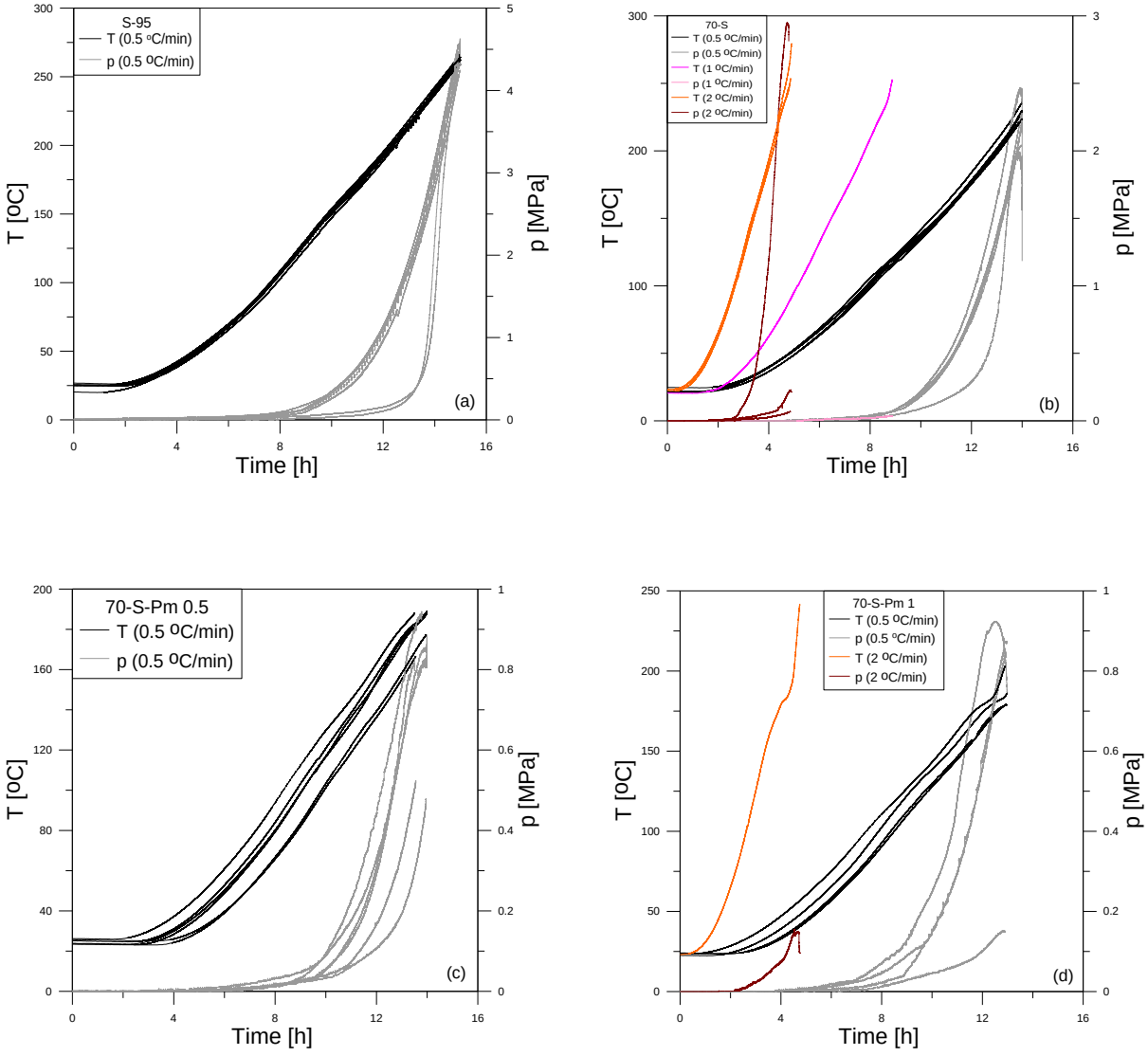

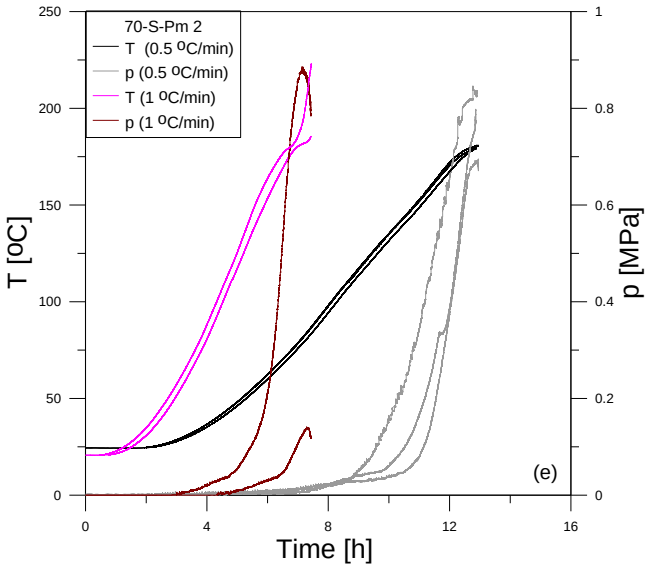

Figure 5.4: Development of temperature and pressure in the centroid of the specimen as a function of time: (a) Mix 95-S,(b) Mix 70-S, (c) Mix 70-S-Pm 0.5, (d) Mix 70-S-Pm 1, (e) Mix 70-S-Pm 2.

Water vaporization is strongly influenced by heating rate: it is very fast for heating rate = 2°C/min (Figures 5.4b,d,e) and low for 0.5°C/min. Polypropylene fibres have sharp plateau in the peak pressure and the pressure release is very fast at the post peak. Most of the pp fibre concrete peak pressures were found at a temperature in between 170 -180°C; at a temperature above 165°C pp start melt and create a large amount of void which enhance the pressure release.

In Figure 5.5, the evolution of the pore pressure as a function of temperature in the mid-section of the concrete specimen is shown. Experimental results of pressure-temperature together with the saturation vapour pressure curve, P_{SV} [$P_{sv} = 0.00611 * 10^{\frac{7.5*T}{237.7+T}}$ bar] are reported; as expected, the saturation curve represents a limit condition of pressure-temperature relation. Theoretically, pressure-temperature curves cannot pass beyond the saturation curve. For many cases, it can be observed that measured pressures follow the P_{sv} curve during the ascending branch. However, all the measured pressures are below the saturation curve and these results are theoretically approved. If the pressure is higher than the saturation curve, vapour pressure is not responsible for this overpressure. This overpressure is often attributed to the partial pressure of the dry air that is enclosed in the porous media. The partial pressure of air in a pore is strongly dependent on its water saturation: the higher the water saturation, the lower is the free volume available to the air to expand during heating (Mindeguia et al., 2010).

In mixes 95-S and 70-S, the experimental curves are very close to P_{sv}, whereas pp fibre concrete pore pressures are little far from P_{sv} (Figure 5.5a,f). For heating rate = 0.5°C/min pore pressures have almost the same branch of the saturation curve, but there is a big gap formed between saturation curve and pressure-temperature curves in the case of 2 °C/min and 1 °C/min.

However, the maximum pressure was found in a narrow thermal range 180-250°C. As abovementioned, pp fibre concrete shows lower pore pressure values than plain concrete.

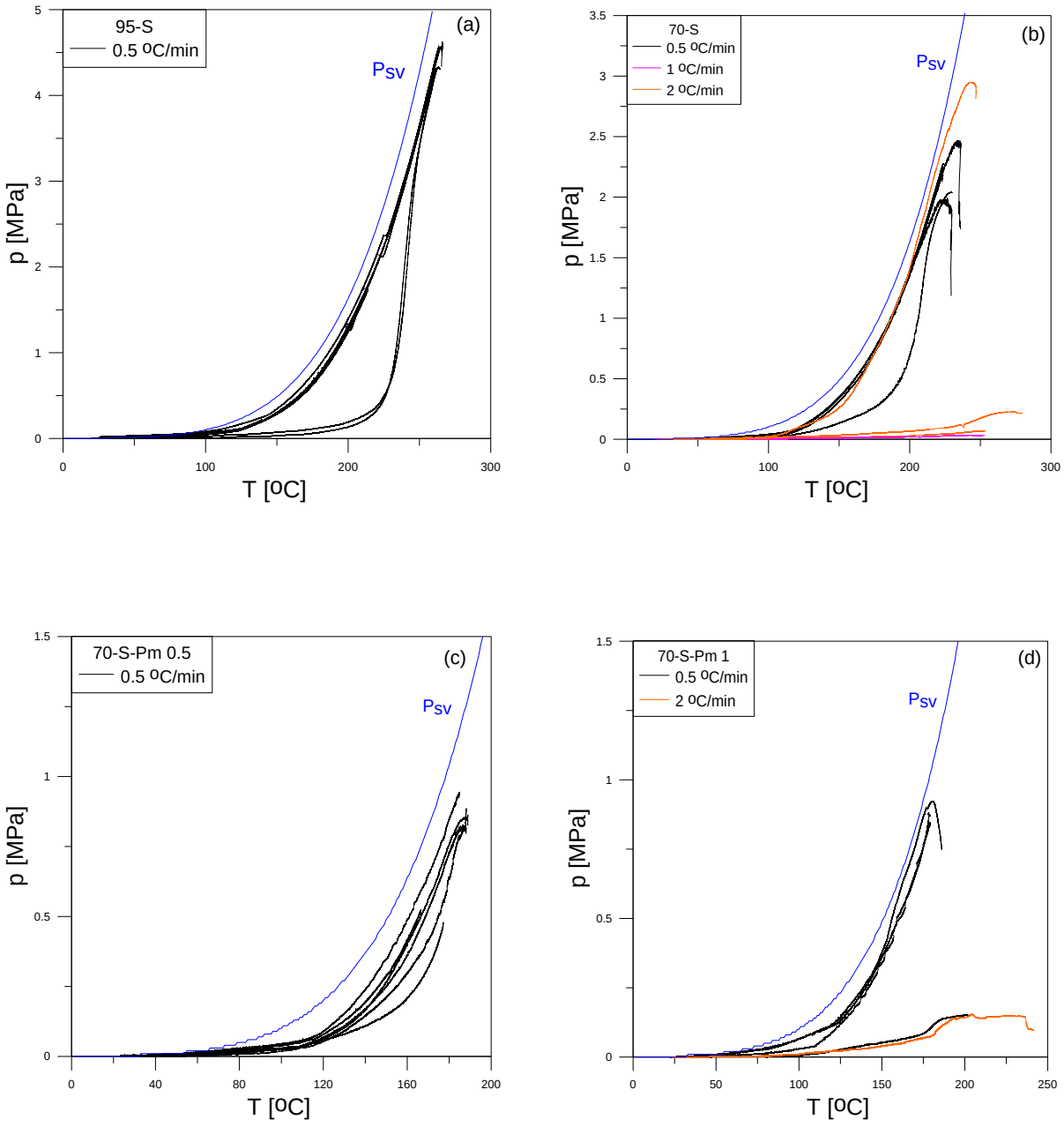

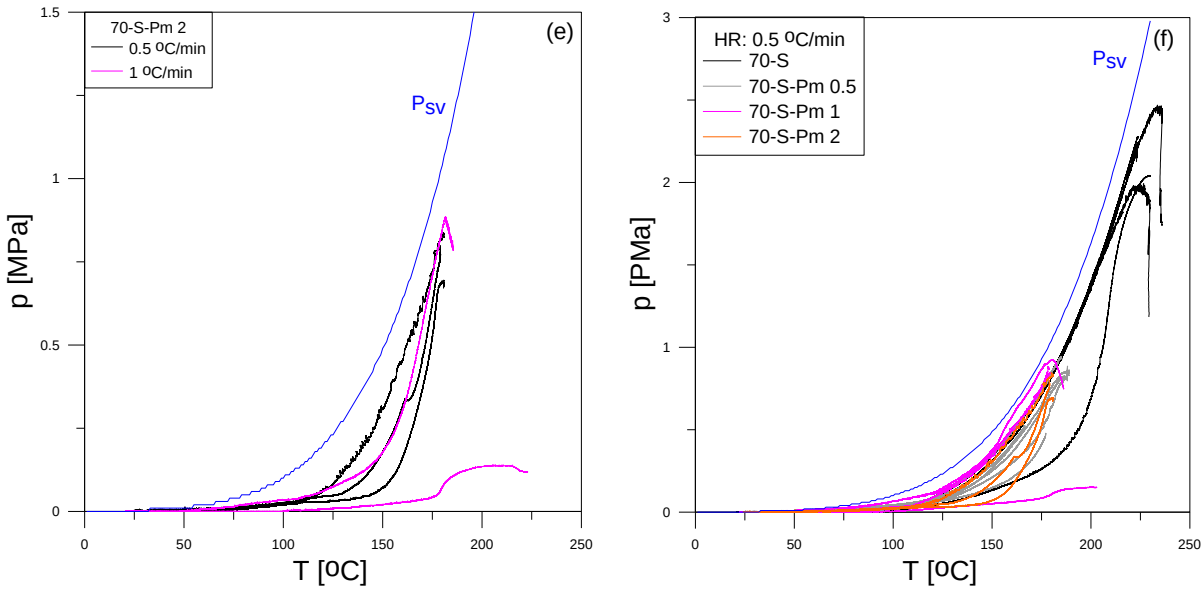

Figure 5.5: Saturation vapour pressure curve (P_{sv}) and pore pressure-temperature curves for the different mixes: (a) Mix 95-S, (b) Mix 70-S, (c) Mix 70-S-Pm 0.5, (d) Mix 70-S-Pm 1, (e) Mix 70-S-Pm 2, and (f) series of 70-S mixes with different dosages of pp fibre.

This is possibly because pp fibers melt above 165°C and generate not only new voids (corresponding to their volume), but create a network of micropores connecting the already-existing pores. In such a way, continuous channels are formed, that allow the vapor to migrate inside the material, towards cooler and lower-pressure zones, and by this way the risk of explosive spalling is reduced.

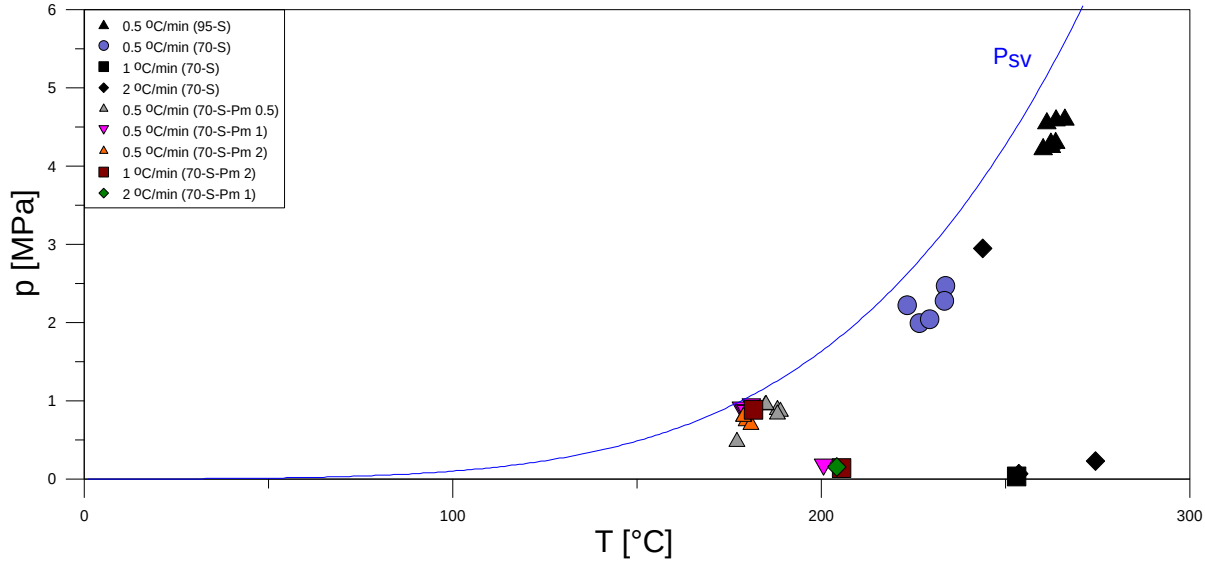

Figure 5.6 Temperature at the peak pore pressure for the 5 mixes.

In Figure 5.6 shows that the peak pressures were achieved in a narrow range of temperature between: 210-240°C for Mix 70-S, 170-185°C for Mix 70-S-Pm 0.5 and 170-180°C for Mix 70-S-Pm 1, Mix 70-S-Pm 2, only higher temperature (250-270°C) shown in Mix 95-S due to highly compactness, with heating rate = 0.5°C/min.

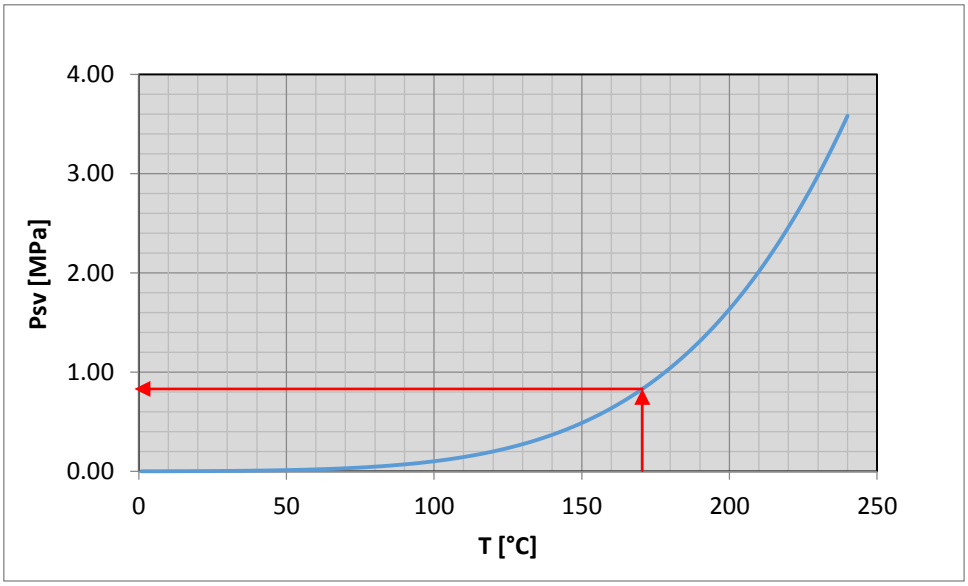

Figure 5.7: Saturation vapour pressure in the temperature range of polypropylene fibre melting.

As abovementioned, all the pp fibre concretes peak pressure reached at the temperature range between 170°C to 185°C and Figure 5.7 shows that the at 170°C temperature water reach the pressure below 1 MPa. The values of the temperature at peak pressure are given (see Table 5.1 and Figure 5.8) for all the 70-S mixes with heating rate = 0.5°C/min. The increasing amount of pp fibre decreases the peak pressure (all the pp fibres concrete peak pressures are less than 1 MPa, Figure 5.8). The additional amount of 0.5 Kg/m^3 pp fibres in the concrete mix can reduce the explosive spalling, so saving a lot of money for the fire exposed structures.

Table 5.1: Temperature at peak pressure for mix all 70-S with heating rate 0.5°C/min

Mix	70-S	70-S-Pm 0.5	70-S-Pm 1	70-S-Pm 2
p_{max} [MPa]	2.47	0.95	0.92	0.85
T at p_{max} [°C]	234	185	181	180

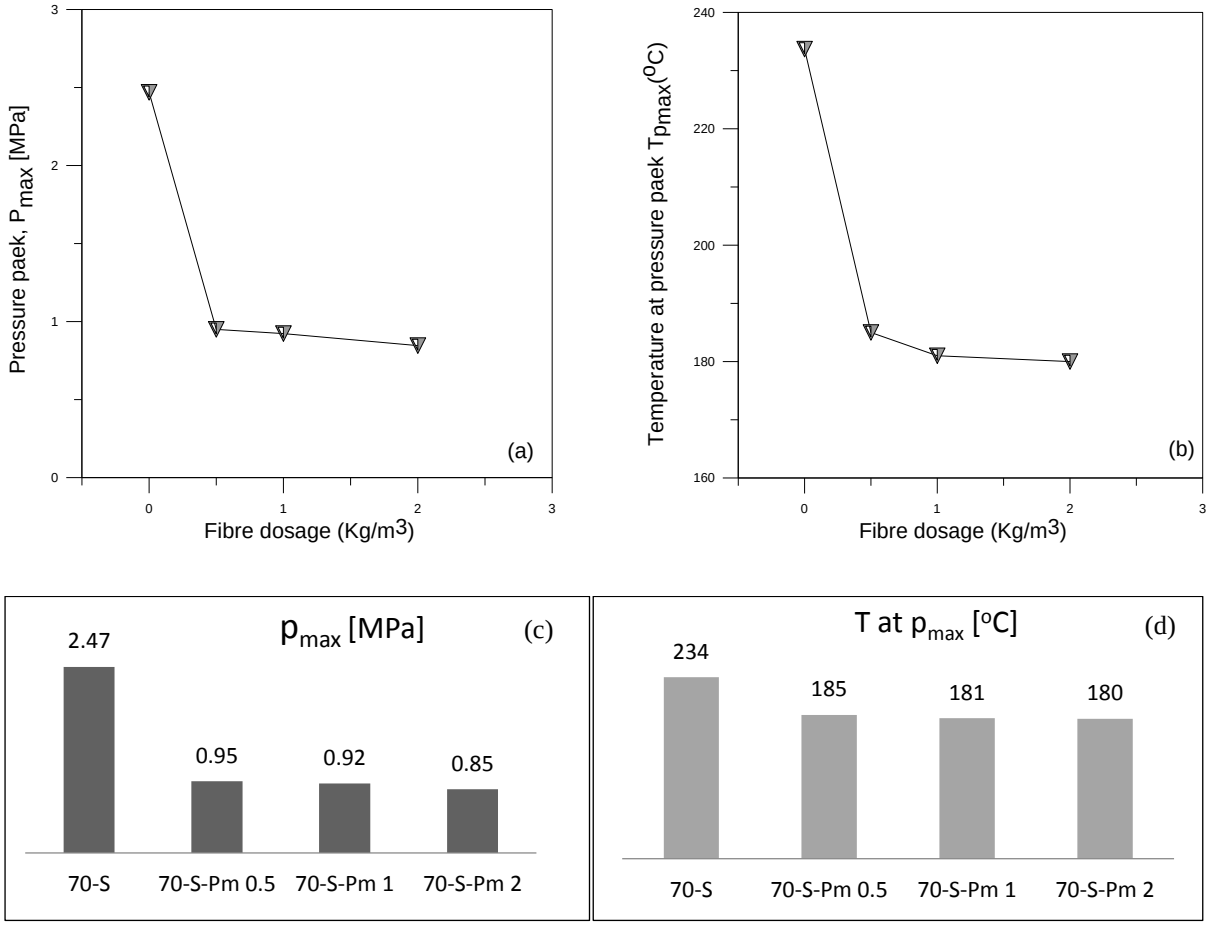

Figure 5.8: Pressure peak versus fibre dosage (a), (c); and Temperature at peak pressure versus fibre dosage (b), (d).Heating rate = 0.5 ^{o}C/min.

To determine the influence of pore pressure on fracture behaviour of high performance concrete with and without pp fibres exposed to fire, splitting tensile test was performed when the peak pore pressure was reached; this means that experiments had not been performed at a specific temperature. However, the peak pressures were achieved in a narrow range of temperature between: 210-240°C for Mix 70-S, 170-185°C for Mix 70-S-Pm 0.5 and 170-180°C for Mix 70-S-Pm 1 , Mix 70-S-Pm 2 (Figure 5.6), only higher temperature (250-270^{o}C) reached in Mix 95-S due to highly compactness, with heating rate = 0.5^{o}C/min. The results obtained from the splitting tests are reported in Figure 5.9 as a function of the pressure measured during the test, with heating rate=0.5°C/min.

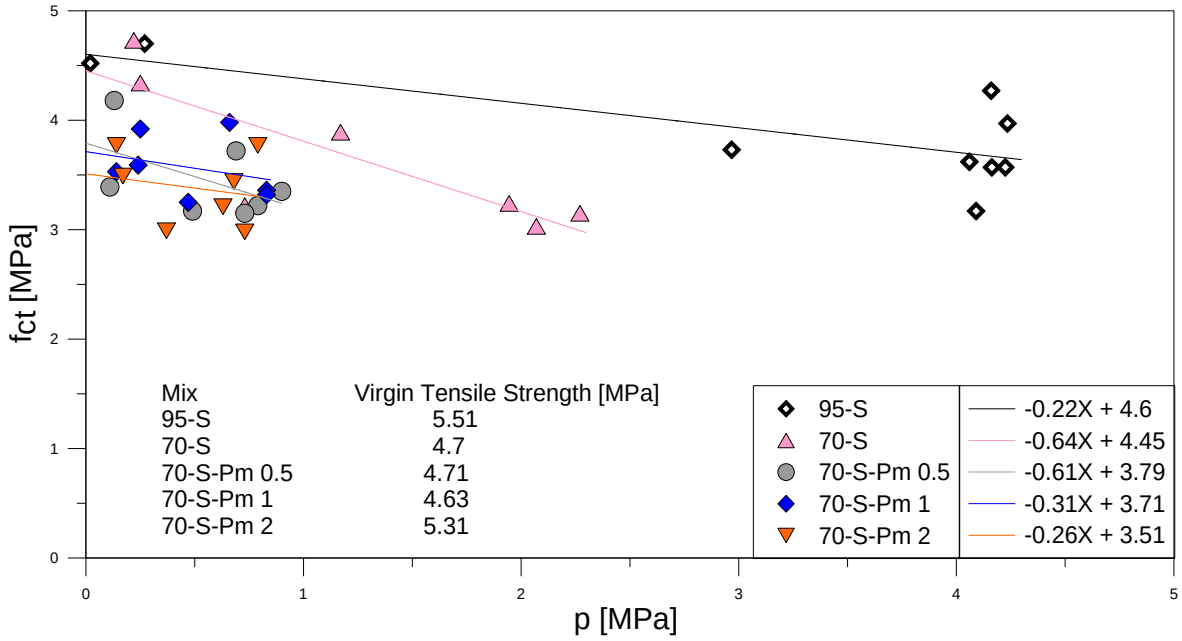

Figure 5.9: Tensile strength-pore pressure plot

In the case of plain concrete shows that pore pressure decreases the apparent tensile strength of concrete of about 0.22 times the pressure for Mix 95-S (negative slope 0.22). We can assume that the pore pressure is zero in virgin condition (because there is no heat increment, so no pore pressure). Almost the same tensile strength was found for Mix 70-S in virgin and zero pressure condition (virgin strength of Mix 70-S is 4.7 MPa and tensile strength at zero pressure is 4.45 MPa). However, almost the similar trend lines were found in the Mix 70-S and Mix 70-S-Pm 0.5 (negative slope: 0.64 for Mix 70-S and 0.61 for Mix 70-S-Pm 0.5). All the polypropylene fibre concrete shows a significant reduction of the tensile strength at zero pressure with respect to virgin tensile strength (around 20% for Mix 70-S-Pm 0.5, Mix 70-S-Pm 1 and 34 % for Mix 70-S-Pm 2) probably due to the melting of the fibres; the further porosity introduced by fibres melting, in fact, makes easier the propagation of the cracks, so increasing the permeability (this leads to low values of pore pressure) and decreasing the tensile strength.

5.2 MICROSTRUCTURAL AND THERMAL CHARACTERIZATION

5.2.1 MERCURY INTRUSION POROSIMETRY (MIP)

The diagrams of the cumulative pore volume and of the relative volume of voids were obtained by means of MIP and are plotted in Figure 5.10 for three concrete mixes (70-S, 70-S-Pm 1 and 70-S-Pm 2), as a function of pore radius. For the sake of comparison, in Figure 5.10 reference is made to Mix

70-S with and without fibers (Mixes 70-S, 70-S-Pm 1 and 70-S-Pm 2). The porosity of the specimens treated at 105°C is considered as a reference, since the evaporable water has been expelled; the porosity at 20°C refers to room-conditioned specimens.

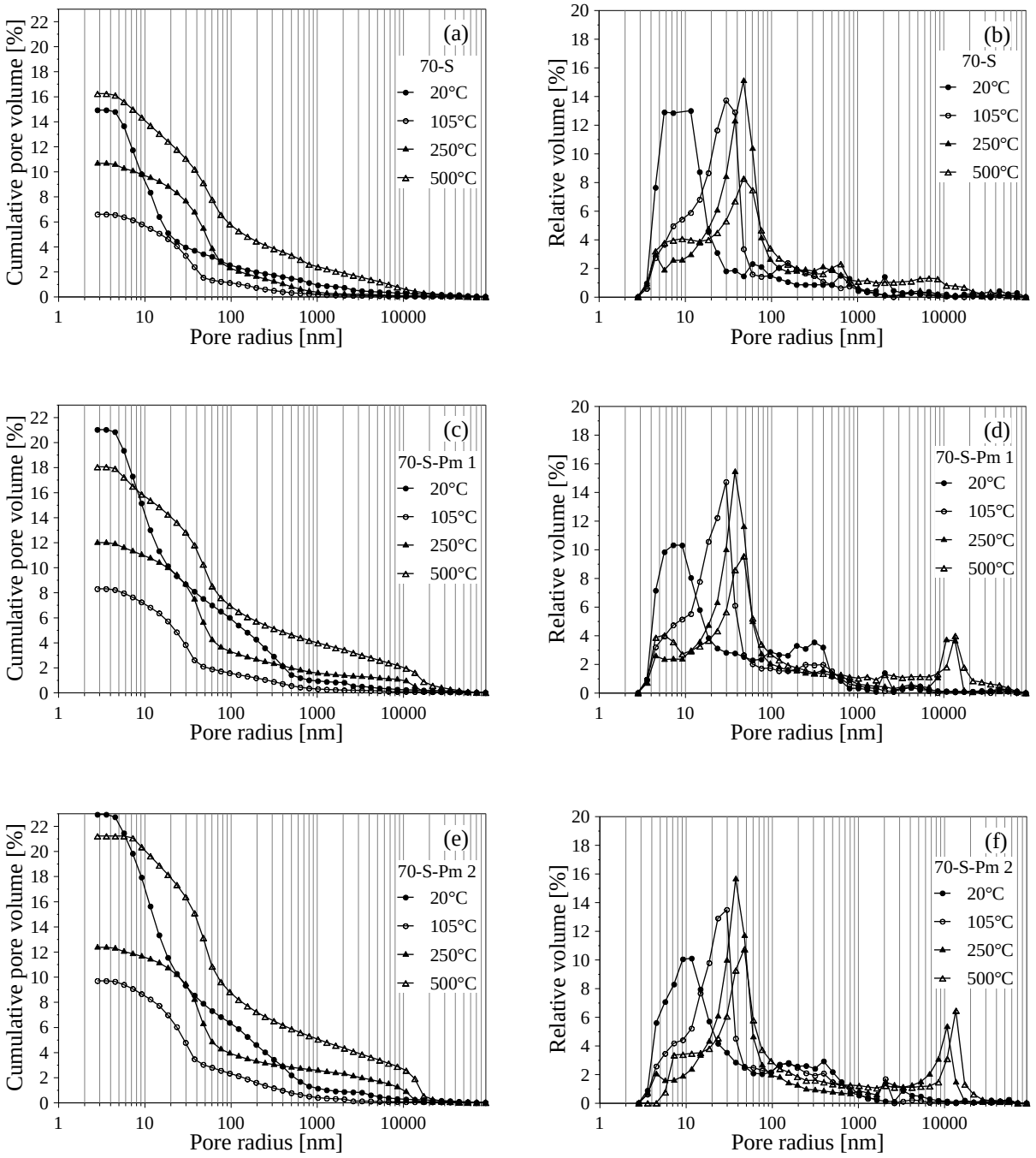

Figure 5.10: Cumulative pore volume for Mixes 70-S (a), 70-S-Pm1 (c), 70-S-Pm2 (e); and relative volume for Mixes 70-S (b), 70-S-Pm1 (d) and 70-S-Pm2 (f) as a function of pore radius at different temperatures.

Figure 5.10 refers to 70-S series and shows that increasing temperature brings in increasing values of the cumulative pore volume. At the same time, adding pp fibers brings in higher values for the cumulative pore volume, at any temperature.

In Figures 5.10b,d,f, the diagrams of pore-size distribution, for different temperatures, move towards larger-radius pores at increasing temperatures, because of the progressive expulsion of both free and bound water (with consequent increase in pore size), and because of concrete dehydration and cracking.

The most significant results concern the pore distribution in the mixes containing pp fibers: microporosities (whose size is of the same order of magnitude as the diameter of monofilament pp fibers) appear in Mixes 70-S-Pm 1 and 70-S-Pm 2, after being heated to 250 and 500°C as a consequence of the melting/degradation of the fibers.

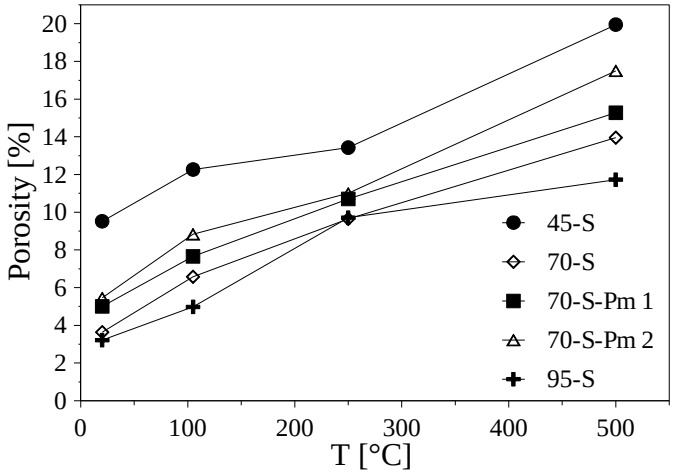

Figure 5.11: Total porosity as a function of the temperature.

The higher the pp-fiber content, the higher the relative volume peaks and the porosity generated by the thermal treatment. Figure 5.11 shows the values of the total porosity as a function of the temperature for the different mixes. As expected, higher-grade concretes have lower porosity at any temperature; pp fibers induce a significant increase of the porosity above 250°C. Room-conditioned specimens (20°C) show a reduced porosity as the pore volume is only partially accessible to mercury. The content of evaporable water at 105°C is about 2% by volume.

5.2.2 SCANNING ELECTRONIC MICROSCOPY (SEM)

The images obtained by means of SEM after concrete heating are shown in Figure 5.12. In the case of polished sections the technique based on Back Scattered Electrons – BSE was used, while fractured surfaces were examined by means of Secondary Electrons – SE. Figures 5.12a-d shows that microcracking occurs mainly after heating to 500°C. In addition, cracking in Mix 45-S (Figure 5.12a) is hardly distributed, being mainly located at the aggregates-matrix interface.

In Mixes 70-S and 95-S (Figures 5.12b, c), cracking appears more distributed and extended to the cementitious matrix. Adding fiber seems to make cracks more distributed (Figure 5.12d). Moreover, observing Mix 70-S-Pm 2 after heating to 250°C (Figure 5.12f), the spaces originally occupied by pp fibers appear empty, because of the melting and subsequent disappearance of the fibers, and a few new cracks propagate through the channels left free by the fibers.

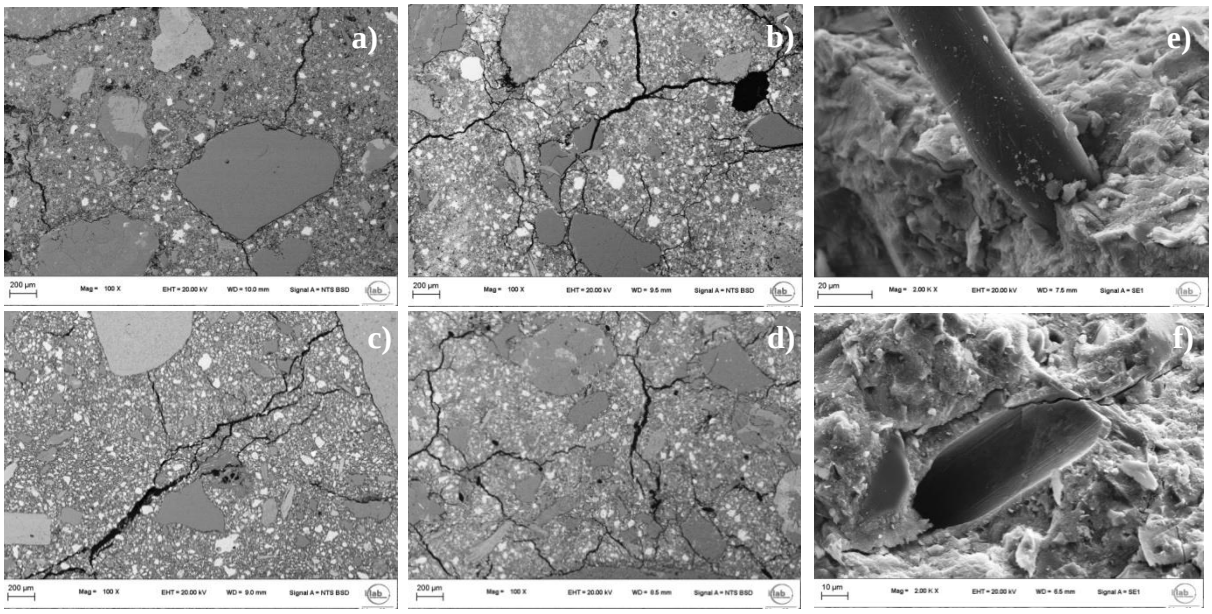

Figure 5.12: BSE images (magnitude: 100X) of polished sections heated to 500°C : (a) Mix 45-S; (b) Mix 70-S ; (c) Mix 95-S; and (d) Mix 70-S-Pm 2; and SE images (magnitude 2.00 KX) of fractured sections, Mix 70-S-Pm 2: (e) a typical monofilament fiber in the virgin material, not heat treated; and (f) typical void left by a fiber after heating to 250°C.

5.2.3 POROSITY, VAPOUR PERMEABILITY AND PORE PRESSURE

The experimental results concerning the vapor permeability of the 4 mixes show that the lower the compressive strength, the higher the vapor permeability, in agreement with the porosity trend

(Figure 5.13). Adding pp fibers does not significantly affect the vapor permeability with respect to the plain mix (Mix 70-S) at room temperature.

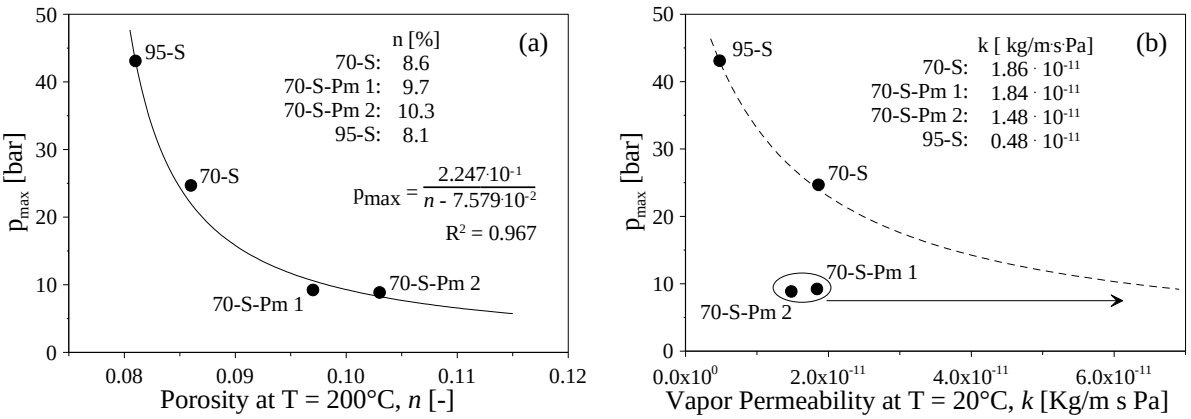

Figure 5.13: Peak values of the pore pressure as function of concrete porosity at 200°C (a) ; and of vapour permeability at room temperature (b).

Since the evolution of pore pressure during the heating process is controlled by vapor permeability (according to Darcy's law [42]) and vapor diffusion (according to Fick's law [42]), both mass transport processes being related to concrete porosity, it is rather interesting to plot the maximum values of pore pressure as a function of total porosity (at 200°C, see Figure 5.13a) and vapour permeability (at 20°C, see Figure 5.13b). In Figure 5.13a the experimental values can be easily fitted by means of a hyperbolic curve with appreciable statistical significance; this confirms the major role played by the total porosity in moisture transport and vaporization, as well as on concrete strength [43]. (For the mathematical formulation of the curve and the R^2 value, see the inserts inside Figure 5.13a).

Figure 5.13b shows that the decrease of pore pressure could be consistent with the increase of vapor permeability at 20°C only for plain mixes (Mixes 70-S and 95-S), while for fiber concrete (Mixes 70-Pm1 and 70-Pm2) the vapor permeability at 20°C does not seem to be a proper parameter to describe the decrease of the peak pressure in the pores as a function of the concrete type. This fact can be ascribed to the much more significant increase of the permeability with the temperature in pp fibers concrete compared to plain concrete (due to the melting and degradation of the fibers - above 165°C - and to the formation of new microcracks starting from the voids left by the fibers [3]).

5.2.4 DIFFUSIVITY

In Figure 5.14a shows that the Mix 95-S has a higher thermal diffusivity, whereas the Mix 70-S has the lower value of diffusivity. Generally diffusivity of concrete varies from 0.3 to 0.8 mm^2/s and the series of 70-S mixes shows that the maximum value of diffusivity is lower than 1.0 mm^2/s, only Mix 95-S has the higher diffusivity in the initial stage. Diffusivity mainly depend on the thermal conductivity, the higher the conductivity of concrete the higher the diffusivity, also its decrease with the increase of density itself.

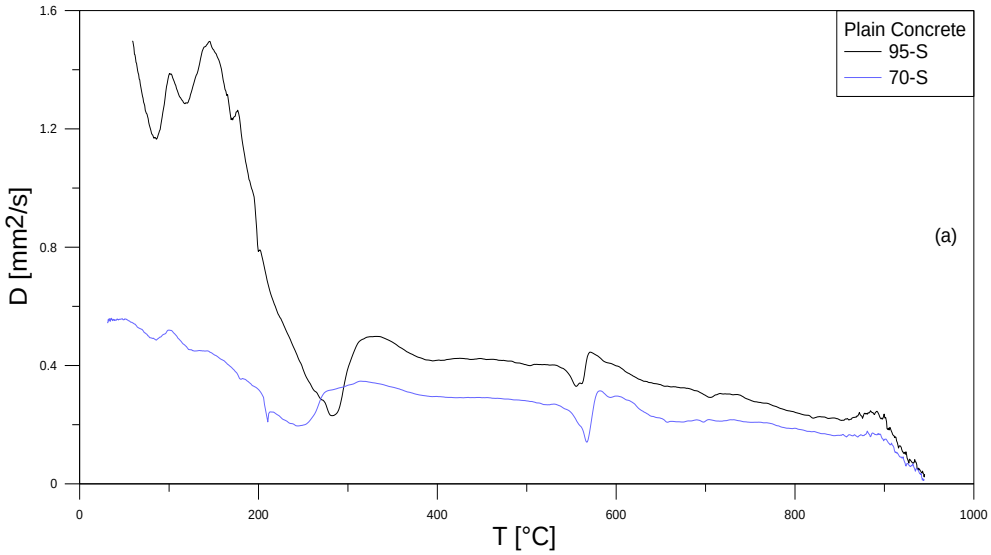

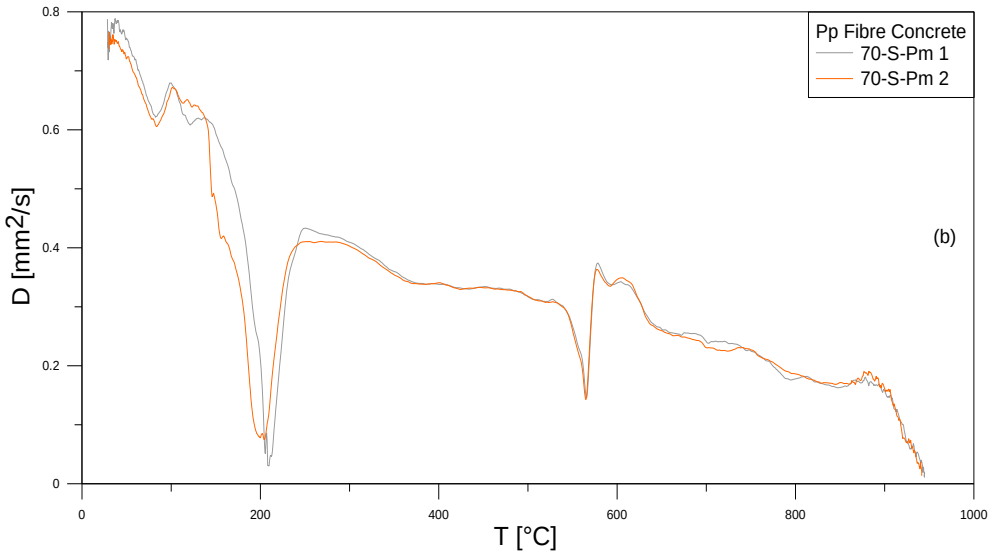

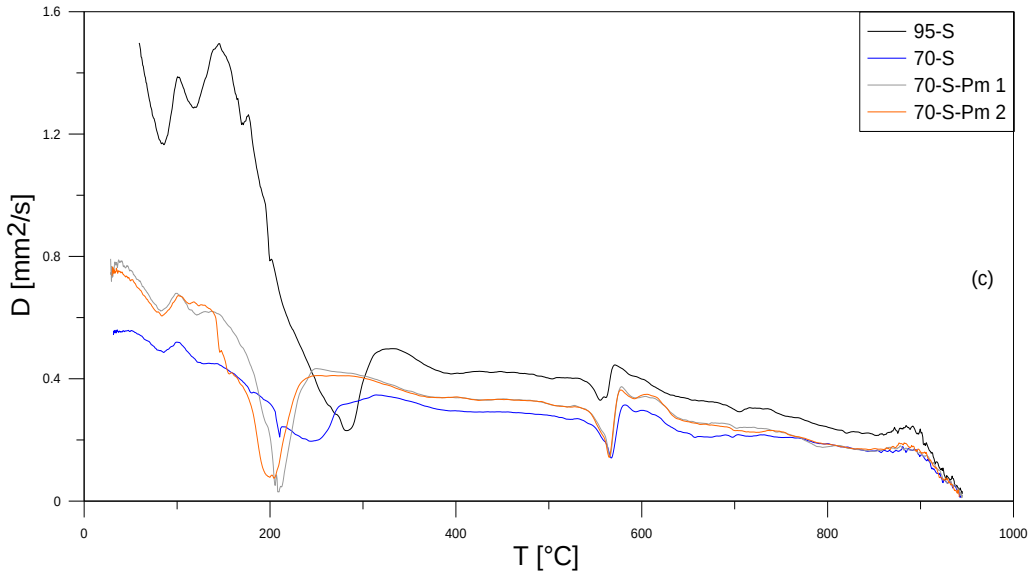

Figure 5.14: Thermal diffusivity of high performance concrete as a function of temperature: (a) Plain concrete, (b) Polypropylene fibre concrete and (c) all the 4 mixes.

On the other hand thermal conductivity of concrete depends on the moisture content, aggregate type, hardened cement paste, pore volume and distribution at the time of heating. However, all the mixes have the sharply drop of diffusivity in the temperature range between 190°C to 270°C and 570 to 580°C. It can be ascribe that, first spike at temperature 200°C due to evaporation of the free water and the partial expulsion of the bound water; second spike about at temperature 570 to 580°C due to the allotropic transition of the quartz contained in the aggregates, from the α to the β crystalline form. Same diffusivity behaviour was found Bamonte and Gambarova, 2010.

CHAPTER - 6

CONCLUSIONS AND RECOMMENDATIONS

Concrete is known to have a good behavior in fire because of its low thermal conductivity and good mechanical response also at high temperature. Several accidents were reported through time and serious damaged occurred, damage concerning both human safety and bearing capacity in terms of stability and integrity. All these factors indicate that concrete exposed to fire represents an important problem that needs further research to be carried out in order to provide a design able to prevent and predict explosive spalling, in particular for the new types of concrete. In this research work, the main objective was to understand the relation between pore pressure and the apparent tensile strength of concrete; establishing this relationship is a complex issue due to the fact that there are many factors governing the problem. Tensile strength of concrete under high temperature is affected not only by pore pressure, but also by temperature, heating rate, fire duration etc.

The main conclusions that can be drawn on the basis of the shown comprehensive experimental program are summarized in the following:

• The higher the water to cement ratio (w/c), the higher the fluid permeability and the lower the pore pressure value. At any temperature, high-performance concretes exhibit a total porosity, that is definitely lower compared to ordinary concrete, mainly owing to the reduced water/cement ratio in the former materials.

• Cracking is more distributed in HPC and tends to propagate through the cementitious matrix, while in ordinary concrete cracking is more concentrated at the aggregate-matrix interface.

• Adding polypropylene fibres (series of 70-S), the peak pressure is reduced of about 2/3 with respect to plain concrete (maximum peak pressure: Mix 70-S is around 3 MPa and Mix 70-S-Pm 0.5 is around 0.9 MPa).

• At any temperature, polypropylene fiber concrete exhibits a higher total porosity than plain concrete; this effect increases with the fiber amount; during or after fibers melting/degradation (above 165°C) - new microcracks form and propagate from the channels left free by polypropylene fibers.

• The peak pressure in the pores is strictly related to the porosity, in both plain and fibre mixes (in these latter mixes, porosity increases markedly after fibers melting and degradation); the relationship between peak pressure and porosity is adequately described by a hyperbole. The same seems to be true for the peak pressure as a function of vapor permeability, although this has been validated so far for plain mixes only.

• Pore pressure in concrete is directly related to porosity, gas permeability and water content. However, in all the tests, it was observed that rapid increase pressure starts at the beginning of the temperature plateau and reaches the peak at the end of the plateau.

• Vapour pore pressure starts rising significantly around 150^{o}C and reaches the peak around 230^{o}C for Mix 70-S, in average 180°C for polypropylene fibre concretes, and 270°C for Mix 95-S. For all the mixes, pore pressure development follows the saturation vapour pressure curve.

• The research result shows that adding 0.5 Kg/m^{3} of polypropylene fibre (Mix 70-S-Pm 0.5) is sufficient to reduce significantly the explosive spalling for very slow heating rate.

•The increasing the strength of the mix, the increasing the diffusivity of the concrete. Polypropylene fibre concrete exhibits the higher diffusivity compared than the plain concrete of same mixes.

• Plain concrete shows that pore pressure decreases the apparent tensile strength of concrete of about 0.22 times the pressure for Mix 95-S and 0.64 times the pressure for Mix 70-S (negative slope: 0.22 for Mix 95-S and 0.64 for Mix 70-S). Moreover, polypropylene fibre concrete shows a significant reduction of the tensile strength at zero pore pressure with respect to virgin tensile strength (around 20% for Mix 70-S-Pm 0.5, Mix 70-S-Pm 1 and 34 % for Mix 70-S-Pm 2) probably due to the melting of the fibres; the further porosity introduced by fibres melting, in fact, makes easier the propagation of the cracks, so increasing the permeability (this leads to low values of pore pressure) and decreasing the tensile strength.

BIBLIOGRAPHY

[1] Khoury A. G. “Effect of fire on concrete and concrete structures”, Progress in Structural Engineering and Materials, 2, pp. 429-447, 2000.

[2] Kalifa P., Menneteau F. D., Quenard D. “Spalling and Pore Pressure in HPC at High Temperatures”, Cement and Concrete Research, 30, pp. 1915-1927, 2000.

[3] Kalifa P., Ghene G., Galle C. “High-Temperature Behaviour of HPC with Polypropylene Fibres: From Spalling to Microstructure”, Cement and Concrete Research, 31, pp. 1487-1499, 2001.

[4] Dal Pont S., Dupas A., Ehrlacher A., and Colina H. "An Experimental Relationship between Complete Liquid Saturation and Violent Damage in Concrete Submitted to High Temperature", Magazine of Concrete Research, 57.8, pp. 455-61, 2005.

[5] Felicetti R., Monte F. L., and Pimienta P. “The Influence of Pore Pressure on the Apparent Tensile Strength of Concrete”, 7th International Conference on Structures in Fire, Zurich, Switzerland, June 6-8, 2012.

[6] Bangi M.R. and Horiguchi T. “Study on Pore Pressure Spalling in Hybrid Fibre- Reinforced High Strength Concrete at Elevated Temperatures”, Cement and Concrete research, 41, pp. 1150-1156, 2011.

[7] Mindeguia J. C., Pimienta P., Carre H., La Borderie Ch. “Experimental Study on the Contribution of Pore Vapour Pressure to the Thermal Instability Risk of Concrete”. 1st International Workshop on Concrete Spalling due to Fire Exposure, Leipzig, Germany, pp. 150-167, 3-5 September 2009.

[8] Mindeguia J. C., Pimienta P., Noumowé A., and Kanema M. "Temperature, Pore Pressure and Mass Variation of Concrete Subjected to High Temperature - Experimental and Numerical Discussion on Spalling Risk", Cement and Concrete Research, 40, pp. 477-487, 2010.

[9] Mindeguia, J. C., Pimienta P., Hager I., and Carrè H. “Influence of Water Content on Gas Pore Pressure in Concretes at High Temperature”, 2nd International RILEM Workshop on Concrete Spalling due to Fire Exposure, Delf, The Netharlands, pp. 113-121, 5-7 October, 2011.

[10] Mindeguia, J. C., Pimienta P., Carrè H., and Borderie C. L. “Experimental Analysis of Concrete Spalling due to Fire Exposure”, European Journal of Environmental and Civil Engineering, 2013.

[11] Bamonte P. and Felicetti R. “High-Temperature Behaviour of Concrete in Tension”, Structural Engineering International, 4/2012, pp. 493-499, 2012.

[12] Zeiml M., Lackner R. and Mang A. "Experimental Insight into Spalling Behaviour of Concrete Tunnel Linings under Fire Loading", Acta Geotechnica, 3, pp.295-308, 2008.

[13] Mindeguia J. C. "Contribution Expérimental a la Compréhension des risqué d'Instabilité Thermiques des Béton", Ph.D. Thesis, Université de Pau et des Pays de l'Adour, 2009.

[14] CEB – fip Model Code 1990, Comité Euro-International du Béton, Lausanne (Switzerland), 1993.

[15] Buchanan A. H. "Structural Design for Fire Safety", 2001.

[16] L. Giuliani et al. "Vulnerability of Bridges to Fire".

[17] Aïtcin and Neville. "High Performance Concrete demnystified", Magazine of Concrete Research, 1993.

[18] EC2-EN1992-1-2. Eurocode 2: Design of concrete structures, part 1-2. Standards Policy and Strategy Committee, 2005.

[19] Yufang Fu and Lianchong Li. "Study on Mechanism of Thermal Spalling in Concrete Exposed to Elevated Temperatures", Materials and Structures, 2010.

[20] T.Z. Harmathy. "Thermal Properties of Concrete at Elevated Temperature," J. of Material 5.pp.47-74, 1970.

[21] Fire Design of Concrete structures-Materials, Structures and Modelling, Bulletin 38, International Federation for Structural Concrete, Lausanne, Switzerland, April 2007.

[22] Z.P. Bazant and M.F. Kaplan. "Concrete at High Temperature: Material Properties and Mathematical Models", Longman, London, United Kingdom, 1996.

[23] C.R. Cruz and M. Gillen. "Thermal Expansion of Portland Cement Paste, Mortar, and Concrete at High Temperature," Fire and Material 4(2), 1980.

[24] P.J.E. Sullivan, G.A. Khoury, and B.N Grainger. "Strain Behaviour Under Uniaxial Compression of Three Concretes During First Heating to 600˚C," Proceedings of 6th International Conference on Structural Mechanics in Reactor Technology, Vol. G-H, Paper 1/3, Paris, France, 1981.

[25] R. Blundell, C. Diamond, and R. Browne. "The Properties of Concrete Subjected to Elevated Temperatures", Report No. 9, Construction Industry Research and Information Association, Underwater Engineering Group, London, United Kingdom, June 1976.

[26] T. Z. Harmathy and L.W. Allen. "Thermal Properties of Selected Masonry Unit Concretes," J. American Concrete Institute 70, 132–142 (1973).

[27] U. Schneider. “Behavior of Concrete at High Temperature”, HEFT 337, Deutscher Ausschuss fur Stahlbeton, Wilhelm Ernst & Sohn, Berlin, Germany, 1982.

[28] K-Y. Shin, S-B. Kim, J-H. Kim, M. Chung, and P-S. Jung. “Thermo-Physical Properties and Transient Heat Transfer of Concrete at Elevated Temperatures,” Nuclear Engineering and Design 212, pp. 233–241 2002.

[29] A. N. Noumowe et al., “Thermal Stresses and Water Vapor Pressure of High Performance Concrete at High Temperature,” Proc. 4th International Symposium on Utilization of High-Strength/High-Performance Concrete, Paris, 1996.

[30] C. Ehm. “Experimental Investigations of the Biaxial Strength and Deformation of Concrete at High Temperatures”, Dissertation, Technical University of Braunschweig, Germany, 1985.

[31] J.C. Marechal, “Variations in the Modulus of Elasticity and Poisson’s Ratio with Temperature”, Paper SP 34-27 in Concrete for Nuclear Reactors, pp. 495-503, American Concrete Institute, Farmington Hills, Michigan, 1972.

[32] C.R. Cruz. “Elastic Properties of Concrete at High Temperatures”, Department Bulletin 191, Journal of the Portland Cement Association Research and Development Laboratories 8(1), pp. 37-45, January 1966.

[33] R.K. Nanstad. “A Review of Concrete Properties for Prestressed Concrete Pressure Vessels”, ORNL/TM-5497, Oak Ridge National Laboratory, Oak Ridge, Tennessee, October 1976.

[34] B. Wu, J. Yuan, and G. Y. Wang. “Experimental Study on the Mechanical Properties of HSC after High Temperature,” Chinese J. Civil Engineering 33(2), pp.8-15, 2000.

[35] J.Zh Xiao, P. Wang, M. Xie, and J. Li. “Experimental Study on Compressive Constitutive Relationship of HPC at Elevated Temperature”, Journal Tongji University 31(2), pp. 186–190, 2003.

[36] M. Zeiml, D. Leithner, R. Lakner, and H. A. Mang. “How do PolypropyleneFibres Improve the Spalling Behaviour of In-Situ concrete?”, Cement and Concrete Research, 36, 2005.

[37] Felicetti R. and Gambarova P. G. “On the Residual Tensile Properties of High Performance Siliceous Concrete Exposed to High Temperature”, Special Volume in honour of Z.P. Bazant’s 60th Anniversary, Prague, March 27-28, Ed. Hermes (Paris), 167-186, 1998.

[38] Mehmet Baran Ulak and Murat Hacioglu. “On the Influence of Pore Pressure On the Apparent Tensile Strength of Concrete”. M.Sc. Thesis. Politecnico di Milano, 2011.

[39] Davide Sciancalepore and Alessandro Simonini. “Il Fenomeno Dello Spacco Esplsivo Del Calcestruzzo Esposto al Fuoco”. Tesi di Laurea Magistrale. Politecnico di Milano, 2012.

[40] CEN European Committee for Standardization, EN 1015-19, Methods of Test for Mortar for Masonry. Determination of Water Vapour Permeability of Hardened Rendering and Plastering Mortars, European Standard.

[41] Felicetti R. and Lo Monte F., Concrete Spalling: Interaction between Tensile Behavior and Pore Pressure during Heating, Proceedings of the 3th International Workshop on Concrete Spalling due to Fire Exposure, Paris, France, 25-27 September, 2013, in press.

[42] Gawin D., Pesavento P and Schrefler B.A., What Physical Phenomena can be Neglected when Modeling Concrete at High Temperature? A comparative study. Part 1: Physical Phenomena and Mathematical Model, *International Journal of Solids and Structures*, 48, 1927-1944, 2011.

[43] Guerrini G.L., Gambarova P.G. and Rosati G.P. Microstructure of High-Strength Concrete Subjected to High Temperature, Proc. Int. Workshop "Fire Design of Concrete Structures: What now? What next?", P.G. Gambarova, R. Felicetti, A. Meda and P. Riva (Eds.), pub. by Starrylink (Brescia, Italy), Milan, Italy, 2-3 December 2004, 89-94, 2005.

[44] CEN European Committee for Standardization, EN 12390-2, Testing hardened concrete – Part 2: Making and curing specimens for strength test, European Standard.

[45] Rossino C., Lo Monte F., Cangiano S., Felicetti R. and Gambarova P.G. "Concrete Spalling Sensitivity versus Microstructure: Preliminary Results on the Effect of Polypropylene Fibres", Proceedings of the 3th International Workshop on Concrete Spalling due to Fire Exposure, Paris, France, 25-27 September, 2013, in press.

[46] Khoury G.A., Polypropylene Fibres in Heated Concrete. Part 2: Pressure Relief Mechanisms and Modelling Criteria, *Magazine of Concrete Research*, 60 (3), 189–204, 2008.

[47] Pistol K., Weise F., Meng B., Schneider U., The Mode of Action of Polypropylene Fibres in High Performance Concrete at High Temperatures, Proceedings of 2nd International RILEM Workshop on Concrete Spalling due to Fire Exposure, E.A.B. Koenders, F. Dehn (Eds.), Delft, The Netherlands, 5-7 October, 289-296, 2011.

[48] CEN European Committee for Standardization, EN 12350-6, Testing fresh concrete – Density, European Standard.

[49] CEN European Committee for Standardization, EN 12350-2, Testing fresh concrete – Slump test, European Standard.

[50] CEN European Committee for Standardization, EN 12390-3, Testing hardened concrete – Compressive strength of test specimens, European Standard.